TARGETING LUNG CANCER BY IDENTIFYING GENES ASSOCIATED WITH RESISTANCE AND DEVELOPING LIPID BASED NANODISPERSIONS FOR THE INHALATION DELIVERY OF THERAPEUTIC PAYLOADS

by

ANDRIY KUZMOV

A dissertation submitted to the

School of Graduate Studies

Rutgers, The State University of New Jersey

In partial fulfillment of the requirements

For the degree of

Doctor of Philosophy

Graduate Program in Pharmaceutical Science

Written under the direction of

Professor Tamara Minko, Ph.D

And approved by

_____

_____

_____

_____

_____

New Brunswick, New Jersey

October, 2018

ABSTRACT OF THE DISSERTATION

TARGETING LUNG CANCER BY IDENTIFYING GENES ASSOCIATED WITH RESISTANCE AND DEVELOPING LIPID BASED NANODISPERSIONS FOR THE INHALATION DELIVERY OF THERAPEUTIC PAYLOADS

By ANDRIY KUZMOV

Dissertation Director:

Tamara Minko

The efficacy of cancer chemotherapy is limited by the development of resistance and intolerable side effects to conventional chemotherapeutic agents. To help overcome these barriers and improve the treatment of lung cancer, we propose the use of local inhalation delivery of chemotherapeutic drugs in combination of siRNA targeting pump and non-pump cellular resistance mechanism. To deliver the poorly soluble small molecule drug paclitaxel in combination with siRNA, we propose the use of a cationic lipid nanodispersion that can deliver the both therapeutic entities at the same time. To increase the targeting of the drug to cancer cells, LHRH peptide is attached to the delivery system. To reduce the particle size, improve the stability of the formulation, and improve its biocompatibility, we evaluate the effect of formulation buffer, solid lipids, and surfactant blends on the characteristics of the lipid dispersions. We report the formulation of gefitinib in the optimized lipid nanodispersions. To investigate the role of the PI3K/AKT pathway in the pathogenesis of cancer and development of resistance, we describe the evaluation of the gene expression of three cell lines with varying sensitivities to the EGFR inhibitor gefitinib.

ACKNOWLEDGEMENTS

I would like to express my gratitude to Dr. Tamara Minko for providing me with the opportunity to pursue my interest in research. Without her support and guidance, this thesis would not have been possible to achieve. Being a mentor professionally and personally, she has provided me with a role model I will look up to as I continue to move forward in life. I would like to thank her for making my time at Rutgers an experience I will always remember.

I would like to thank my committee members Dr. Colaizzi, Dr. Garbuzenco, and Dr. You for the time they took to serve as members on my committee. I would also like to thank them for serving as additional mentors during my time at Rutgers by proving valuable insight on the process of transitioning from student to professional.

I would like to thank all the former and current members of the Minko lab that I have had the pleasure of seeing everyday during my time at the lab. Without your guidance, support, and scientific discussions, I would not be the person that I am today. I would also like to thank Fei Han, Sharana Taylor, Hui Pung, and Marianne Shen with their help throughout the program and supporting all the students in our department.

Lastly, I would like to thank my parents, my sister, and grandparents for all the support they have provided me with throughout my life. Without their guidance, caring and support, I would not have been the person I am today.

Contents

List of Tables

List of Figures

1. Introduction

To enhance the efficiency of the treatment of lung cancer and prevent severe adverse side effects on healthy tissues, the toxicity to tumor cells of anticancer drug should be increased while the adverse side effects to the healthy cells in the lungs and entire body should be reduced. This can be achieved by simultaneous (1) targeting of the treatment specifically to lung tumor cells, (2) increasing the amount of antineoplastic agent delivered to the tumor site by local drug delivery, and (3) suppressing the pump and non-pump drug resistance in cancer cells. It is known that siRNA is capable of effectively suppressing the synthesis of proteins which are responsible for multidrug resistance in lung cancer cells.[1] siRNA functions by activating the RNA inducible silencing complex (RISC) which preferentially binds to mRNA with the complementary sequence of the siRNA. Once bound, the RISC proteins cleave the mRNA via ribonucleases preventing the expression of the targeted gene. siRNA, however, is very unstable in the blood stream due to the action of peripheral ribonucleases, uptake by macrophages of the reticuloendothelial system, and excretion by the kidneys, and it is characterized by poor cellular uptake. A nanoparticle delivery system capable of tumor targeted co-delivery of anticancer drugs and siRNA as suppressors of pump and nonpump cellular resistance can be used to achieve optimization of drug therapy of lung cancer.[2]

Over the years, lipid based drug delivery systems, including liposomes, have been used for increasing efficacy of different cancer treatments. However, liposomes have a few disadvantages such as low circulation time due to the action of the reticuloendothelial system and a reduced efficacy in the encapsulation of lipophilic drugs.[3] To help overcome some of the limitations of liposomes, solid lipid

nanoparticles (SLN) and nanostructured lipid carriers (NLC) have been developed as novel drug delivery systems to improve treatment efficacy and safety. Solid lipid nanoparticles are composed of surfactants and melted lipids which are solid at body temperatures. They are manufactured using various methods such high pressure homogenization and sonication.[4] NLC are the next generation of lipid carriers which are produced using the same methods as SLN, however, they use a mixture of lipids which can lead to higher drug loading capacity as compared to SLN.[3] NLC can be used to carry siRNA by using DOTAP, a lipid with a positive head, to make a positively charged exterior which can bind the negatively charged backbone of the siRNA. Poly-ethylene glycol (PEG) can be used to provide steric stabilization and decrease the clearance of the nanoparticles by the immune system. [2, 3]

For lung diseases, aerosol technology has been developed to deliver therapeutics directly to the lung tissue. The most important advantage of a pulmonary route for drug administration is a large absorptive surface of lungs for aerosol deposition, avoidance of the first-pass metabolic degradation, and the reduced exposure of the rest of the body to the delivery system which contains the chemotherapeutic agent.[5] It has been shown that lipid nanoparticles delivered to the lung are mainly cleared through lymphatic drainage as compared to absorbance into the blood stream of free drug delivered to the lungs. [6] This can be used to potentially increase the amount of drug that accumulates in the tumor tissues as many solid tumors have been shown to have impaired lymphatic drainage.[7] To decrease the side effects of the NLC loaded with chemotherapeutic agents, targeting ligands, such as an anti-bodies or peptides, can be attached to the delivery system to specifically target the tumor cells in the lungs. In this case, a synthetic LHRH peptide is

attached to the distal end of the PEG molecules to help target the nanoparticle system to the lung cancer cells that over express the LHRH receptor. [3]

2. Background and Significance

2.1 Lipid Dispersions

For the preparation of a lipid dispersion two immiscible phases, surfactant, and energy input are needed to begin the formulation process.[8-10]The dispersed phase is the one that breaks up into smaller and smaller components that are suspended in the continuous phase. When the dispersed phase is liquid at room temperature, an emulsion is formed while a solid dispersion is formed when the lipids are solid at room temperature.[11] To prepare dispersions using higher melting point lipids, the components can heated to about 10 degrees above the melting point of the solid lipid, and the parameters that govern emulsion formation can be applied in this situation.[4] The interaction of two immiscible fluids leads to the creation of an interphase with a certain area and surface tension.[9] If introduced into a container with no other stimulation, the two phases segregate and take a thermodynamically favorable orientation where they minimize the area of their interaction. A decrease in the size of the droplets leads to an increase in the size of the interphase requiring the addition of energy for the formation of the dispersion. Initially, the formation of droplets is relatively easy requiring relatively low speed mechanical mixing to produce droplets that are in the micron range in size.[9, 12] The oil droplets are mainly broken into smaller components by either laminar flow or turbulent flow of the continuous phase. Laminar flow of liquids applies sheer stress to the droplets as two layers of fluid travel past one another at different speeds. Turbulent flow causes the

decrease in droplet size by the effects of cavitation and the sheer stresses that can be caused by cavitation of the liquid. During formulation, the decrease in droplet size is countered by two factors. One, coalescence can occur when two droplets come together to form one larger droplet.[8, 9, 12] Two, the increase in the Laplace pressure of the droplets as their size decreases which increases the amount of energy needed to further destabilize the droplet. The droplet's Laplace pressure is directly proportional to the surface tension of the oil phase and inversely proportional to the radius of the droplet, which means there is a need to add more energy and surfactant to the system for the formation of smaller particles. The presence of the emulsifier in the formulation helps overcome these two forces in two ways. One, the surfactant can stabilize the droplets that are formed during emulsification preventing their coalescence. Two, the incorporation of the surfactant onto the droplet surface lowers the surface tension of the oil helping to overcome the effects of the increase in Laplace pressure on droplet deformation ability.[9] The more surfactant added to the system the smaller the droplet size that can be achieved, to a degree. This is due to the presence of abundant amounts of surfactant that can adsorb into the interface, which keeps increasing with decreasing droplet size. The type of surfactant used will also determine its ability to partition into the newly formed interphases. Smaller non-ionic surfactants tend to partition onto the interphase much quicker than larger polymeric or peptide based surfactants. The type of emulsion prepared is therefore dependent on the types of oils, the surfactant, and the amount of energy that is applied to the system. The three types of lipid dispersions that can be prepared are coarse emulsions, nanoemulsions, and microemulsions. Each type of emulsion has different characteristics, properties, and production parameters which make

it more or less attractive for a given application. The summary their characteristics are listed in table 2.1.[10, 12-14]

2.1.1 Coarse Emulsions

Coarse emulsions are thermodynamically unstable systems that are formed by low energy mechanical perturbations. Coarse emulsions are kinetically stable, meaning the surfactants used during their formation prevent phase separation for various lengths of time, days to years. The emulsions could degrade via flocculation where the individual drops clump together to from larger aggregates which can be somewhat reversible with mechanical agitation. Coalescence leads to the formation of large drops from smaller ones and is irreversible. Creaming results from the rising of droplets to the top of the formulation due to buoyancy forces. Sedimentation of the dispersed phase occurs due to the effects of gravity on the dispersed droplets. Coarse emulsions are generally in the range of 0.5 to 50 microns in size and can be created as oil in water, water in oil, or mixed water in oil in water emulsions depending on the intended applications. Due to the micron range size of the particles they usually appear as white cloudy dispersions. Relatively low amounts of surfactants are used in the preparation of course emulsions.[9, 14, 15] These dispersions are not good candidates for delivery of payloads directly into cells as they can be too large for effective uptake by individual cells.[16]

2.1.2 Nanoemulsions

Nanoemulsions sometimes referenced as miniemulsions, submicron emulsions, or ultrafine emulsions, are thermodynamically unstable systems which are formed by high energy perturbations of the continuous phase. They are kinetically stable systems that are in the range of 50 to 500 nanometers in diameter. These systems appear to be transparent

in the 50 to 200 nanometer range and somewhat opaque in the 200 to 500 nanometer range. These systems are created using more surfactant than coarse emulsions with the need to use multiple emulsifiers to create the most stable systems. Nanoemulsions have advantages over coarse emulsions in that they are less susceptible to the effects of flocculation due to the ability of the higher surfactant content to form a more stable interfacial layer at the oil water interface. There is no creaming or sedimentation seen with nanodispersions due to effects of Brownian motion. The particle diffusion rate in the continuous phase is higher than the effects of gravity on the droplets. Nanoemulsions can show signs of separation and destabilization if the droplet size increases to the point where creaming and sedimentation become possible. The increase in droplet size can occur due to coalescence, aggregation, and Oswald ripening if the correct components are not utilized.[8-10, 14, 15]

Nanodispersions offer some practical advantages over coarse emulsions due to the size of the droplets. The small droplet size and large surface area also allow for the better adsorption of the droplets onto surfaces where they can act as controlled release reservoirs. [9, 10] They can help increase the total amount of hydrophobic substances that can be incorporated into the aqueous phase as well as well as provide a controlled release of the active ingredients.[4] The improved effects of nanoencapsulated active ingredients may be due to the increase in the mass transfer of the active ingredient throughout the area where the nanodispersion is applied or due to the ability to deliver the payload inside cells as nanoparticles can be internalized by individual cells.[17, 18] The wide spread use of nanodispersions for commercial purposes has been limited by a number of factors. The preparation of nanoemulsions requires the use of specialized equipment, such as

homogenizes, microfluidisers, and sonicators, or specialized formulation techniques such as the concept of phase inversion temperature preparation methods. There is a need to understand the role that surfactants and co-surfactants play in the formation of the nanodispersion and the appropriate ratios of each one that need to be applied to a specific lipid phase and how each component affects stability, drug loading, and toxicity.[8, 9]

2.1.3 Microemulsions

Microemulsions are thermodynamically stable systems that are formed without the need for high energy perturbation mechanisms. The thermodynamically favorable formation of microemulsions is due to the presence of high surfactant concentrations which lower the interfacial tension to the point that the entropy of emulsion droplet formation becomes greater than the effects of the increase in the size of the interface. Preparation of microemulsions occurs spontaneously with low speed mixing of two immiscible liquids in the presence of high amounts of surfactants and cosurfactants, typically in the range of 15-20% of the formulation.[10, 19, 20] Microemulsions are truly stable systems as application of high sheer stress will not change the size distribution of the droplets. The size of the microemulsion droplets must be altered by changing the types and amounts of surfactants or lipids used in the formulation.[10, 14] Heating may need to be added to the low speed mixing to increase the rate of formation of the microemulsion or to prepare microemulsions with high melting point lipids.[21] Microemulsions seem to be great alternatives to nanoemulsions and emulsions; however, they do have some challenges that need to be considered. One, their formation relies on the presence of high concentrations of surfactants[10, 14] Some types of surfactants may not be able to reach high enough concentrations in the continuous phase for microemulsion formation. The

excess surfactant concentrations may not be appropriate for all intended applications. The need to use high surfactant concentrations can also affect the ability to dilute the emulsion beyond its preparation conditions. This likely due to the changes in the structure and organization of the interactions between the lipid phase, surfactants, and aqueous phase as the surfactant concentration decreases and the continuous phase increases.[20]

2.1.4 Formulation Methods

Many methods of emulsification have been identified including pipe flow, colloid mills, high speed mixing, high pressure homogenization, microfluidics, sonication, membrane emulsification, phase inversion temperature formation, and many others. However, the following methods are commonly used to prepare nanodispersions.

High pressure homogenization techniques are commonly used to create nanoemulsions for research purposes. These techniques may vary somewhat in their set up, but they all rely on the application of pressure to a fluid and the creation of shearing forces produced by the high pressure flow. Usually, high pressure homogenization refers to high pressure valve homogenization. In this set up, a crude coarse emulsion is prepared and subject to high pressures, usually up to 300 Mpa, as the fluid is forced through a small opening. As the fluid flows through the opening, laminar elongation forces are experienced by the coarse emulsions. After the valve, the fluid is subjected to turbulent flow. These shearing forces work to break up the coarse emulsion into smaller droplets. This method is attractive as it can be scaled up for large scale production. However, there are some draw backs. Generally, coalescence can occur during this process requiring multiple passes through the valve homogenizer to produce the smallest droplets for a given oil,

surfactant, and water mixture. The type of surfactants can also affect the number of passes needed to achieve minimum droplet size.[12, 22]

Microfluidic approaches are a different type of high pressure homogenization. This method relies on the high pressure flow of two streams of fluid which collide with each other at varying angles and forced out through one opening. The streams are usually in the 50-150 micron range in diameter. In a microfluidic device, the droplets are broken down by the shearing and turbulent flow which occurs when the two streams collide. Microfluidics provides some advantages over valve homogenization as the minimum droplet size can be reached with fewer passes through the homogenization process, and microfluidic preparation produces a more monodispersed emulsion. Microfluidics is currently used primarily in research applications as there are limitations in large scale production using this method.[12, 22]

Ultrasonication or sonication emulsification relies on the use of an ultrasound generator to propagate sound waves though the continuous phase. Often, probe sonicators are used for the preparation of emulsions. Two proposed mechanisms exist for the formation of the emulsion using this method. One, the ultrasonic waves can disrupt the oil water interface increasing the interaction between the two phases. Two, cavitation bubbles are formed as the waves propagate though the continuous phase. Upon rupture, these cavitation bubbles can cause high pressure shock waves and increases in temperature which can help to further break down the droplets of the dispersed phase. During sonication, the emulsification potential is concentrated at the tip of the probe and dissipates as you move away from it. There have been many studies of emulsification using batch sonication methods and some investigations into continuous sonication

designs to help improve the scale up potential of this emulsification method. Sonication is limited by the generation of heat during the process, and the relatively small volumes which can be prepared using the batch sonication set up.[13, 23, 24]

Two low energy methods for nanoemulsion formation are the phase inversion temperature(PIT) and the phase inversion composition(PIC) methods. These methods rely on the ability of the surfactants to change their behavior at with changing parameters. In the PIT method, non-ionic surfactants have different behaviors at different temperatures. At high temperatures, many such surfactants will have a negative curvature. As the temperature decreases, they can transition to a state of zero curvature and finally to a state of positive curvature where they can stabilize oil in water nanoemulsions. The PIC method relies on the continuous phase to a mixture of the dispersed phase and surfactant such as gradually adding water to a surfactant and oil mixture. Initially, a water in oil emulsion is created with a negative curvature of the surfactant which stabilizes the water in oil emulsion. As more water is added, the curvature of the surfactant becomes zero and an intermediate bi-continuous phase is formed. Eventually, as more water is added, an oil in water nanoemulsion is formed. The advantage of these low energy methods lies in the fact that they do not require excessive processing with expensive equipment. However, they have the disadvantage of generally requiring higher amounts of surfactant, and the need to understand surfactant behavior at different temperatures and concentrations.[25]

2.1.5 Solid Lipid Nanoparticles and Nanostructured Lipid Carriers

Solid lipid nanoparticles (SLN) and nanostructured lipid carriers (NLC) are two types of lipid dispersions that can be created using lipids that are solid at room temperature. These

systems are the same as emulsion based systems but differ in the use of only solid or mixtures of solid and liquid lipids as the dispersed phase.[4] The interest in developing these systems lies in the fact that these systems have a number of proposed advantages. The SLN and NLC systems can be used to provide controlled release and targeting of the payload to a specific site. They can increase drug stability by protecting the payload from chemical degradation that can occur in aqueous formulations of free drug. Depending on the drug molecule, very high drug loading can be achieved.[11] Drug loading can be described by the entrapment efficiency and drug loading percent. Drug loading efficiency is described by the amount of drug loaded into the formulation as compared to the amount of drug added to the initial mixture. Drug loading percent relates to the total amount of drug in the system as it compares to the total weight of the lipid dispersed phase. [4] The matrix of these systems is made from biocompatible and biodegradable lipids that limit acute and chronic toxicity concerns and have virtually no concerns of accumulation of the ingredients in the body.[11, 26] Formulation of the lipid dispersions can be accomplished with little to no use of highly toxic organic solvents as compared to the preparation of some polymeric drug delivery systems.[11, 27] The lipid dispersions can be scaled up for the production of quantities necessary for commercial applications. Although preparation methods such as sonication and microfluidics have limited scalability, the fabrication of large quantities of lipid dispersions can be achieved using high pressure homogenization techniques. [4, 11] The wide range of available components makes it difficult to create one system that can be used in every application. Therefore, it is necessary to not only show the system can be used to deliver cargo to a specific site but also to optimize the system for the particular application.

The core of the systems can be made of triglycerides, hard fats, oils, free fatty acids, and other components. These lipids have different properties in terms of melting point, crystal structure, and rate of degradation. Some lipids are provided as a mixture of two or more species of glycerides which can alter the above properties of the blend. These differences must be considered when designing the formulation parameters used during the preparation process as the particle characteristics can change when using different lipid core components.[11] The surfactants used in the formulation of lipid nanoparticles can be classified into two major categories, ionic and non-ionic surfactants. The most common non-ionic surfactants include poloxamers, polysorbates, and pegylated fatty acids. They generally consist of a hydrophobic polymer or fatty acid conjugated to long segment of hydrophilic polymer, most commonly, polyethylene glycol (PEG). Non-ionic surfactants stabilize the lipid droplets in the aqueous phase by the steric hindrance that is provided by the PEG chains. The ionic surfactants can be broken down into cationic, anionic, and zwitterion surfactants. Cationic surfactants include substances such as cetyl trimethylammonium bromide (CTAB), cetylpyridinium chloride (CPC), dimethyldioctadecylammonium bromide (DDAB), N-[1-(2,3-dioleoyloxy)propyl]-N,N,N-trimethylammonium chloride (DOTAP), 1,2-distearoyl-3-dimethylammonium-propane (DAP) and many others. The cationic surfactants generally contain some form of an amine functional group in the hydrophilic portion of the molecule which provides the positive charge of the molecule when introduced into an aqueous environment. Anionic surfactants create particles with a negative surface charge which is usually achieved by the presence of a carboxylic acid or a phosphate group in the hydrophilic portion of the surfactant. The zwitterion surfactants contain both a positively and a negatively charged

group in the hydrophilic portion of the molecule leading to an overall neutral charge. The most commonly used zwitterion surfactants are the many types of phospholipids available for commercial use. The surfactants based on fatty acid derivatives differ in terms of the length of their lipid tails, the degree of unsaturation, and the number of fatty acid tails present which leads to changes in the ability of the surfactant to stabilize nanodispersions.[4, 11, 26, 28, 29]

The loading of therapeutic small molecule compounds into lipid nanoparticles is believed to occur by one of the following models, homogeneous matrix model, enriched shell model, and enriched core model as seen in figure 2.1. In the homogeneous model, the drug is believed to be completely dissolved in the lipid phase and distributed evenly throughout the matrix of the lipid core. In this scenario, the drug is released by one of two mechanisms, diffusion from the lipid phase or by degradation of the particles either in the gut or after internalization by individual cells. The drug enriched shell model comes into effect when drug has an increased solubility in the aqueous phase during formulation when the temperature is elevated in the presence of abundant surfactant. As the droplets are formed and subsequently cooled, the lipid phase forms an empty core first, followed by a shell that is enriched with drug as it partitions into the lipid phase as the temperature is lowered. The drugs that partition into the particles in this manner have been shown to exhibit a burst release when administered to animals. The drug enriched core model occurs when the drug precipitates before the lipid phase during cooling leading to higher drug content in the core which is then surrounded by lipids and surfactants. Drug loading by this mechanism has been shown to lead to prolonged drug release profiles. [4]

2.2 Lung Cancer

According to the Center for Disease Control cancer statistics, cancer claims the life of more than five hundred thousand Americans each year. Cancer is the second leading cause of death in the population of the United States and contributes to one out of every four deaths. According to the incidence rates data on the top ten cancers in the United States in 2007, prostate cancer, female breast cancer, and lung cancer are the most common types of cancers with incidence rates of 156.9, 120.4, and 65.6 cases per one hundred thousand people, respectively. Among the top three cancers mentioned, lung cancer has the highest death rate among both men and women at 50.7 deaths per one hundred thousand persons. The death rate due to lung cancers is more than twice exceeds the death rate of prostate cancer, the next deadliest cancer with a death rate of 23.5 per one hundred thousand.[30] Lung cancer is one of the deadliest cancers found in the United States with 70 % of patients being diagnosed with tumors that do not respond well to therapy, and, when the cancer is discovered early and treated, it is prone to relapse in patients. The main causes of lung cancer include exposure to tobacco smoke, asbestos, radon, coal tar, benzene, and halogenated ethers. These compounds are able to enter into the lungs during breathing, induce mutations and alter the gene expression of the stem cells of the lung epithelium tissue.[31] Although smoking is considered to be the major cause of lung cancer, every smoker does not develop lung cancer leaving other risk factors to be explored. It has been noted that first degree relatives of lung cancer patients are at an increased risk of developing lung cancer themselves. Patients who suffer from chronic obstructive pulmonary disease and asthma have also been recognized as having as increased risk for developing lung cancer. Lung cancer can be divided into two general

types: small cell lung cancer (SCLC) and non-small cell lung cancer (NSCLC) with small cell lung cancer generally being the more aggressive of the two. [32, 33]

Non-small cell lung cancer accounts for 80% of all the lung cancer cases in the United States. If detected early, the five year survival rate can be as high as 80% while the five year survival rate of patients diagnosed at later stages drops below 5%. During the early stages of disease progression, patients often do not show any signs or symptoms of tumor growth. They present with symptoms such as cough, hemoptysis, wheezing, stridor, dyspnea, and post obstructive pneumonia which can all be caused by a number of conditions. If left untreated, early tumors of NSCLC tend to metastasize to other parts of the body with the lymph nodes, pleura, and other areas of the lungs being the three most common areas of local infiltration.[33]

NSCLC can also metastasize to areas outside the lung such as the bones, liver, and the CNS with each point of metastases presenting with unique symptoms. Based on the location of extra pulmonary metastases, patients can present with bone pain, liver dysfunction, and neurologic changes. NSCLC can be further characterized into one of three sub groups: squamous cell, adenocarcinoma, and large cell. Squamous cell carcinoma is most often seen in smokers and men. It usually grows slowly, but it can metastasize to lymph nodes, liver, adrenals, kidneys, bone, and the gastrointestinal area. Adenocarcinoma is the most common histology of lung cancer and can have a number of different sub-classifications based on the site of origin. Adenocarcinoma often metastasizes before the initial tumor is detected making it more dangerous for the patients with this histology, and it leads to patients that can initially present in a number of different stages of disease. Adenocarcinoma can metastasize to a number of different

sites that include the lung, liver, bone, adrenal glands, CNS, and the kidneys.[32, 33] The NCCN guidelines recommend that patients with adenocarcinomas be tested for epidermal growth factor receptor (EGFR) and anaplastic lymphoma kinase (ALK) mutations as these patients may be candidates for targeted therapy.[34] It was found that patients with mutations in the EGFR that respond to EGFR blockade fare better on targeted therapy as compared to traditional agents.[35] Large cell carcinomas are similar to adenocarcinomas in the sites that it metastasizes to as well as the risks it poses to the patients who are diagnosed with it. When it comes to treatment, the different classes of NSCLC are generally treated in the same way as they respond to the same therapies.[32]

2.2.1 Treatment of Lung Cancer

The treatment of NSCLC is based on the stage of disease the patients present with when they are diagnosed as well as the patients' ability to tolerate the treatment. Patients that present with local stage 1A disease are primarily treated with surgery with curative intent. These patients often do not receive additional chemotherapy after surgery, even if the margins are positive. In such a case, a second surgery is recommended; however, patients can be treated with radiation therapy with or without concomitant chemotherapy. In patients who are diagnosed with Stage IB, Stage IIA, and some with Stage IIB disease are treated first with surgical removal of the tumor with adjuvant chemotherapy to follow. The exact patients in which to use chemotherapy as well as the best first line chemotherapy option is not clear, however, cisplatin based regimens are most often used to treat these patients. In patients who have positive margins after histologic evaluations of the removed tissue may receive radiation therapy along with the chemotherapy. Patients who present with stage IIB or IIIA disease are treated with a multifaceted

approach. If they are candidates for surgery, the tumor tissue is resected, and the patients are treated with adjuvant chemotherapy. For those who are not candidates for surgery, chemotherapy and radiation are used to treat the patients to help prologue survival. The treatments of choice here are again a platinum containing regiment. The common platinum agents used early in disease are either cisplatin of carboplatin. They are often used in combination with one of the following agents: vindesine, vinorelbine, etoposide, vinblastine, or paclitaxel. In later stage disease, surgery is less often a viable treatment option and chemotherapy becomes the backbone of treatment.[32, 33]

The majorities of patients who are diagnosed with NSCLC are diagnosed with stage IIIB or IV disease and are not candidates for surgical removal as they often have many sites of metastases. These patients are treated with chemotherapy to help relieve symptoms, improve the patient's quality of life, as well as help improve survival. The treatment of choice is again a platinum agent, either cisplatin of carboplatin, and another agent such as paclitaxel, pemetrexed, vinorelbine, gemcitabine, or docetaxel for a total of four to six cycles.[32, 34] For those who cannot tolerate platinum based therapy, a combination of gemcitabine and a taxane can be used. After the initial therapy is complete, it is not recommended to continue maintenance therapy for all patients, however, there is a benefit seen in patients who have stable disease or have responded to their initial therapy. In patients with non-squamous cell histology, maintenance with pemetrexed has prolonged the median overall survival by about three months. In patients who cannot tolerate the first line combination therapy, single agent treatment is used even though there is only minimal survival benefit. The drugs that are considered for single agent treatment include cisplatin, carboplatin, docetaxel, paclitaxel, etoposide,

gemcitabine, ifosfamide, irinotecan, topotecan, mitomycin, vinblastine, vinorelbine, and pemetrexed. In the event that a patient does not respond to the initial treatment or there is a relapse of disease after induction therapy, the patients can be treated with single agent therapy consisting of docetaxel, pemetrexed, or erlotinib. Docetaxel and pemetrexed have similar efficacy when used as second line agents but have different toxicities. Along with these treatments, there are a number of targeted therapies that may be used if the cancer harbors certain mutations.

The targeted agents used include epidermal growth factor receptor (EGFR) inhibitors, vascular endothelial growth factor receptor (VEGF) inhibitors, and ALK mutation inhibitors. The EGFR inhibitors used in the treating patients with NSCLC are erlotinib, gefitinib, and cetuximab. Gefitinib and erlotinib are two small molecule tyrosine kinase inhibitors that interfere with kinase signaling downstream of the EGFR. Gefitinib was the first drug to reach the market and was FDA approved for the monotherapy of patients who had failed cisplatin based and docetaxel therapy.[32]

The traditional agents that are used often in the treatment of lung cancer as previously mentioned include cisplatin, carboplatin, pemetrexed, irinotecan, vinorelbine, docetaxel, paclitaxel, and others. The combination of a platinum agent with one of these new agents has increased the NSCLC survival time; however, these drugs are toxic substances and have many side effects which may be intolerable to the patients who are given these drugs. Although the targeted therapies are generally better tolerated than traditional therapy, some patients develop intolerable side effects that may lead them to discontinue their therapy.[32]

2.2.2 Inhalation Delivery for Lung Cancer Treatment

The delivery of therapeutic compounds to the lungs has long been established as a viable method for the treatment of lung diseases. Primarily, inhalation delivery of therapeutics is used in the treatment of asthma and chronic obstructive pulmonary disease (COPD). The challenges of reaching the lungs with systemic therapy and some benefits of local delivery are outlined in figure 2.2.[36] The major draw backs of systemic therapy targeting the lungs centers on the low retention of drugs in the lungs of many drugs when they are given systemically as well as the development of side effects due to wide spread exposure of the system to elevated drug levels. The main benefits of inhalation delivery include higher accumulation of the active ingredients directly to the site of action, limiting systemic exposure, and improved outcomes due to higher drug levels in the lungs. Challenges in the local delivery of therapeutics to the lungs come from the inability of many drugs to be retained in the lungs for extended periods of time due to the high absorptive surface area of the lungs and the inability of some free drugs to be easily delivered without special formulation needs.[36] The use of nanoparticle based delivery systems can help overcome these challenges by providing a formulation that can carry and deliver various types of payloads, increase the retention time in the lungs, and provide a controlled release profile for extended action of the therapeutic. It has been shown that delivery of nanoparticles to the lungs can increase the retention time of the system in the lungs and reduce their detection in other organs in the body. [6, 36] It has also been demonstrated that lipid nanoparticles are mostly cleared from the lungs by lymphatic drainage from the tissues. This property of lipid nanoparticles can be used to

help target cancer by the following mechanisms. One, it is well established that many solid tumors do not have well developed vascular and lymphatic systems. In the case of systemically administered nanoparticles, the particles can be passively target the tumor via the enhanced permeability and retention effect. The particles are able to more readily access the tumor microenvironment due to the leaky vasculature of the tumor, as compared to the distribution into other organs. Once in the tumor microenvironment, the nanoparticles are retained there for a longer period of time due to their decreased clearance from the tumor tissues due to the poorly developed lymphatics system. In the case of local delivery to the lungs, we will not observe the enhanced permeability as can be seen with systemically administered nanoparticles; however, we can have an increased retention of the nanoparticles in the tumor tissues due to their poor lymphatic drainage as described above. Two, lung cancer cells have been described to spread through the lymphatic system, which can lead to development of metastasis and spread of the disease. The propensity of lipid nanoparticles to be cleared through the lymphatics could be advantageous in targeting any cancer cells that have spread to the lymph nodes.[6, 7]

The use of inhalation chemotherapy for lung cancer treatment has been explored by a number of groups in early phase clinical trials. Some have focused on the delivery of free immune modulating peptides such as GM-CSF and IL-2, however, they have had limited success in the treatment of the disease. The authors of the IL-2 trials, however, reported decreased side effects as compared to therapy with standard doses of systemic therapy. Other trials evaluated the inhalation administration of free drug solutions such as doxorubicin, gemcitabine, and carboplatin.[37-40] G. Otterson et al. reported the results of a dose escalation study using doxorubicin nebulized via an OncoMyst device which

consisted of a Pari LC Plus nebulizer contained within a system to capture stray aerosols. The dose limiting toxicity was observed at inhalation doses of 9.4 mg/m^2. During the trial, it was found that absorption into the blood stream occurred after inhalation, but the Cmax was much lower than that observed after intra-venous administration. The investigators found that the patients experienced some of the expected toxicities associated with the use of doxorubicin, but patients also developed side effects associated with the inhalation of the drug solution such as sore throat, hoarseness, dyspnea, and chest pain. When the investigators performed a phase two study of inhaled doxorubicin in combination with systemic therapy, they found that 35% of the study participants had a positive response, however, this was not decide to proceed to a large scale study.[41, 42]

E. Lemarie et al. demonstrated feasibility of inhaled gemcitabine in eleven patients in combination with 99mTc-diethylene triamino pentaacetic acid to study the distribution of the inhaled solution in the patient population. It was found that 43% of the inhaled dose was able to reach the lower airways while on average 47% of the inhaled dose ended up in the upper airways and stomach. The identification of almost 50% of the dose in the upper airways and stomach can be attributed to the deposition of the droplets in the upper airways and subsequent mucociliary clearance of the solution towards the pharynx where it is then swallowed. The authors reported limited absorption of the drug into circulation; the reported side effects included bronchospasm, cough, fatigue, nausea, anorexia, and others. The appearance of gastrointestinal and upper respiratory side effects could be attributed to the deposition of the gemcitabine in those locations.[43] P. Zarogoulidis et al. reported the use of inhaled carboplatin in combination with 100 mg/m2 IV docetaxel in various dosing groups. It was found that those in the inhalation group saw reduced

systemic side effects such as neutropenia, however, those patients experienced increased pulmonary and gastro intestinal side effects with increasing doses of inhaled carboplatin.[44] The increase in pulmonary and gastrointestinal side effects can be attributed to the increased deposition of the inhaled therapeutic in those areas as described by E. Lamarie et al.

It is proposed that the use of lipid nanoparticle based delivery systems can be used to help target lung cancer tissues in the lungs. The nanoparticle delivery system can provide an increased accumulation of drugs in the lungs while limiting systemic exposure. The nanoparticle formulation may also help alleviate some of the pulmonary and gastrointestinal side effects reported as it can provide a slower more controlled release as compared to the inhalation of free drug solution.

2.2.3 Resistance

The efficacy of chemotherapy is also limited by the rapid development of tumor resistance with repeated courses of chemotherapy. The mechanisms of this resistance are dependent on a number of factors. Some resistance is related to the drug metabolism, alterations in target proteins with in the cells, and over expression of repair enzymes.[45] Cancers can also develop multidrug resistance through the expression of “pump” and “non-pump” resistance proteins. The pump resistance is caused by membrane transporters that pump out drugs from cells, decreasing the efficacy of the treatment. The main proteins associated with pump resistance in lung cancers are the multidrug resistance associated protein (MRP) family of drug transporters. Lung cancer cells show

the ability to induce the over expression of MRP1 transporters after exposure to chemotherapeutic agents in order to increase their chance of survival. The other main efflux pump found in cancer cell types is the multidrug resistance protein (MDR) which functions in a similar fashion as the MRP family of proteins.[46]The mechanism of non-pump resistance includes the activation of anti-apoptotic cellular defense in the cancer cells. One of the proteins associated with non-pump resistance is the BCL2 protein which becomes over expressed after exposure to chemotherapeutic agents.[1]

2.2.4 Efflux Pumps

The MRP and MDR are two families of closely related efflux pumps that can become over expressed after exposure to xenobiotics. The MRP family is composed of nine members of transporter proteins which are distributed throughout the body and have varying substrates. The MRP1 protein is found in large quantities in lungs, testes, muscles, placenta, and macrophages especially on the basement membrane of bilayers.[47, 48] The MRP1 has many substrates that include glutathione, glucuronate, and sulfate conjugates, anthracyclines, vinca alkaloids, etoposide, camptothecins, and the cysteine leukotriene LTC4. Through these substrates, the MRP transporter can impart significant resistance to the treatment of cancer using the above groups of drugs. MRP1 is also thought to mediate the immune inflammatory response due to the ability to transport LTC4. The MRP1 protein is also able to transport methotrexate and other reduced folates, however, the poly-glutamated forms of methotrexate are not substrates for this transporter.[47]The MDR family of trans-membrane transporters can also recognize a wide variety of therapeutic compounds which are similar to the MRP profile. The MDR family of transporters is located on the lumen side of cells such as those found in renal

proximal tubules, the large and small intestines, hepatocytes, endothelial cells of the brain and testes, and the placenta. The localization of the MDR transporters suggests that these transporters are important in the clearance of foreign drug substances from the body as well as the protection of important tissues such as the brain, testes, and developing fetus from exposure to harmful chemicals.[49] The MDR transporter can effectively transport following group of antineoplastic agents: vinca alkaloids such as vincristine and vinblastine, anthracyclines, etoposide and teniposide, paclitaxel, topotecan, and others.[50] In one study where mdr1 positive cells were exposed to paclitaxel, subsequent exposures to paclitaxel led to decreased susceptibility to paclitaxel treatment. The same cells were also displayed decreased sensitivity to vinblastine, vincristine, doxorubicin, and etoposide.[51] Together, the MDR and MRP family of transporters provide for the development of pump resistance in many different cancer types that extends to a number of therapeutic agents.

2.2.5 Non-Pump Resistance

The BCL2 family of proteins is an important group of proteins that regulate the process of cell survival. This family is broken down into three groups of important proteins which include a pro-survival group of proteins, a pro-apoptotic group of proteins, and a regulatory group of proteins. The anti-apoptotic group of proteins includes BCL-2, BCL-xl-BCL-w, MCL-1, and BCL-b and has important functions in tissue development and function.[52] In one study, BCL-xl deficient mice showed decreased development of nervous tissues as well as the development of hematopoietic cell lines.[53] The MCL-1 protein seems to be important in embryogenesis, especially the implantation of a

fertilized embryo during development.[54] The knockout of the BCL-2 gene leads to mice that have deficiencies in lymphocytes, decreased production of colored fur, and deficiencies in kidney function due to the development of polycystic kidney disease.[55] Mice who are lacking the BCL-w gene sterile as this is an important part of spermatogenesis. [56] The pro-apoptotic proteins are BAX and BAC. These function as regulators of mitochondrial membrane permeability leading to the release a number of different proteins, including cytochrome c, into the cytoplasm activating the apoptosis process. The regulatory elements of the BCl-2 family is composed BH3- proteins which include BAD, BIK, BID, HRK, BIM, BME, NOXA, and PUMA proteins. These proteins work to regulate the anti-apoptotic effects of BCL-2 helping to inhibit its anti-apoptotic effects.[52] This group of proteins plays a key role in the processes mentioned above, as well as others, and deregulation of this system can lead to unwanted effects such as neoplastic transformation.[57]

When it comes to the role of BCL-2 in cancer, it plays a role as an anti-apoptotic signaling protein rather than a pro-survival signal.[57] BCL-2 plays an important role as an oncogene in the transformation to malignant states when it works together with c-myc. C-myc is an oncogene that has both pro-proliferative and apoptotic properties. Over expression of c-myc can promote the progression of the cell cycle, increase the cellular protein load, and alter glucose and iron balance. On the other hand, c-myc can cause DNA damage and activate the p53 apoptotic cascade. When combined with BCL-2 over expression, the apoptotic signals of c-myc are overcome by the BCL-2 signaling allowing the proliferative effects to work unchecked.[58]

To further investigate genes associated with cellular resistance, we explore the gene expression profile of the PIK3/AKT signaling pathway as it has been found to be correlated with resistance of lung cancer cells to tyrosine kinase inhibitors such as gefitinib.[59-62] Understanding the genes that are over expressed in sensitive and resistant cell line can help us understand the mechanisms that drive the development of resistance in cancers and undertake possible methods to overcome such resistance.

	Coarse Emulsions	Nanoemulsions	Microemulsions
Stability	**Kinetic**	**Kinetic**	**Thermodynamic**
Formation	**Low energy agitation**	**High energy agitation**	**Spontaneous**
Droplet Size	**500-50,000 nm**	**50-500 nm**	**10-100 nm**
Types of Emulsions	**W/O, O/W, or multiple emulsions W/O/W**	**O/W or W/O**	**O/W, W/O, or bicontinuous**
Surfactant Concentration	**Low Up to 1%**	**Medium 1-5%**	**High 15-20%**
Cosurfactant	**No**	**Yes**	**Yes**
Appearance	**Cloudy/White**	**Transparent/Opaque**	**Transparent**

Table 2.1 Types of emulsions.

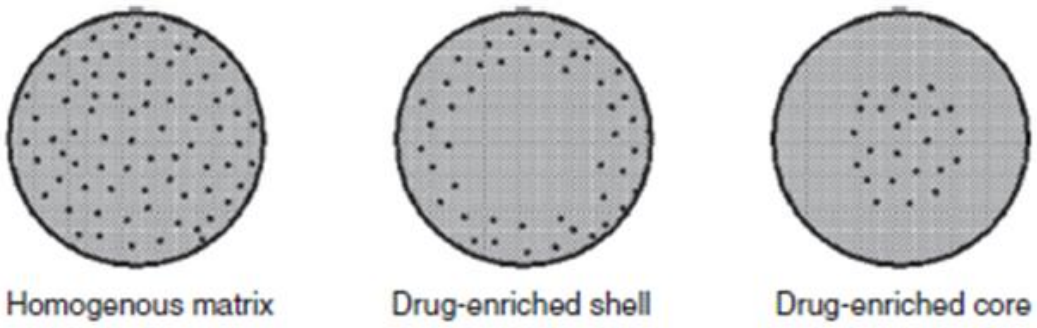

Figure 2.1 Representation of drug loading models. [4]

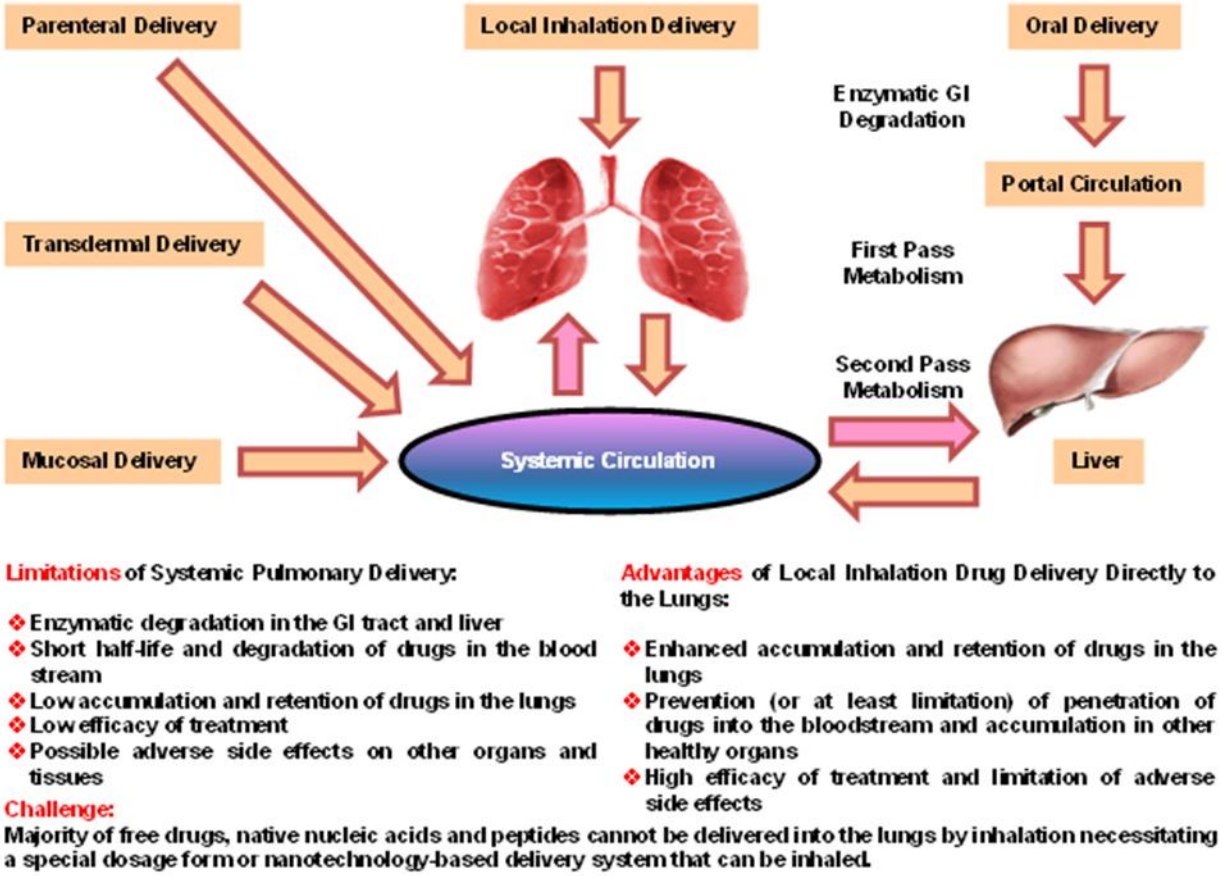

Figure 2.2 Review of the advantages and disadvantages of various routes targeting the lungs for therapeutic purposes. [36]

3. Specific Aims

Specific Aim 1: Development of a cationic lipid dispersion based system for the co-delivery of chemotherapeutic drug and siRNA as inhibitors of cellular resistance for the inhalation treatment of lung cancer.

The effectiveness of chemotherapy is hampered by the toxic side effects experienced at high doses as well as the rapid development of resistance to traditional chemotherapy drugs. To help limit the exposure of healthy organs to toxic chemotherapy drugs, we propose the development of a drug delivery system that can be used for the inhalation delivery of active agents directly to the lungs via nebulization. By targeting the lungs by local delivery, we can increase the amount of drug delivered to the lungs while limiting the amount of drug that reaches other organ tissues. To help target mechanisms of resistance, the addition of siRNA targeting pump and non-pump cellular resistance is proposed. Together, the combination of local delivery and the inclusion of inhibitors of cellular resistance, the treatment of lung cancer can be improved while at the same time limiting the toxic side effects of traditional chemotherapy.

Specific Aim 2: Optimization of the formulation parameters, continuous phase, dispersed phase, and surfactant blends in the preparation of highly stable biocompatible lipid nanodispersions for gefitinib drug delivery.

The preparation of lipid nanodispersions has been reported by many authors. These formulations use a wide variety of lipids and surfactants that are generally considered safe by the FDA. When trying to determine the best lipids and surfactants to use, it is

difficult to use the available literature as most groups use different methods of preparation and develop their systems for very specific applications. One analysis found that there is very little correlation between the size and toxicity of lipid dispersions as it relates to the components used to fabricate those lipid dispersions. To clarify which components are best suited for development of lipid dispersions for delivery to lung tissues, we propose the optimization of the formulation parameters such as the choice of core lipids, surfactant mixtures, and types of surfactants used.

Gefitinib is a small molecule tyrosine kinase inhibitor targeting the epidermal growth factor receptor (EGFR). It is approved for the treatment of patients that have activating mutations in the EGFR gene. It is dosed by mouth once daily until disease progression or the developments of unacceptable toxicity. Considered a form of targeted therapy, gefitinib generally has lower incidence of side effects such as decreases in the levels of various types of blood cells, however, there is an increased incidence of dermatologic side effects such as rash, xeroderma, and others. To help improve the tolerability of this daily treatment, we propose the formulation of gefitinib in optimized nanostructured lipid carriers for inhalation delivery of gefitinib for the treatment of non-small cell lung cancer.

Specific Aim 3: Investigation of the genes in the PI3K/AKT pathway that are differentially expressed in normal cell lines versus cancer cell lines.

The PI3K/AKT pathway has been shown to harbor changes in a number of different types of cancers. Some genes in this pathway have even been shown to contribute to the development of drug resistance. To investigate the role of this pathway in the sensitivity to gefitinib, we compare the gene expression of a small airway epithelial cell line to that

of three non-small cell lung cancer cell lines with varying sensitivity to gefitinib. The identification of the relative levels of gene expression in these cell lines can help direct future studies aimed at improving the sensitivity of cancer cells to chemotherapy treatment.

4. Development of a cationic lipid dispersion based system for the co-delivery of chemotherapeutic drug and siRNA as inhibitors of cellular resistance for the inhalation treatment of lung cancer.

4.1 Introduction

Short interfering RNA (siRNA) is a class of short 20-25 base pair double stranded RNA molecules that can be used for therapeutic purposes. The can be used to control the level of proteins in target cells and tissues by degrading the mRNA molecules that are used to synthesize proteins. These molecules function via the activation of the RNA induced silencing complex (RISC). When siRNA interacts with the RISC proteins, the two strands dissociate from one another leaving one strand associated with the RISC proteins which then can guide the whole complex to a complementary sequence found in mRNA molecules. When the complex binds to its complementary sequence, the RISC proteins chop the mRNA into pieces and the complex can move on to degrade another mRNA molecule. The 20-25 base pair sequence is long enough to provide efficient and specific targeting of sequences in the mRNA molecules that are specific for only one gene. The wide spread use of such a gene silencing machinery is limited by the low plasma stability

of siRNA, due to degradation by plasma esterase, and the low permeability of siRNA across the plasma membrane, due to the high negative charge of the phosphate backbone. Successful introduction of siRNA into cells has been achieved by the use of a wide variety of cationic polymers, dendrimers, lipids, and liposomes. The use of cationic delivery systems allows for the protection of the siRNA from degradation by serum esterases and improves the amount of siRNA that can be internalized by cells. 1,2-dioleoyl-3-trimethylammonium-propane (DOTAP) is one of the lipids that has been extensively studies for its ability to transfect cells with both, plasmid DNA and siRNA molecule. Generally, DOTAP is combined with a few other lipids to form liposomes which are then used to make lipoplexes with the negatively charged siRNA or DNA capable of delivering the genetic material across cell membranes.

Lipid nanoparticles that are based on the formation of cationic lipid nanodispersion have also been described. One of the advantages of the lipid nanodispersions is the ability to deliver nucleic acid material along with small molecule therapeutics in the same delivery system. In our lab, it was previously shown that the co-delivery of small molecule compounds along with gene therapy targeted at cellular resistance mechanisms was more effective than delivering the components independently. Lipid nanoparticles have also been widely described for their ability to deliver a wide range of lipophilic small molecule compounds. The drugs are able to be encapsulated within the lipid core of the nanoparticles which can protect the drug from degradation, allow for controlled release properties, and increase the amount of drug that can be solubilized in the aqueous phase. The majority of lipids used in the formation of lipid nanoparticles are generally regarded as safe and used in other applications for formulation development. Precirol has been

used to previously develop lipid nanoparticles, but it is also widely used for the preparation of oral dosage forms. Squalene is a biocompatible lipid that has been used as a carrier for various formulations of various vaccines.

We propose the use of precirol, squalene, DOTAP, and a combination of other stabilizers for the preparation of cationic paclitaxel loaded lipid nanoparticles for inhalation delivery to the lungs. Paclitaxel is a hydrophobic drug that has very poor water solubility and a good candidate for delivery using lipid nanoparticles. The use of paclitaxel is combined with siRNA targeted towards BCL-2 and MRP-1 to help improve the efficacy of the treatment by targeting both pump and non-pump resistance mechanisms that can be developed by the cancer cells.

4.2 Materials and Methods

4.2.1 Materials

Paclitaxel was purchased from Polymed Therapeutics, Huston Texas. siRNA targeted to BCl2 and MRP1 was obtained from Ambion, Grand Island New York. For Nanostructured Lipid Carrier (NLC) preparation, squalene was purchased from Sigma Life Science, St. Louis, Missouri. Glyceryl palmitostearate (Precirol) was gifted from Gattefossé, Paramus, New Jersey. 1,2-di-(9Z-octadecenoyl)-3-trimethylammonium-propane (chloride salt) (DOTAP), soy L-α-phosphatidylcholine PC), 1,2-distearoyl-sn-glycero-3-phosphoethanolamine-N-(carboxy(polyethylene glycol)-2000) (ammonium salt) (DSPE-PEG-COOH) was purchased from AVANTI polar lipids, Alabaster, Alabama. A synthetic analog of Luteinizing Hormone-Releasing Hormone (LHRH) peptide (Gln–His–Trp–Ser–Tyr–DLys–Leu–Arg–Pro–NH–Et) was synthesized according

to our design[63] by American Peptide Company, Sunnyvale, California. Polysorbate 80, dimethyl sulfoxide (DMSO), and sodium phosphate were purchased from Fischer scientific. Dimethylformamide (DMF), Triethylamine (TEA), and 1-ethyl-3-(3-dimethylaminopropyl) carbodiimide (EDC), dimethyl amino pyridine (DMAP), ethylenediaminetetraacetic acid (EDTA), and 4′,6-Diamidino-2-phenylindole dihydrochloride (DAPI) were purchased from Sigma Aldrich, St. Louis, Missouri. Dichloromethane (DCM) was purchased from Acros Organics, Geel, Belgium. 12-15 kDa molecular weight cut off regenerated cellulose dialysis membrane was ordered from Spectrum Laboratories 18617 Braodwick Street, California.

4.2.2 Cell Culture

A549 lung cancer cells were grown using RPMI-1640 media (Morristown, NJ) mixed with 10% fetal bovine serum (Sigma, St. Louis, MO), 1% penicillin-streptomycin , and 2.5% sodium bicarbonate (Fisher Scientific, Waltham, MA). The cells were grown in an incubator at 37° C and 5% (v/v) carbon dioxide. All experiments using cells were performed while the cells were in the exponential growth phase.

4.2.3 DSPE-PEG-LHRH Synthesis

The targeting moiety used was the LHRH peptide. To incorporate it into the drug delivery system, the peptide was conjugated to the distal ends of DSPE-PEG-COOH via a peptide bond. 15 mg of DSPE-PEG and 10 mg of LHRH peptide were dissolved in 3 ml of dimethylformamide and 5 ml of dichloromethane. Next, 5.3 mg of 1-ethyl-3-(3-dimethylaminopropyl) carbodiimide (EDC) and 8 mg of dimethylaminopyridine were added to the reaction mixture. Finally, 400 µl of triethylamine was added to the mixture. The components were placed under slow speed stirring for 24 hours. After 24 hours,

precipitates formed as a byproduct of the reaction and were separated from the solution by centrifugation at 13,000 RPM. Finally, the sample was purified using a Buchi rotary evaporator to remove the excess DCM.

4.2.4 Nanostructured Lipid Carrier Preparation

NLC were synthesized via a homogenization sonication technique. Synthesis began with the preparation of the lipid and aqueous phases. The lipid phase consisted of 100 mg of precirol, 100 mg of squalene, 5 mg of soy PC, and 10 mg of paclitaxel (TAX) in 1 ml of DMSO. For placebo particles, the same components and procedures were used except paclitaxel was not added to the formulation. The aqueous phase consists of 250 mg of polysorbate 80, 50 mg of DOTAP, and 5.5 mg of DSPE-PEG-LHRH with water added to reach a final volume of 10 ml. The phases are vortexed and placed in an oil bath that is heated at 65-70 °C. After about 10-15 minutes, the two phases were ready for high speed homogenization. During homogenization, the lipid phase was added to the aqueous phase and homogenized on a low-medium speed for 5 minutes. Next, the mixture was homogenized at medium-high speed for an additional 5 minutes. Finally, the mixture was sonicated using pulse sonication for another 5 minutes. After sonication, the solution was kept on ice for 30-60 minutes to make sure the particles solidified before they formed larger aggregates. Small Interfering RNA (siRNA) loading was achieved by mixing a suspension of the NLC with the desired amount of siRNA, vortexing the mixture, then allowing 30-60 minutes for the siRNA to form nanoparticles with NCL via electrostatic interactions. The sequences of siRNA targeted to BCL2 and MRP1 mRNA were: 5'-GUGAAGUCAACAUGCCUGCTT -3' and 5'- GGCUACAUUCAGAUGACACTT -3',

respectively. siRNA was synthesized by Applied Biosystems/Ambion (Austin, TX) according to our design.

4.2.5 Particle Characterization

A dynamic light scattering technique was used to characterize the nanoparticle dispersions using a Malvern ZetaSizer Nanoseries instrument (Malvern Instruments, UK). The size and zeta potential of the nanoparticles was measured at room temperature.

4.2.6 siRNA Complexation

siRNA complexation studies were performed. 1 µM siRNA was added to 10 µg, 20 µg, 30 µg, 40 µg, 50 µg, and 80 µg of cationic NLC. The particles and siRNA were vortexed and allowed to stand at room temperature for 30-60 minutes to allow siRNA to complex to the NLC. Next, the amount of free siRNA was visualized by running a gel with one well representing 1 µM free siRNA and the rest of the wells representing the complexes above. After the gel was loaded, and it finished running, the image of the gel was obtained using a Gel Logic 440 Imaging System (Kodak).

4.2.7 Cellular Drug Internalization

NLC loaded with doxorubicin, which has an inherent red fluorescence, and FAM labeled siRNA, which has a green fluorescence, were prepared as described above. A549 lung cancer cells were plated in 6 well plates and treated with the NLC loaded with doxorubicin and FAM labeled siRNA for three hours. Before visualization, the nuclei were stained with DAPI. The cells were then visualized using a fluorescence microscope from Olympus America Inc., Melville, NY.

4.2.8 Cytotoxicity Assay

Cytotoxicity of the cationic NLC loaded with both paclitaxel and siRNA, NLC loaded with paclitaxel, and free paclitaxel was assessed using a modified 3-(4,5-Dimethylthiazol-2-yl)-2,5-diphenyltetrazolium bromide (MTT) assay. The A549 cells were seeded on a 96 well plate at 10,000 cells per well with 100 µl of growth media in each well and placed in the incubator for 24 hours. After the 24 hours, the media was removed and the cells were treated with varying concentrations of either free non-bound paclitaxel or the variants of the drug delivery system. The concentrations of tested substances were prepared using a serial dilution (1:2) to make 12 different working concentrations. The control cells received fresh media. The 96 well plates were then placed in the incubator for 24 hours; the media was suctioned out of every well and replaced with 100 µl of fresh media. To each well, 20 µl of 5 mg/mL MTT solution in Dulbecco's Phosphate Buffered Saline (DPBS) was added. Following MTT addition, the plates were placed back into the incubator for 3 hours. 90 µl of detergent solution was then added to each well to dissolve any formazan crystals that had formed. The plates were then placed in the incubator overnight. The detergent solution was made by mixing 10.5 g sodium dodecyl sulfate, 25 ml of dimethylformamide, and 25 ml of de-ionized water and adjusting the pH to 4.7 using acetic acid. The absorbance of the samples was then measured using a plate reader with the wavelengths set at 570 and 630. The absorbance readings were used to calculate the cell viability by comparing the treatment measurements to control measurements.

4.2.9 Gene Expression

The following formulations were evaluated for their influence on the BCl2 and MRP1 mRNA expression: control (untreated cells); NLC loaded with TAX; NLC loaded with siRNA (no TAX); NLC loaded with TAX and siRNA; and a 75% lower concentration of NLC loaded with TAX and siRNA. A549 cells were seeded into a twenty five square centimeter flask and placed into the incubator for 24 hours at 37 ºC. The next day, the media was changed; the formulations were added; and the cells were placed back into the incubator for another 24 hours. The cells were then collected and total RNA was extracted using QIAshredder micro spin homogenizer (Qiagen, Valencia, CA) and RNeasy KIT (Quiagen, Valencia, CA). After extraction, the RNA concentrations for each sample were measured and used in subsequent calculations. For each treatment group, 3 samples of 4 µg of RNA and 3 µl of random primers were prepared for cDNA conversion. RNA was converted into cDNA by following manufacturer's procedures provided with the Ready-To-Go™ You-Prime First-Strand Beads (GE Healthcare, Piscataway, NJ). After the conversion, a Polymerase Chain Reaction (PCR) was used to amplify the genes of interest for analysis using gel electrophoresis. To set up the PCR reaction, each sample was evaluated for the expression of 3 genes, BCL2, MRP1, and β2-microglobulin (β2-m) which was used as an internal standard. To make the PCR reaction mixture, the 33 µl of cDNA, 2 µl of polymerase, and 6 µl of primers for the desired gene (3 µl of the forward primer and 3 βl of the reverse primer) for a total volume of 100 µl. The following pairs of primers were used (5' to 3'): MRP1 - ATG TCA CGT GGA ATA CCA GC (sense), GAA GAC TGA ACT CCC TTC CT (antisense); BCL2 - GGA TTG TGG CCT TCT TTG AG (sense), CCA AAC TGA GCA GAG TCT TC (antisense); β2-

m - ACC CCC ACT GAA AAA GAT GA (sense), ATC TTC AAA CCT CCA TGA TG (antisense). The samples were then placed into a PCR machine. After the PCR reaction was complete, the samples were stored at 4 °C until gel electrophoresis was carried out. Gel electrophoresis was performed using the Reliant ® Gel system (Lonza, Rockland, ME) using 4% NuSieve ® 3:1 Plus agarose using Tris/Borate/EDTA buffer supplemented with Ethidium Bromide. To prepare each sample for loading onto the gel, 15 µl of sample and 3 µl of loading dye (Glycerol & bromophenol blue) were mixed then loaded into the wells on the gel. The gels were then visualized using the Gel Logic 440 Imaging System (Kodak).

4.2.10 Lung Cancer Model Development

Nude mice were ordered from Taconic Farms, Inc.(Cranbury, NJ). A549 non-small cell lung cancer cells transfected with luciferase were grown, collected, and injected into the lungs of the mice at about 5.0x10^6 cells per injection. The tumors were allowed to develop over time and were periodically imaged using IVIS optical imaging by injecting mice with luciferin before visualizing the tumor. The mice were anesthetized with isoflurane during the imaging procedures. The tumors were also visualized using MRI (Aspect imaging , Shoham, Israel) and CT (Carestream molecular imaging, Woodbridge, CT) imaging systems.

4.2.11 Body Distribution of NLC

Cy5.5 labeled NLC were administered to mice either by inhalation or i.v. injection. The mice were anesthetized with isoflurane and images were taken using an IVIS imaging system. After the mice were sacrificed, the lungs were extracted and kept frozen until the tissues were visualized using a fluorescent microscope.

4.2.12 Treatment of Mice with Tumors

Nude mice were induced with lung tumors by intra-tracheal injection of luciferase transfected A549 lung cancer cells and tumors were imaged as described above. Once the tumors were large enough, the mice were treated with controls and the NLC delivery system using nose only exposure chambers for inhalation. The mice were treated on days 0, 3, 7, 11, 14, 17, 21, and 24. The treatment groups were as follows: untreated mice, mice treated with i.v. injection of paclitaxel, inhalation of LHRH-NLC, inhalation of LHRH-NLC-Taxol, and inhalation of LHRH-NLC-Taxol-siRNA targeted to MRP1 and BCL2. The paclitaxel dose in all treatments was 2.5 mg/ kg. The dose of siRNA in each treatment was 170 µg/kg. The change in tumor volume was used to track the effectiveness of the treatment.

4.2.13 Statistical Analysis

Data obtained were analyzed using descriptive statistics, single factor analysis of variance (ANOVA) and presented as a mean value ± standard deviation (SD) from five independent measurements. We analyzed data sets for significance with Student's t test and considered P values of less than 0.05 as statistically significant.

4.3 Results

4.3.1 Particle Size and Zeta Potential

The particle size was measured for both the cationic and non-cationic NLC. The average number size for the cationic NLC was 111.3 ± 20 nm with a polydispersity index of 0.4. These are depicted in figure 4.1. The zeta potential was measured to be 60.3 mV with a reduction of the zeta potential to 45.5 mV after complexation with siRNA.

4.3.2 siRNA Complexation

To show that siRNA attached to the delivery system, a gel retardation assay was performed with the results shown in Figure 4.2. In figure 4.2, 1 µM of siRNA is incubated with increasing amounts of the NLC preparation. As the siRNA complexes with the particles, it is no longer able to travel down the gel and the bands seen on the gel become smaller until they disappear. After a ratio of 40 µg NLC to 1 µM siRNA concentration there is no more band seen on the gel showing that all the siRNA that was introduced into the mixture was complexed to the particles.

4.3.3 Cellular Drug Internalization

To show that drug was internalized into the cell, Doxorubicin and fluorescently labeled siRNA were loaded onto the particles. Cells treated and fluorescent microscopy was used to obtain the images in Figure 4.3. Figure 4.3A shows the cell under the microscope using light. Figure 4.3B shows the nucleus stained with DAPI. Figure 3C shows the fluorescence of Doxorubicin which is colored red. Here, it can be seen that the Doxorubicin fluorescence is seen throughout the cell, this includes the cytoplasm and the nucleus of the cell. Figure 4.3D shows the fluorescence of the labeled siRNA. In the image, it can be seen that the siRNA is localized in the cytoplasm where it exerts its gene silencing effects.

4.3.4 Cellular Viability

The delivery system was evaluated for its ability to treat lung cancer cells in vitro. Figure 4.4 shows the results of cell viability (MTT Assay) studies using free paclitaxel and 2 different formulations, NLC with paclitaxel only and NLC with paclitaxel and siRNA targeted to BCL2 and MRP1. The black line shows the results of cell viability of cells

treated with free paclitaxel with a resulting IC:50 value (concentration of drug that kill 50% of cells) at 98 µg/ml. When the paclitaxel is encapsulated into the nanocarrier, the cytotoxicity of the drug was enhanced, the IC:50 dose decreased down to 13 µg/ml. When siRNA is introduced into the delivery system, there is a further lowering of the IC:50 concentration of paclitaxel to 0.8 µg/ml. The results are shown in figure 4B.

4.3.5 Silencing of BCL-2 and MRP-1 Genes

The delivery system was evaluated for its ability to effectively deliver the siRNA to the cells and decrease the expression of the target genes, BCL2 and MRP1. Figure 4.5 shows the results of untreated cells, cells treated with NLC loaded with paclitaxel, and NLC loaded with paclitaxel and siRNA targeted to BCL2 and MRP1. The expression of B2M is used as an internal standard to show that the same amounts of RNA were taken from each sample. The results show that the bands of B2M are the same throughout the samples meaning that any differences seen in other genes can be considered significant. When looking at the expression of the MRP1 gene, the untreated group is set as the baseline of 100% expression. When the cells are treated with NLC loaded with paclitaxel, there is a slight bump in the expression of the MRP1 gene. However, when the siRNA is added to the delivery system, there is a marked decrease in the expression of the MRP1 gene. Similar results can be seen with the BCL2 gene. When the cells are treated with NLC loaded with paclitaxel, there is a slight increase in the expression of the BCl2 gene in the cells. However, when the cells are treated with NLC loaded with paclitaxel and siRNA, there is an almost complete down regulation of the BCL2 gene expression.

4.3.6 Confirmation of Lung Cancer Model

The confirmation image of the development of lung cancer in the mice was obtained using optical, MRI, and CT imaging modalities as seen in figure 4.6. Images show the clear development of tumor in the mice as compared to control mice. The tumors are well defined and can be easily identified on the images as distinct from the healthy lung tissues.

4.3.7 In Vivo Distribution of Cationic NLC

The in vivo distribution of cy 5.5 labeled inhaled targeted and non-targeted NLC as well as IV injection of non-targeted was evaluated using IVIS imaging systems and fluorescence microscopy. IVIS images showed that the inhaled NLC had greater distribution into the lungs as compared to the IV injection of the NLC as seen in figure 4.7A. When looking at the inhaled targeted and non-targeted NLC, the NLC targeted with LHRH peptide had a greater accumulation in tumor tissues as compared to the rest of the healthy lung tissue. This was further confirmed by using fluorescence microscopy Figure 4.7B. Overall, the targeted inhaled NLC were able to selectively target tumor tissues as compared to healthy lung lungs.

4.3.8 In Vivo anti-tumor activity of Cationic NLC

The anti-tumor activity of four treatments and one control were evaluated by observing mice over 24 days and recording the tumor volume as a marker of activity. When looking at the mice treated with the NLC without drug and siRNA, the tumor did not show any change in volume and increased at a similar rate as the untreated mice (figure 4.8).

Looking at the mice treated with IV paclitaxel, the tumor kept growing with time, but at a slower rate than the untreated mice (figure 8). The mice treated with the paclitaxel loaded NLC showed that the tumor growth could be controlled and led to a decrease in the size of the tumor in the mice (figure 4.8). When the mice were treated with NLC loaded with paclitaxel and siRNA, the tumor growth was controlled and there was a further decrease in the tumor size as compared to with the NLC loaded with only paclitaxel. This indicates that the addition of siRNA targeted to MRP1 and BCL2 plays a role in increasing the effectiveness of the proposed delivery system.

4.4 Discussion

The first step in attempting to deliver siRNA to the inside of the cell involves the ability of the delivery system to successfully be loaded with siRNA. The difficulties in effectively detecting loaded siRNA lie in the ability to distinguish the loaded siRNA from any free siRNA in the system. To help get around the problem, the gel retardation assay was performed with the assumption that any siRNA that is seen on the gel has not been attached to the particles. If there is a trend of seeing smaller and smaller bands on the gel, it is because the siRNA is attached to the particles which cannot easily travel down the gel with any free siRNA. Observing the gel closely, there appears to be only one band on the gel after visualization raising the question of why is there not a second band depicting the distance traveled by the particles and the siRNA complexed with the particles. This can be explained by the method of attachment and its effects of the nucleotide ethidium bromide interaction. The method of attachment of the siRNA was a static interaction between the surface of the particles and the siRNA. Here, the siRNA is tightly bound to the surface of the particles. When free nucleic acids are exposed to ethidium bromide, it

inserts itself into nucleic acids causing an increase in florescence. When a nucleic acid binds to the surface of the particles, the ethidium bromide is displaced from the nucleic acid decreasing its florescence. The displacement of the ethidium bromide from the bound siRNA could explain why there is not a second band seen on the gel that would in represent the distance the particles and siRNA have traveled together on the gel.

The drug internalization studies are important to show that the payload carried by the particles is able to be delivered to the inside of the cell. As the results show, the NLC were able to effectively deliver the doxorubicin and the siRNA to the inside of the cell. The NLC are able to deliver the siRNA to its site of action. Looking at the results, the siRNA is distributed throughout the cytoplasm of the cell while very little of the siRNA marking is seen in the nucleus. This is important as the siRNA functions to decrease the expression of proteins by destroying mRNA that has made its way into the cytoplasm. The distribution of siRNA is seen to be throughout the cell, however, it is difficult to quantify exact amount of siRNA in the cytoplasmic compartment itself and how much is in contained within vesicles. Based on these in vitro results, one can project that the system will be able to deliver the siRNA to the tissues in an in vivo setting. It has been reported that by using cationic liposomes, siRNA can effectively be delivered to many areas inside the liver after systemic administration of the liposome siRNA complexes[64]. If the siRNA does not get into the cytoplasm, it is not able to silence its targeted mRNA. One way to confirm the siRNA is escaping to the cytoplasm is to perform gene suppression studies to verify the mRNA of the target genes is being reduced.

The silencing of MRP1 and BCL2 genes was important for verifying that the siRNA was successfully delivered inside the cells as well as improving the efficacy of the proposed treatment. The fact that the system was able to effectively silence these genes confirms that the siRNA was able to effectively escape the delivery system to interact with the RISC proteins to lead to target mRNA degradation. It is interesting to note that the extent of mRNA silencing was different for MRP1 and BCL2. This can be due to the localization of the mRNA during the translation process. Others have also used NLC like carrier systems and effectively achieved mRNA knockdown of target genes. The major difference in the siRNA delivery method is that the siRNA was loaded into the NLC and a sustained siRNA release profile was attained[65]. The silencing of the target genes is also one reason that can be attributed to the increased effectiveness of the treatment when siRNA is introduced into the system. This supports the original hypothesis that the treatment could be improved by the addition of mechanisms to overcome cellular resistance. It should be noted, however, that the targeted genes are two of a number of possible resistance pathways that can develop with in cancer cells.[33, 66] The other mechanisms of cellular resistance can be related to the mechanisms of action of the drug. There could be an over expression of repair enzymes, increase in the production of the target enzyme, or changes in the target of the drug which alters its activity at its site of action. Because cancer is a complex disease with many mutations occurring within cells, the cells with the most beneficial mutations will survive and continue to grow without regulation.

The cellular viability of A549 cancer cells was evaluated using the two formulations previously discussed. The cationic paclitaxel loaded NLC produced an

increased effectiveness of the treatment as compared to paclitaxel treatment alone. This effect was further increased by the addition of siRNA targeted to MRP1 and BCL2 as suppressors of cellular resistance. The delivery system was able to effectively deliver the siRNA to the cells leading to silencing of the mRNA of the target genes. These findings are consistent with others who have incorporated anticancer drugs into lipid nanoparticles. Subedi et al showed that by incorporating doxorubicin into solid lipid nanoparticles, the efficacy of the drug was improved when compared to equivalent doses of the free drug.[67] Liu et al showed similar results when evaluating docetaxel loaded NLC. They compared a commercially available docetaxel formulation and docetaxel loaded NLC. The findings show similar results of decreased IC:50 values as compared to the free drug formulations. [68]

The in vivo distribution studies show that the NLC can be targeted to the tumor site through the use of a targeting peptide and the use of local delivery methods. The injection of non-targeted NLC had a distribution that is not ideal for the treatment of lung cancer. These particles were distributed largely into the liver with some distribution into the kidneys and spleen. The distribution of non-targeted lipid particles is similar to that of siRNA loaded liposomes reported by Shi et.al. When liposomes loaded with cy5 labeled siRNA were injected into the mice, it was found that cy5 labeled siRNA was observed in the liver, spleen, and the kidneys but not in the other organs of the body. These results were also confirmed using stem-loop qPCR to detect the siRNA levels in the various tissues. Their results showed that the liposomes distributed mostly to the liver as that was the area where the most siRNA was localized[64]. When the NLC solutions were subject to local delivery using a nebulizer, there was an increase in the accumulation of NLC in

the lungs. With the increased accumulation in the lungs, both the targeted and non-targeted inhalation treatments showed a decreased exposure to the rest of the organs in the body. The increased targeting to the lungs with local delivery meets one of the goals of nanoparticle delivery set out at the beginning of the experiment. When the NLC was targeted to the tumor using the LHRH peptide, there was a greater distribution of the NLC to the tumor tissue as compared to the healthy lung tissue. With local delivery and the use of a targeting peptide, the NLC can be targeted effectively to the tumor tissue in the lungs and help decrease the unwanted effects of chemotherapy in the other organs of the body and help increase the anti-tumor effect of the treatment.

The cationic NLC were evaluated for the ability to inhibit tumor growth in a mouse model of lung cancer. The results showed that paclitaxel loaded NLC were able to effectively inhibit tumor growth in vivo while showing no antitumor activity when treated with the delivery system alone. The anti-tumor activity of the paclitaxel loaded NLC was further increased when siRNA targeted to BCL2 and MRP1 was added to the formulation. These two siRNA's are able to help overcome cellular resistance and increase the effectiveness of the treatment. Again as observed with the in vitro studies, the NLC loaded with paclitaxel alone was more effective than the paclitaxel alone. In a recent study, Gao et al reported the results of docetaxel loaded NLC. When looking at the results, they showed that docetaxel loaded NLC and folate targeted NLC were two and four times more effective at reducing the tumor volume, respectively. This support the observations seen in our experiments that by encapsulating the drug in a nanocarrier and targeting the drug using a specific peptide can lead to improved efficacy of treatment.[69]

4.5 Conclusion

In conclusion, the NLC systems developed can effectively target and deliver their payload to the tumor tissue. The internalization of the drug inside a carrier helps improve the efficacy of the treatment as seen in these experiments and those reported by others. With the improved localization at tumor tissues, this system can help improve the effectiveness of current treatments by limiting the toxicity of the treatments as well as well as helping to overcome cellular resistance that develops after repeat exposures to chemotherapeutics.

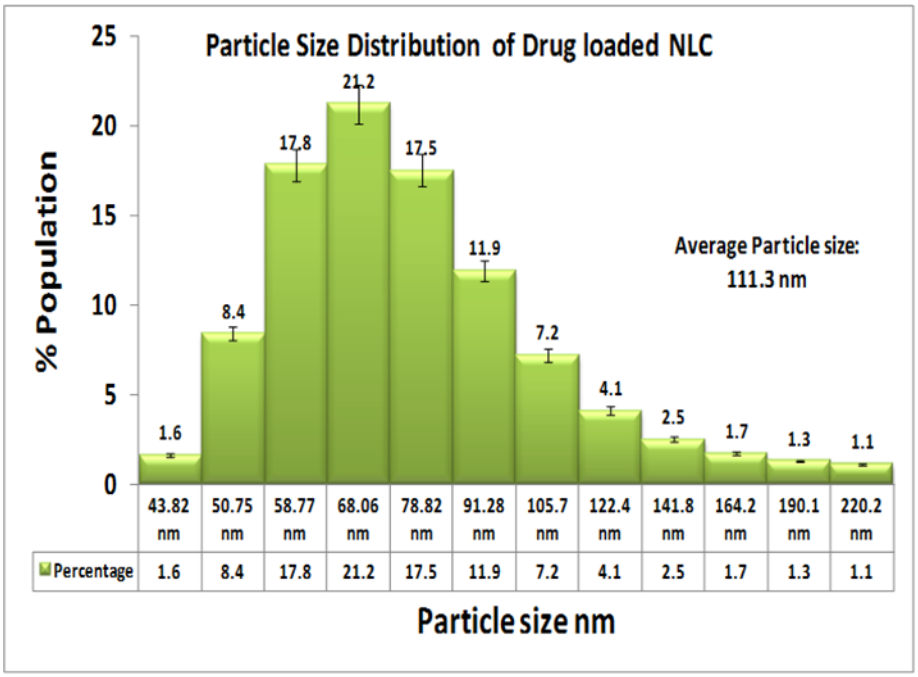

Figure 4.1. Cationic NLC particle size distribution.

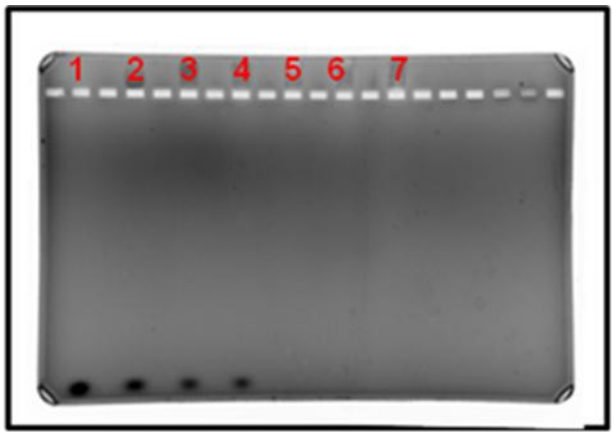

1. 1 µM siRNA
2. 1 µM siRNA incubated with 10 µg of NLC
3. 1 µM siRNA incubated with 20 µg of NLC
4. 1 µM siRNA incubated with 30 µg of NLC
5. 1 µM siRNA incubated with 40 µg of NLC
6. 1 µM siRNA incubated with 50 µg of NLC
7. 1 µM siRNA incubated with 80 µg of NLC

Figure 4.2. Complexation of siRNA with increasing amounts of NLC.

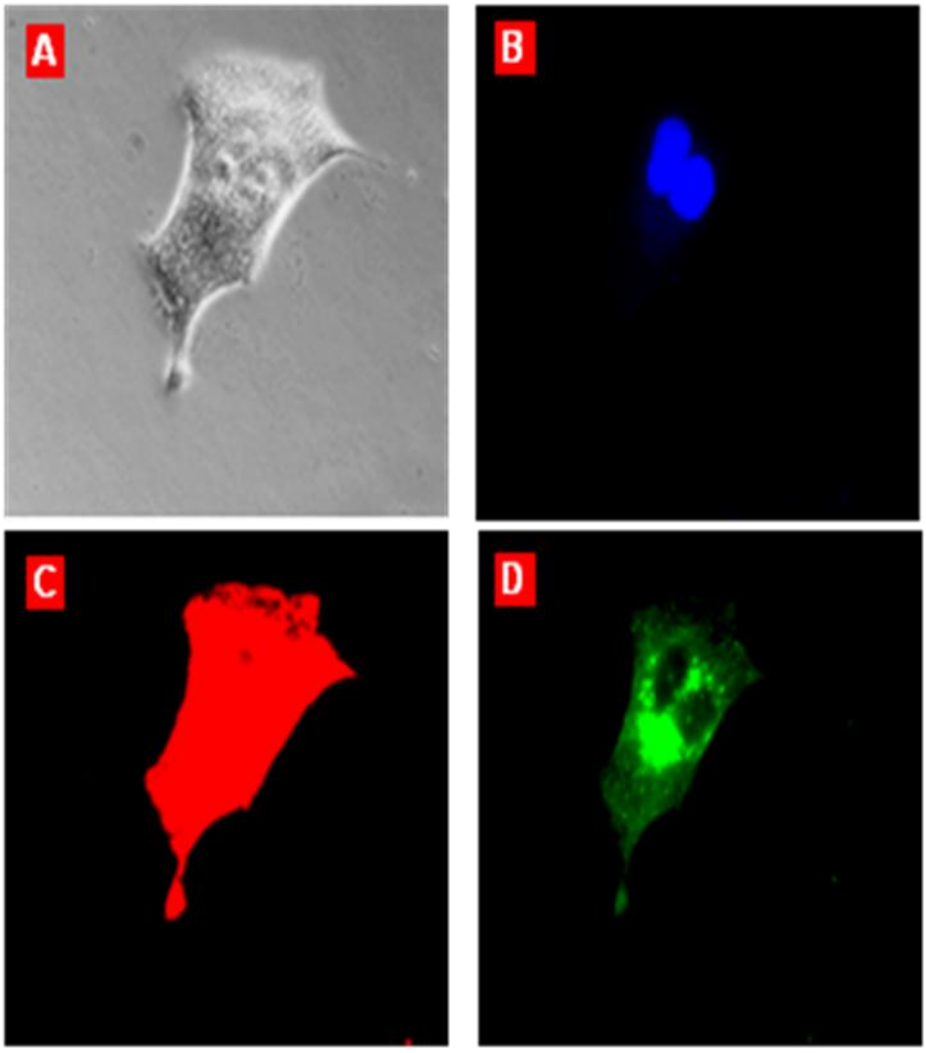

Figure 4.3. Cellular Internalization of drug and siRNA delivered by Nanostructure Lipid Carrier: A – light image; B – Nuclei stained with fluorescent dye DAPI; C – Doxorubicin (intrinsic fluorescence); D - siRNA labeled by fluorescent dye FITC.

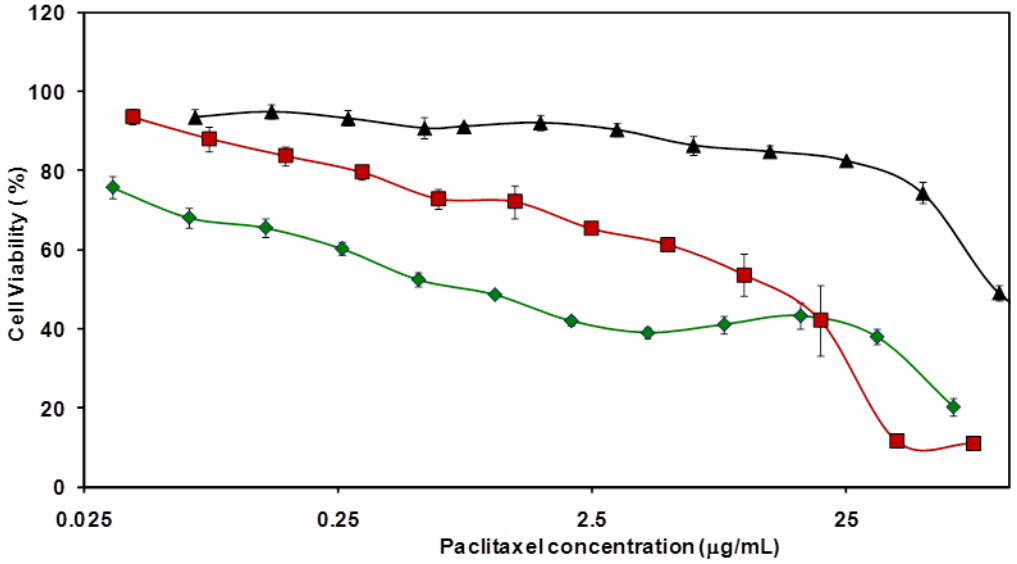

▲ Paclitaxel ■ NLC-PTX-PEG-LHRH ◆ NLC-PTX-siRNA *-PEG-LHRH

*-Targeted to MRP1 and BCL2

Paclitaxel	NLC-PTX-PEG-LHRH	NLC-PTX-siRNA *-PEG-LHRH
IC_{50} = 98 µg/mL	IC_{50} = 13 µg/mL	IC_{50} = 0.8 µg/mL

Figure 4.4. Cytotoxicity of the drug loaded formulation and IC 50 values of the various treatments.

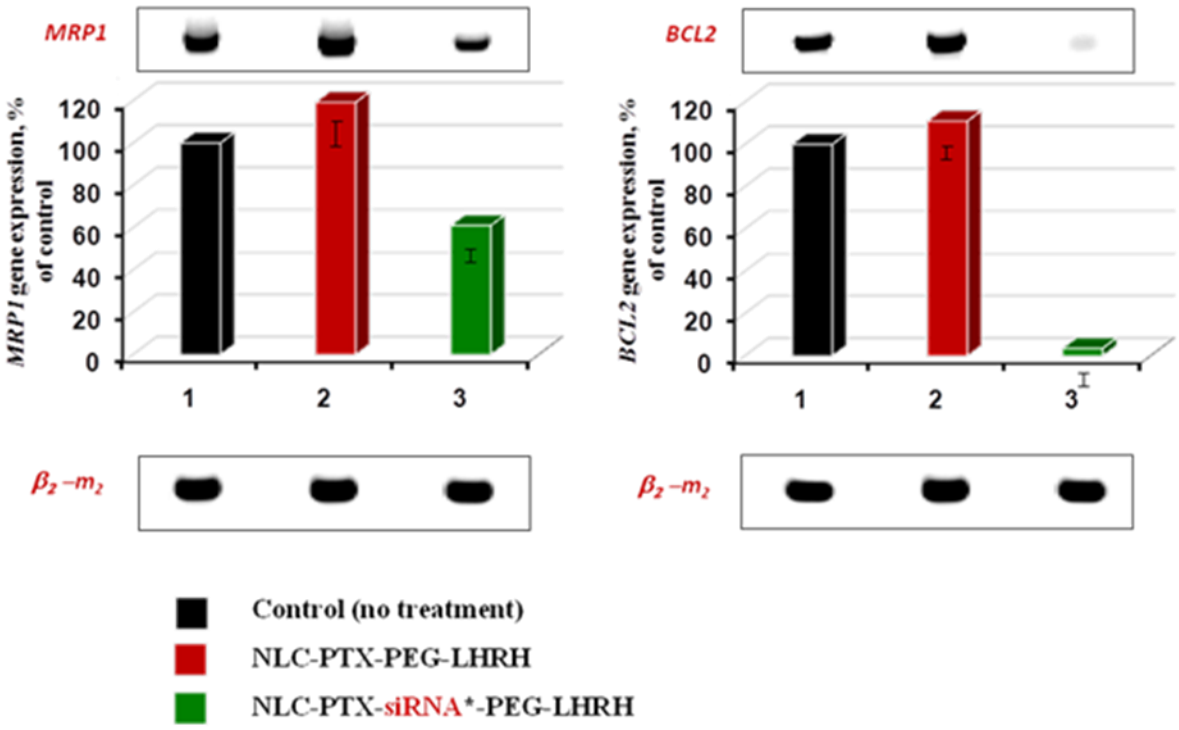

Figure 4.5. Gene suppression of target genes MRP-1 and BCL-2.

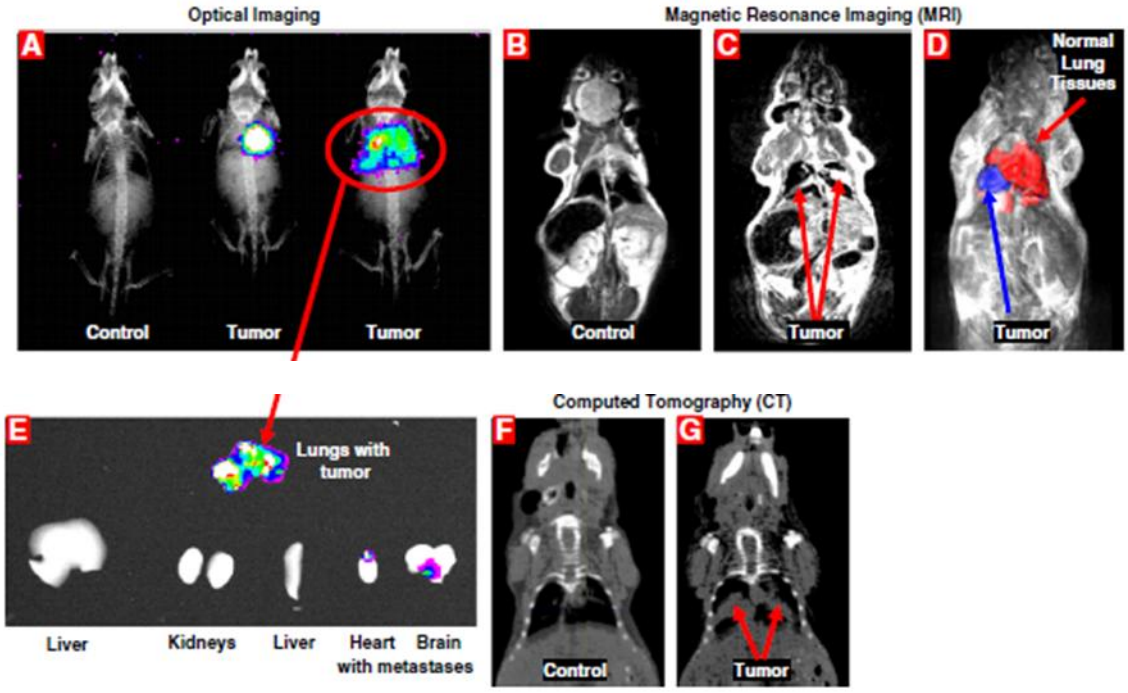

Figure 4.6. Orthotopic lung cancer model as seen by various imagine techniques. (A) Bioluminescence optical imaging of control mouse and mice with lung tumors of different size. (B–D) Magnetic resonance imaging of control mouse (B) and mice with lung tumors of different size (C, D). Lung tumor (blue) and healthy lung tissues (red) are shown (D). (E) Optical imaging of excised organs. (F–G) Computed tomography images of control mouse (F) and mouse with lung tumors (G).

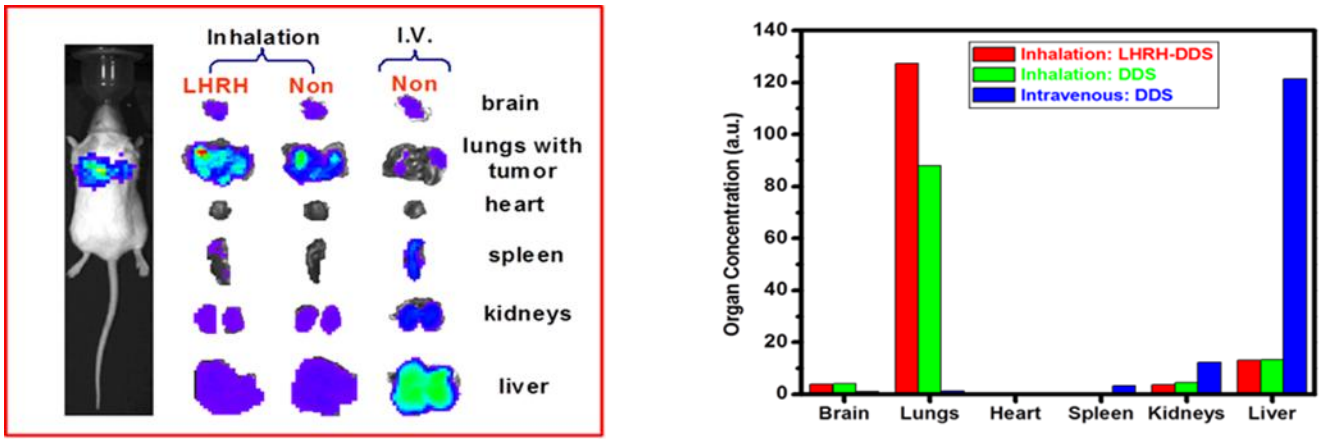

Figure 4.7A. Organ distribution of NLC as administered via inhalation or intravenous administration.

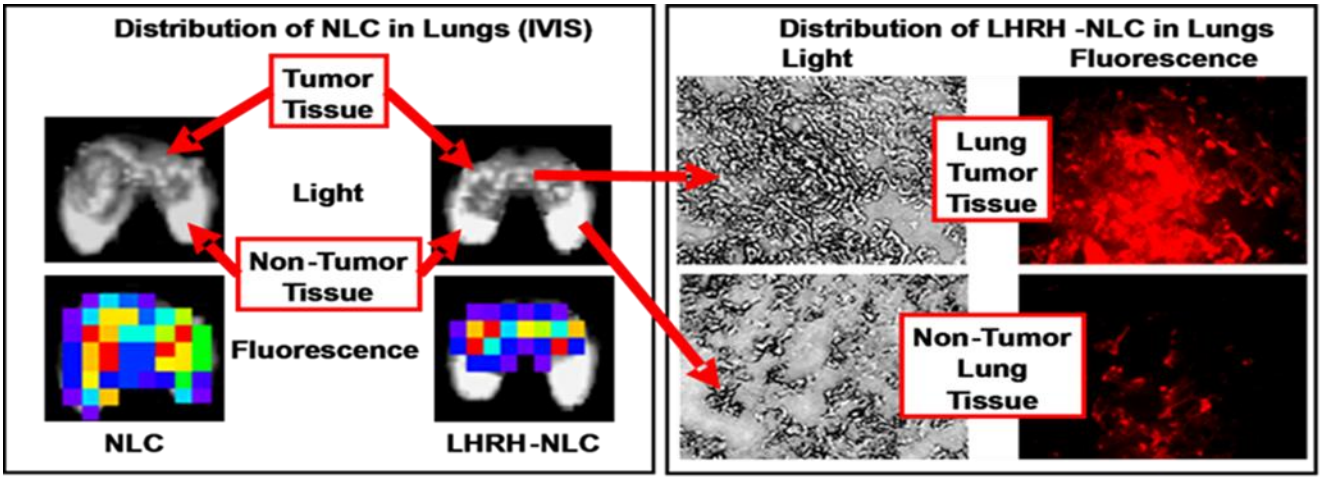

Figure 4.7B. Distribution of drug delivery system as seen at the tissue level using IVIS and florescence microscopy imaging.

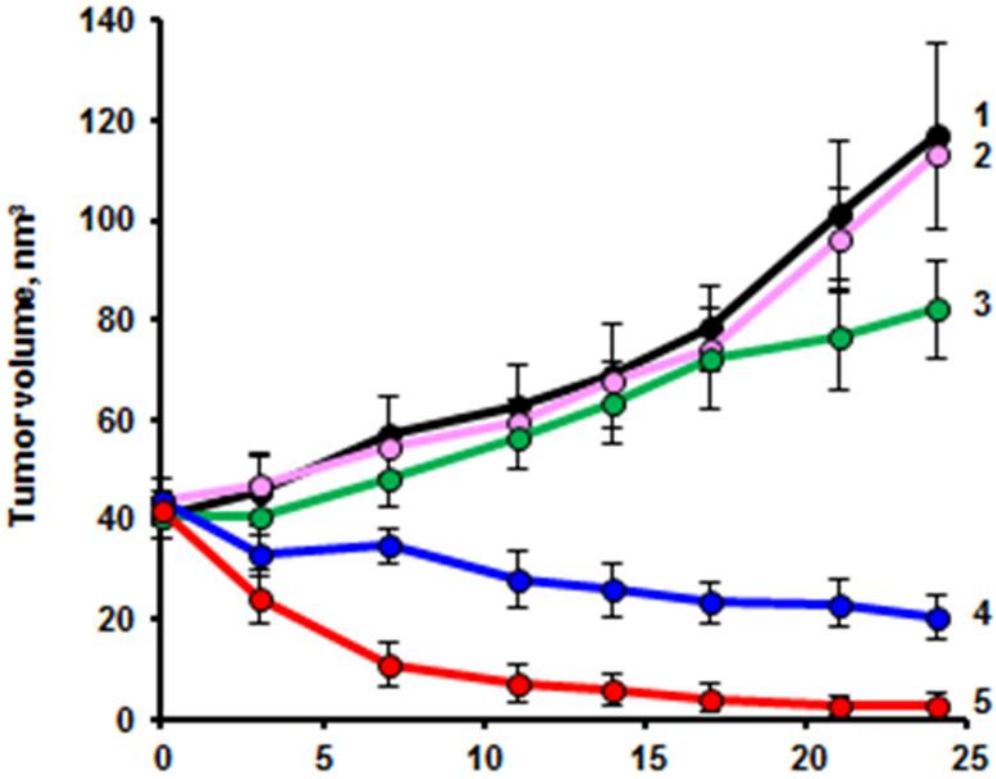

Figure 4.8. In vivo treatment efficacy. Lung tumor volume change over time after various treatments. 1.) Untreated mice. 2.) Inhaled LHRH-NLC. 3.) TAXOL (I.V.). 4.) Inhaled – LHRH-NLC-TAX. 5.) Inhaled – LHRH-NLC-TAX-siRNA targeted to MRP1 and BCL2. The mice were treated on days 0, 3, 7, 11, 14, 17, 21, and 24.

5. Specific Aim 2: Optimization of the formulation parameters, continuous phase, dispersed phase, and surfactant blends in the preparation of highly stable biocompatible lipid nanodispersions for drug delivery.

5.1 Introduction

The formulation of lipid dispersions has been widely studied by many investigators. In the case of lipid dispersions, the hydrophobic lipid is the dispersed phase, or portion of the mixture that is broken up into individual droplets that are suspended in a second phase. The continuous phase is the aqueous medium that surrounds the lipid droplets. Generally speaking, the dispersed phase will be portion of the formulation that is present in a lower percentage of the total mixture as it possible to prepare water in oil as well as oil in water dispersions. Each describes the use of unique combinations of core lipids, surfactants, co-surfactants, loaded drugs, formulation methods, and charge on the surface of the particles. When looking at the biocompatibility of such formulations, it is often difficult to make direct interpretations as to the effects each component of the formulation could have on the size, biocompatibility, and long term stability of the formulation. This can be attributed to the fact that each laboratory uses different methods and conditions for the formulation of their nanodispersions. When looking at the core lipid components of the formulation, it is difficult to definitively attribute a difference in the size of the particles to any particular lipid as the type, amount, and combination of surfactants will greatly affect the final characteristics of the formulation. The core lipids may also respond differently to various types of surfactants as some may be more compatible for effective stabilization with one type of surfactant versus another.[70]

The types of surfactants also greatly affect the characteristics of the final lipid dispersion. The general structure of a surfactant molecule consists of a hydrophobic portion and a hydrophilic portion allowing these molecules to position themselves at the interface that occurs when hydrophobic and hydrophilic substances come into contact with one another. The surfactants can differ in terms of the size and characteristics of the hydrophobic and hydrophilic portions. If the surfactant has a large lipophilic segment relative to the hydrophilic portion, it will be more soluble in the lipid phase. Surfactants with large hydrophilic portions relative to the hydrophobic segment will be more soluble in the aqueous portion. In theory, the most efficient surfactants at stabilizing a lipid dispersion will be localized at the interface without partitioning too heavily into either phase. The size and nature of the hydrophobic and hydrophilic segments of the surfactants can determine whether they are best suited for the preparation of oil in water or water in oil type dispersions. The size of the surfactant also affects the rate at which it can adsorb onto the interphase of the two phases and can have implications on the size of the dispersions that can be achieved with a particular surfactant. In an aqueous environment, surfactants can exist as free monomers in the solution, but above a certain concentration they assemble into micellar structures. These properties of the surfactants change based on the characteristics of their hydrophobic and hydrophilic segments. Surfactants can be classified into ionic and non-ionic surfactants and both classes of surfactants. As seen with the use of phase inversion methods for the preparation of lipid dispersions, surfactants can behave differently when exposed to different temperatures and buffer conditions. Notably, non-ionic polyethylene glycol surfactants show a propensity for increased lipid affinity when heated to high temperatures. Ionic surfactants

have been shown to undergo phase inversion if they are exposed to high strength ionic solutions. [9, 25, 71, 72]

Doktorovova et al. performed a systematic review of the nanotoxicology of various SLN and NLC formulations and were not able to find many clear patterns relating to which characteristics of the lipid dispersions lead to the more biocompatible formulations. They found no correlation in the toxicity on the particles as it relates to the particle size or the types of surfactants used for the formation of the lipid dispersions . They also found that the same lipid core material can have a measured IC:50 of 0.247 mg/mL or an IC:50 greater than 1 mg/mL. These differences can be attributed to the fact that various labs use different cell lines, surfactants, and production procedures which may affect the outcome of their viability studies. [70] The same pattern can be seen with the various types of surfactants used for the preparation of these lipid dispersions as the same surfactant can be found in formulations with low IC:50 and those with a high IC:50. [70]

We propose the investigation into the effects that various parameters and formulation components have on the size, zeta potential, toxicity, and stability of the lipid nanoparticle formulations. Here, we will be using the same preparation procedures and evaluate the formulations in the same cell lines and methods. The evaluation can help us determine the optimal formulation parameters and composition of the formulation that will lead to the formation of more stable and biocompatible particles. We report the effects of a number of liquid lipids such as glycerol trioctanoate and oleic acid have on the characteristic of the fabricated nanodispersions. We further report the effects various formulation buffers have on the characteristics of the lipid dispersions. Lastly, we report the effects solid lipids such as precirol ®, compritol ®, trilaurin, and others have on the

size and toxicity of the lipid nanodispersions. This data taken together can help determine the optimal components to use in the preparation of nanoparticles for inhalation delivery of actives to the lungs.

5.2 Materials and Methods

5.2.1 Materials

A lab scale probe sonicator and probe thermometer were obtained from Fisher Scientific, Hampton, NH. Glycerol trioctanoate, ethanol, glycerol, N-[Tris(hydroxymethyl)methyl]-2-aminoethanesulfonic acid (TES), sodium chloride, stearic acid, palmitic acid, myristic acid, erucic acid, eladic acid, 3-(4,5-Dimethylthiazol-2-yl)-2,5-Diphenyltetrazolium Bromide (MTT yellow), squalene, fetal bovine serum, Span 60, tween 60, and sodium dodecyl sulfate were obtained from Sigma Aldrich, St. Louis, Missouri. Gelucire 43/01, precirol, compritol, geleol mono and diglycerides were generously donated by Gattefossé, Paramus, New Jersey. DSPC, cholesterol, DSPE-PEG-2K-COOH and DC-cholesterol were ordered from AVANTI polar lipids, Alabaster, Alabama. Trilaurin, trimyristin, and triglycerol monostearate were ordered from Fisher Scientific, Hampton, NH. DSPE-PEG-2K-methoxy and DSPE-PEG-5K-methoxy were ordered from NOF America Corporation, White Plains, NY.

5.2.2 Cell culture

A549 lung cancer cells were grown using RPMI-1640 media (Morristown, NJ) mixed with 10% fetal bovine serum (Sigma, St. Louis, MO), 1% penicillin-streptomycin, and 2.5% sodium bicarbonate (Fisher Scientific, Waltham, MA). The cells were grown in an

incubator at 37° C and 5% (v/v) carbon dioxide. All experiments using cells were performed while the cells were in the exponential growth phase.

5.2.3 Effects of sonication parameters and bath temperature on the temperature achieved during fabrication

To evaluate the effects of the sonication and bath settings on the temperature of the dispersion, 2 mL of deionized water was sonicated under various conditions. First, the length of the pulse time was evaluated when 2 mL deionized water was sonicated for 5 and 10 minute intervals. The water was kept at room temperature and sonicated at 35% amplitude with the following pulse settings, 15 second on- 5 seconds off, 10 seconds on-5 seconds off, and 5 seconds on- 5 seconds off. The total sonication was set to 5 minutes. The temperature of the water was measured using a probe thermometer placed into the water and measured in real time. The temperature was recorded after the first 5 minute cycle and then another 5 minute cycle. Next, the maximum temperature reached during sonication when starting at various temperatures was investigated. The pulse was kept constant at 15 second on- 5 seconds off. At a starting temperature of 30 degrees Celsius, amplitudes settings of 35% and 40% were evaluated. At a starting temperature of 51 degrees Celsius, amplitude at 35% was evaluated. At a starting temperature of about 60 degrees Celsius, amplitudes of 25%, 35%, and 50% were evaluated. For two of the experiments, the temperature was measured at 15 minutes as well. From this initial information, we created two sonication schedules based on a starting bath temperature of 35 degrees Celsius and a pulse setting of 15 second on 5 seconds off and varying amplitude settings. Schedule one was as follows, amplitude 30%, 35%, 40%, and 45%.

Schedule two was as follows, amplitude 35%, 40%, 45%, and 50%. These parameters were used for most of the experiments, and the differences are noted where other conditions were used.

5.2.4 Effects of the formulation and cooling buffers on the size and PDI of lipid nanodispersions

The feasibility of creating various nanodispersions using various combinations of formulation and cooling buffers was evaluated. To prepare the nanodispersions, the lipids were initially dispersed in 1.5-2 mL of aqueous buffer using probe sonication then immediately diluted into 5-18 mL of ice cold aqueous buffer under stirring with a magnetic stir bar. The effects of a 5 mM sodium chloride and 5 mM TES buffer on the size and polydispersity index of lipid nanodispersion was evaluated. Briefly, 15 mg glycerol trioctanoate, 35 mg gelucire 43/01, 10 mg DSPC, 12.5 mg DSPE-PEG- 2K-methoxy, 7.5 mg cholesterol were formulated in DI and cooled in DI, formulated in DI and cooled in the buffer, or formulated in the buffer and cooled in the buffer,. All the formulation buffers also contained 10% ethanol. These were prepared using sonication schedule two.

The feasibility of using normal saline solution as the cooling buffer was also evaluated. Using a lipid blend of 13 mg glycerol trioctanoate, 40 mg precirol, 10 mg DSPC, and 10 mg DSPE-PEG-2K methoxy, the lipids were formulated in a 10 % ethanol in DI buffer using sonication schedule one, and poured into a solution of 8 mL normal saline.

If a stable nanodispersion was achieved, the z-average size, number size, and PDI of the dispersion was measured using MALVER zetasizer instrument using dynamic light

scattering technique. The dispersions were diluted in the formulation buffer of 5mM sodium chloride and 5 mM TES and allowed to equilibrate for at least one hour. The measurements provided represent the average of three measurements.

5.2.5 The effects of varying amounts of ethanol on the size, PDI, zeta potential, and cell viability on lipid nanoparticle dispersions

To evaluate the effects of ethanol in aqueous phase, 0%, 5%, and 10% ethanol was added to the aqueous phase containing 5 mM sodium chloride and 5 mM TES. The lipid phase consisted of the following: 10 mg squalene, 40 mg precirol, 10 mg DSPC, and 12.5 mg DSPE-PEG-2k-methoxy. The lipid phase was mixed in a vial, heated to 80 ° C to melt and mix the lipids well, and allowed to solidify. They were then placed in a dry bath at 35 °C and the aqueous buffer that has been heated to the same temperature was added. The mixture was allowed to rest for 5 minutes before sonication for 2 minutes to create a coarse emulsion. After the two minutes, the vial was placed in the dry bath and sonication schedule two was followed, and the temperature monitored with a probe. After completion of the sonication schedule, the hot lipid dispersion was dissolved into 20 mL of ice cold 5 mM sodium chloride buffered with 5 mM TES at pH 7.

Once all the samples were prepared, they were allowed to rest for 24-48 hours. The samples were diluted one to five into 5 mM sodium chloride buffered with 5 mM TES at pH 7 and allowed to equilibrate for at least one hour. The size, zeta potential, and PDI were determined using Malvern zetasizer.

The cell viability of the formulation was evaluated using a modified MTT assay. The A549 cells were seeded on a 96 well plate at 5,000 cells per well with 100 µl of growth

media in each well and placed in the incubator for 48 hours. After the 48 hours, the media was removed and the cells were treated with varying concentrations of the formulations which were diluted using a serial dilution procedure. The control cells received fresh media. The 96 well plates were then placed in the incubator for 24 hours; the media was suctioned out of every well and replaced with 100 µl of fresh media. To each well, 20 µl of 5 mg/mL MTT solution in Dulbecco's Phosphate Buffered Saline (DPBS) was added. Following MTT addition, the plates were placed back into the incubator for 3 hours. 90 µl of detergent solution was then added to each well to dissolve any formazan crystals that had formed. The plates were then placed in the incubator overnight. The detergent solution was made by mixing 10.5 g sodium dodecyl sulfate, 25 ml of dimethylformamide, and 25 ml of de-ionized water and adjusting the pH to 4.7 using acetic acid. The absorbance of the samples was then measured using a plate reader with the wavelengths set at 570 and a reference at 650. The absorbance readings were used to calculate the cell viability by comparing the treatment measurements to control measurements.

5.2.6 Effects of the solid lipid on particle characteristics and cell viability

To compare the effects of the solid lipid on the characteristics of the lipid dispersion, the following batches were prepared. To compare the effects of precirol, cetyl palmitate, and compritol on the dispersion characteristics, lipid dispersions were created using a 50:50 average mole ratio of glycerol trioctanoate, the liquid lipid, to the solid lipids above. These lipid mixes were kept to a final lipid core weight of 50 mg combined of the solid and liquid lipid. The surfactants used for this preparation were as follows: 10 mg DSPC,

12.5 mg DSPE-PEG-2K-methoxy, and 7 mg cholesterol. These batches were formulated in 2 mL of 10% ethanol 5 mM sodium chloride buffered with 5 mM TES at pH 7. The lipids and surfactants were melted at 80 ˚C and allowed to mix evenly. The lipids were solidified and placed in a 35 ˚C dry bath and 2 mL of the buffer was added. In the case of compritol, 50 ˚C bath was used as compritol has a melting point approaching 70 ˚C. The lipids were then sonicated according to sonication schedule number two and poured into 8 mL of ice cold 5 mM sodium chloride buffered with 5 mM TES pH 7. The particles size and zeta potential were measured as described above using a Malvern zetasizer. The cell viability of the formulations was evaluated using a modified MTT assay as previously described using a seeding density of 10,000 cells per 96 well plate.

Comparison of precirol and trimyristin lipid dispersions was performed using the following formulation using 35 mg of each solid lipid combined with the following components: glycerol trioctanoate 15 mg, DSPC 7.5 mg, SPAN 60 2.5 mg, cholesterol 7 mg, DSPE-PEG-2K-methoxy 15 mg. These batches were formulated in 2 mL of 10% ethanol 5 mM sodium chloride buffered with 5 mM TES at pH 7. The lipids and surfactants were melted at 80 ˚C and allowed to mix evenly. The lipids were solidified and placed in a 35 ˚C dry bath and 2 mL of the buffer was added and sonicated following sonication schedule number two and poured into 8 mL of ice cold 5 mM sodium chloride buffered with 5 mM TES pH 7with 1.25% glycerol. The size and zeta potential was measured as described above. The cell viability was measured as described above using a seeding density of 10,000 cells per well in a 96 well plate.

Comparison of precirol, gelucire 43/01, trilaurin, and geleol mono and diglycerides was performed using 35 mg of each solid lipid and the following ingredients: glycerol

trioctanoate 15 mg, DSPC 7.5 mg, SPAN 60 2.5 mg, DSPE-PEG-2k-methoxy 20 mg, and cholesterol 7.5 mg. These batches were formulated in 2 mL of 10% ethanol 5 mM sodium chloride buffered with 5 mM TES at pH 7. The lipids and surfactants were melted at 80 ˚C and allowed to mix evenly. The lipids were solidified and placed in a 35 ˚C dry bath and 2 mL of the buffer was added and sonicated following sonication schedule number two and poured into 18 mL of ice cold 5 mM sodium chloride buffered with 5 mM TES pH 7. The size and zeta potential were measured as described above. The cell viability was measured as described above using a seeding density of 7,500 cells per well. These lipid dispersions were stored in 2-4 ˚C and monitored for long term stability by looking for signs of phase separation at 6+ months after formulation.

5.2.7 Effect of the use of various surfactant combinations on the size, zeta potential, and cell viability of lipid nanodispersions

The first investigation of the surfactants used to create lipid dispersions focused on the use of various phospholipid combinations for the preparation of lipid nanodispersion. The early formulations were prepared in 1.5 mL deionized water, heated to 65 ˚C and sonicated at 50% amplitude for 10 minutes, and poured into 15 mL of ice cold deionized water. For the following experiments, 30 mg squalene, 70 mg precirol, and 200 microliters of ethanol was used as the lipid phase. Formulation 1 contained 40 mg DSPC as the surfactant in the lipid phase. Formulation 2 was a mixture of 20 mg DSPC and 20 mg DSPE-PEG-2K-methoxy added to the lipid phase. Formulation 3 contained 40 mg

DSPC in the lipid phase and 3% Tween 60 in the aqueous phase. The particles were diluted one to five in deionized water and characterized using a Malvern zetasizer for size and zeta potential. Cell viability of A549 cells exposed to the formulation was performed as described above with a seeding density of 7,500 cells/well.

The role of the amount of DSPE-PEG-2k-methoxy in the lipid dispersion on particle size and zeta potential was investigated using the following procedures. The formulations consisted of 15 mg glycerol trioctanoate, 35 mg precirol, 7.5 mg DSPC, 2.5 mg SPAN 60, 7 mg cholesterol, with the amount of DSPE-PEG-2k-methoxy in varying as follows, 12.5 mg, 15 mg, 17.5 mg, and 20 mg for formulations 4, 5, 6, and 7, respectfully. The formulation was performed in 2 mL of 10% ethanol in 5 mM sodium chloride buffered with 5 mM TES. The formulation was performed according to sonication schedule 2 and poured into ice cold 5 mM sodium chloride buffered with 5 mM TES pH 7 with 1.25% glycerol. The formulation was allowed to cool for 24-48 hours before the size and zeta potential was measured using Malvern zetasizer. The effects of the formulation on cell viability was performed as previously described with a seeding density of 10,000 cells per well.

The role of a carboxylic acid functional group on the distal end of the DSPE-PEG-2k molecule on particle size and zeta potential was investigated using the following two formulations. The formulation consisted of 10 mg squalene, 40 mg precirol, 10 mg DSPC, and 12.5 mg of DSPE-PEG-2K-methoxy or 12.5 mg of DSPE-PEG-2K-COOH formulations 8 and 9, respectfully. The buffer consisted of 5% ethanol in 5 mM sodium chloride buffered with 5 mM TES at pH 7. The cooling buffer was 20 mL of 5 mM

sodium chloride buffered with 5 mM TES pH7. The particles were evaluated for their size and zeta potential using a Malvern zetasizer instrument.

The effects of triglycerol monostearate instead of span 60 as a cosurfactant were investigated. At the same time, the effects of using DSPE-PEG-2K versus DSPE-PEG-5K were investigated. The lipid phase consisted of 15 mg glycerol trioctanoate and 35 mg trilaurin. The surfactant blend for formulation 10 consisted of 10 mg triglycerol monostearate, 7.5 mg DSPC, 20 mg DSPE-PEG-2K-methoxy, and 7.5 mg cholesterol. Formulation 11 consisted of 15 mg glycerol trioctanoate, 35 mg trilaurin, 10 mg triglycerol monostearate, 7.5 mg DSPC, 10 mg DSPE-PEG-2K-methoxy, and 7.5 mg cholesterol. Formulation 12 consisted of glycerol trioctanoate 15 mg, trilaurin 35 mg, triglycerol monostearate 10 mg, DSPC 7.5 mg, DSPE-PEG-5K-methoxy 10 mg, and cholesterol 7.5 mg. Formulation 13 consisted of glycerol trioctanoate 15 mg, trilaurin 35 mg, DSPC 7.5 mg, SPAN 60 2.5 mg, DSPE-PEG-2k-methoxy 20 mg, and cholesterol 7.5 mg. The buffer consisted of 10% ethanol in 5 mM sodium chloride buffered with 5 mM TES at pH 7. The cooling buffer was 8 mL of 5 mM sodium chloride buffered with 5 mM TES pH7. The formulations were characterized for their size and zeta potential using a Malvern zetasizer instrument and formulations 10 and 12 were evaluated for their effects of the cell viability of A549 cells using a MTT assay as described above with a seeding density of 7,500 cells per well.

5.2.8 Ability of lipid nanodispersions to internalize into A549 cells

The ability of lipid nanodispersions prepared using DSPE-PEG-2K and DSPE-PEG-5K was evaluated using confocal microscopy. The two formulations were labeled with 0.1% of the lipophilic molecule nile red. Formulation 1 contained glycerol trioctanoate 15 mg,

trilaurin 35 mg, DSPC 7.5 mg, cholesterol 6.5 mg, triglycerol monostearate 10 mg, DSPE-PEG-2K 15 mg, and 50 micrograms of nile red. Formulation 2 contained glycerol trioctanoate 15 mg, trilaurin 35 mg, DSPC 7.5 mg, cholesterol 6.5 mg, triglycerol monostearate 10 mg, DSPE-PEG-5K 10 mg, and 50 micrograms of nile red. The particles were characterized for their size, zeta potential, and used in subsequent experiments for confocal microscopy at a treatment concentration of 1 mg/mL for each formulation. To set up the experiments for confocal microscopy, 4 well chambered cover glass slides were seeded with 40,000 cells per well and placed in the incubator for 24 hours. The following day the cells were treated with the formulation and incubated for 24 hours. After 24 hours of incubation, the cells were washed 5 times with dubelco's phosphate buffered saline, fixed using 4% formaldehyde, and the nuclei were stained using 300 nanomolar 4′,6-diamidino-2-phenylindole (DAPI) dissolved in dubelco's phosphate buffered saline. After staining was complete, the chambers were wrapped in foil to protect the samples from light. The samples were then examined using a Leica TCS SP8 Confocal microscope. Z- stack images were taken of the cells to confirm the internalization of the particles by measuring the florescence of the nile red for particle internalization while the DAPI stain was used as a contrast.

5.2.9 Testing gefitinib solubility in various lipid mixtures

Gefitinib solubility in various lipid mixtures was assessed by attempting to dissolve 2-5 mg of drug in a total of 50-65 mg of lipid. The combinations of lipids evaluated include the following: 20 mg oleic acid and 30 mg trilaurin; 15 mg glycerol trioctanoate and 35 mg trilaurin; 15 mg trioctanoate, 20 mg trilaurin, and 10 mg stearic acid; 15 mg glycerol trioctanoate, 35 mg trilaurin, and 15 mg dipalmitoyl hydroxyproline; 15 mg glycerol

trioctanoate, 35 mg trilaurin, and 11 mg dipalmitoyl hydroxyproline. The lipids plus drug were added to a glass vial and heated to 80 ˚C to allow the lipids to melt and dissolve the drug. The lipids were observed for the dissolution of the drug in the lipid melt. Drug was deemed to be dissolved in the lipid if no drug powder was observed in the clear lipid melt.

5.2.10 Formulation of gefitinib loaded nanoparticles with oleic acid as the liquid lipid to help solubilize gefitinib in the lipid phase

The formulation of empty and gefitinib loaded nanoparticles with oleic acid was evaluated. Empty nanoparticles were formulated using the following lipid phase: 20 mg oleic acid, 30 mg trilaurin, 4 mg egg PC, 10 mg DSPE-PEG-5k-methoxy, 5 mg DSPC, 7 mg cholesterol, and 3 mg triglycerol monostearate. Drug loaded formulation was made with the same lipid phase plus 5.5 mg gefitinib dissolved in the lipid phase. The aqueous phase for both formulations consisted of 10% ethanol in 5 mM sodium chloride buffered with 5 mM TES buffer at pH 7. The lipids were sonicated following sonication schedule two. After formulation, the particles were evaluated for particle size, zeta potential, and stability in media.

5.2.11 Ability of carboxylic acid containing lipids to form sub 200 nanometer lipid dispersions

The effects of various carboxylic acid containing lipids on the ability to form lipid dispersions were evaluated. The formulations were based on the following core lipids and surfactant mixtures: glycerol trioctanoate 15 mg, trilaurin 35 mg, cholesterol 6.5 mg, triglycerol monostearate 10 mg, DSPC 7.5 mg, and DSPE-PEG-5K-methoxy 10 mg. The carboxylic acid containing lipids were mixed to the above lipid. The following were

added in various batches: 20 mg stearic acid, 10 mg myristic acid, 10 mg palmitic acid, 15 mg eladic acid, and 15 mg erucic acid. The particles were formulated in 2 mL of 10% ethanol in 5 mM sodium chloride buffered with 5 mM TES at pH 7. They were sonicated using sonication schedule 2 and poured into 8 mL of 5 mM sodium chloride buffered with 5 mM TES at pH 7. The particles were allowed to rest for 24 hours before characterized using a Malvern zetasizer for their particle size and zeta potential in 5 mM sodium chloride buffered with 5 mM TES pH 7. The stable particles were evaluated for stability in media and the batch formulated with erudic acid was evaluated for stability in normal saline to investigate possible mechanisms of destabilization that occurs as seen with oleic acid formulated lipid dispersions.

5.2.12 Formulation of gefitinib loaded lipid dispersions with dipalmitoyl hydroxyproline with and without DC-cholesterol

The formulation of gefitinib loaded lipid dispersions containing dipalmitoyl hydroxyproline with and without 3ß-[N-(N',N'-dimethylaminoethane)-carbamoyl]cholesterol hydrochloride(DC-cholesterol) was evaluated. To help increase the stability of the formulation in media, DC-cholesterol was used to help counter act the presence of negatively charged groups that are formed when the carboxylic acid groups are exposed to aqueous buffer above pH 5.5. Gefitinib formulation one consisted of the following: glycerol trioctanoate 15 mg, trilaurin 35 mg, gefitinib 2.5 mg, dipalmitoyl hydroxyproline 15 mg, DSPC 8.5 mg, triglycerol monostearate 10 mg, DSPE-PEG-5K 10 mg, cholesterol 6.5 mg and gefitinib 3.4 mg. Gefitinib formulation two consisted of the following: glycerol trioctanoate 15 mg, trilaurin 35 mg, gefitinib 2.5 mg, dipalmitoyl hydroxyproline 11 mg, DSPC 8.5 mg, triglycerol monostearate 10 mg, DSPE-PEG-5K-

methoxy 10 mg, cholesterol 6.5 mg, and 3ß-[N-(N',N'-dimethylaminoethane)-carbamoyl]cholesterol hydrochloride 6.5 mg. In the second formulation, the mole ratio of amine containing compounds of gefitinib and DC-cholesterol to dipalmitoyl hydroxyproline was 50:50. The particles were measured using a Malvern zetasizer and evaluated for their stability in media.

5.3 Results

5.3.1 Effects of sonication parameters on bath temperature achieved during sonication.

The results are summarized in table 5.1. Looking at the temperatures obtained after 5 minutes and 10 minutes of sonication, there seems to be minimal increase in the temperature after the first 5 minutes of sonication. It appears that after the first five minutes of sonication the increase in temperature reaches a plateau. The two measurements of the temperature at 15 minutes of sonication further show the plateau of the temperature with extended sonication periods. The first round of sonication raises the temperature anywhere from 10-20 ˚C depending on the amplitude settings. The largest increase in temperature occurs with the highest amplitude settings, which corresponds with the higher amount of energy that is put into the system. The temperatures reached during sonication schedules one and two are summarized in tables 5.2A and 5.2B, respectfully. With these schedules, the temperature of the formulation is controlled with in two degrees at each amplitude level. The use of the sonication schedule provides for the ability to fine tune the formulation conditions that are achieved during the

formulation process. For lower melting point lipids, the lowest final temperatures are used. For higher melting point lipids, the temperature of the bath can be adjusted to reach temperatures sufficiently high enough to melt the lipid.

5.3.2 Effects of formulation and cooling buffer on the size and PDI of the lipid nanodispersion

When cooling the hot lipid melt into the normal saline solution, the batch destabilized immediately and formed large aggregates in the buffer. Initially, after completion of the sonication cycle, the dispersion looked like nanodispersion; however, the addition into the saline completely destabilized the system. Testing the batches made using combinations of the sodium chloride and TES buffer showed much more promising results. When formulated in DI and cooled in DI, the dispersion formed has a z-average size of 91.52(1.387), a PDI of 0.167 (0.008), and a number size average of 44.22 (9.856). When formulated in DI and cooled in the buffer, the dispersion formed had a z-average size of 96.94 (0.9603), PDI of 0.174 (0.023), and a number size of 50.43 (5.271). When formulated in the buffer and cooled in the buffer, the dispersion had a z-average size of 90.94 (0.1266), PDI of 0.150 (0.007), and number size of 48.58 (5.923).

5.3.3 Effects of ethanol in the formulation buffer

The addition of ethanol into the aqueous buffer of the formulation was found to reduce the size of the particles without changing any of the components of the formulation. With zero ethanol in the formulation buffer, the lipid dispersion created had the following

characteristics: z-average size 105.5 nm (0.9074), PDI 0.109 (0.009), number size 70.21 nm (1.305), and zeta potential -11.6 mV (0.666). With 5% ethanol in the aqueous buffer, the lipid dispersion showed the following characteristics: z-average size 95.25 nm (0.3780), PDI 0.130 (0.003), number size 59.68 nm, and zeta potential – 18.7 mV (0.306). With 10% ethanol in the aqueous buffer, the lipid dispersion had the following characteristics: z-average size 74.76 nm (0.3035), PDI 0.107 (0.009), number size 46.93 nm (0.6806), and zeta potential – 18.5 mV (0.693). The addition of ethanol into the aqueous phase leads to a reduction of the size of the particles with the largest effect seen with the 10% ethanol. The number size distribution is shown in figure 5.1

The effects of the formulations on the cell viability of A549 cells was shown in figure 5.2. The IC:50 of each formulation is near 1 mg/mL with very small differences between their IC:50 values.

5.3.4 Effects of the solid lipid on particle characteristics and cell viability

Comparing the particles characteristics between precirol, cetyl palmitate, and compritol lipid dispersions created using the surfactant mixture described above. With precirol, the surfactant blend used led to particles with a z-average of 81.65 nm (0.5305), PDI of 0.126 (0.015), number size of 52.53 nm (1.28), and a zeta potential of -19.7 mV (1.05). Cetyl palmitate lipid dispersion had the following characteristics: z-average size 119.6 nm (3.252), PDI of 0.15 (0.006), number size average 73.84 nm (1.45), and zeta potential of -17.9 mV (0.85). Compritol as the solid lipid led to particles with the

following characteristics: z-average size 86.89 nm (0.54), PDI of 0.109 (0.003), number size average 55.86 nm (0.3557), and zeta potential -15.5 mV (0.289).

The results comparing the effects of precirol, cetyl palmitate, and compritol on cell viability are shown in Figure 5.3A. Precirol appears to be the most biocompatible of these lipids with an IC:50 between 3 and 4 mg/mL and a viability of 79% at a concentration of 2 mg/mL. Looking at cetyl palmitate and compritol, the cell viability appears to plateau at 50% as the concentrations get above 1 mg/mL. At 1 mg/mL, cetyl palmitate lipid nanoparticles reduce the cell viability to 60% while compritol nanoparticles reduce the cell viability to 52%. Using the above formulation conditions, it is clear that precirol is the more biocompatible lipid as compared to ceytyl palmitate and compritol as evaluated via MTT assay in A549 lung cancer cells.

Evaluating the effects of precirol and trimyristin on the particles size characteristics using the surfactant blend described above. Precirol lipid dispersion had the following characteristics: z-average size 84.35 nm (2.172), PDI 0.214 (0.008), number size average 42.98 nm (0.6768), and zeta potential -19.6 mV (0.208). Trimyristin lipid dispersion had the following characteristics: z-average size 91.7 nm (1.135), PDI 0.127 (0.017), number size average 59.8 nm (2.33), and zeta potential -16.9 mV (0.321).

The effects on cell viability of precirol versus trimyristi as the solid lipid were evaluated. The results are shown in Figure 5.3B. Here, the precirol lipid particles showed an IC:50 near 1.5 mg/mL while those with trimyristin had an IC:50 near 0.5 mg/mL. It is interesting to note at elevated concentrations, the precirol particles showed a dose

dependent decrease in the cell viability while the trimyristin based lipid particles appear to plateau around 40% as the concentration was increased past 1 mg/mL.

The evaluation of precirol, gelucire 43/01, trilaurin, and geleol mono and diglycerides as the solid lipid using the surfactants described showed the following results. Precirol lipid dispersions had a z-average size 71.9 nm (0.005), PDI 0.161 (0.016), number size average 37.8 nm (2.048) and zeta potential of -16.6 mV (0.808). Trilaurin lipid dispersions showed a z-average size of 71.83 nm (0.147), PDI 0.118 (0.005), number size 46.13 nm (0.7499), and zeta potential of -15.3 mV (0.451). Gelucire 43/01 lipid dispersion had a z-average size of 85.62 nm (0.4279), PDI of 0.178 (0.004), number size average 46.41 nm (1.972), and zeta potential of -16.9 mV (0.551). Geleol mono and diglyceride lipid dispersions showed a z-average size of 80.1 nm (0.405), PDI 0.149 (0.006), number size average 45.57 nm (2.445), and zeta potential of -16.5 mV (0.802).

The effects of the solid lipids precirol, gelucire 43/01, trilaurin, and geleol mono and diglycerides on cell viability were evaluated and results plotted in Figure 5.3C. Out of the four lipids evaluated, the trilaurin and gelucire 43/01 lipid blends showed the least reduction of cell viability with 2.18 mg/mL treatment concentration showing a 51.4% and 52.8% cellular viability, respectfully. The precirol based lipid dispersion showed an IC:50 near 1 mg/mL while the dispersion based on geleol mono and diglycerides showed an IC:50 near 0.5 mg/mL. At concentrations above 0.3 mg/mL, all the dispersions appear to show a cell viability above 70%. Comparing these three formulations, it is clear that trilaurin and gelucire 43/01 are the preferred solid lipids to be used for the fabrication of lipid nanodispersions. When looking for signs of phase separation at 6+ months of storage at 2-4 ˚C, the formulations containing geleol mono and diglycerides and precirol

show the formation of white precipitates, while the dispersions made with trilaurin and gelucire 43/01 maintain their transparent appearance without forming any large precipitates (Figure 5.4).

5.3.5 Effects of surfactant blends on lipid dispersion characteristics

The formulation characteristics were as follows. Formulation one did not lead to the formation of a homogeneous lipid dispersion as large aggregates were seen throughout the white dispersion. Formulation two had the following characteristics: z-average size 96.81 nm (0.3853), PDI 0.331 (0.009), number size average 4.147 nm (1.111) and zeta potential of -42.2 mV (0.651). Formulation three had a z-average size of 122.7 nm (1.179), PDI 0.251 (0.009), number size average 24.2 nm (4.818), and zeta potential of -17.5 mV (0.493). Since formulation one was not a homogenous dispersion, only formulations 2 and 3 were evaluated for their effects on cell viability in A549 cells. Figure 5.5 shows the data. Formulation 2 showed a higher cell viability across all concentrations evaluated reaching 100% viability above 0.5 mg/mL. Formulation three, however, showed a cell viability of 60% at a concentration of 0.03 mg/mL.

Formulation 4 had a z-average size of 93.64 nm (0.3686), PDI 0.136 (0.004), number size 56.09 nm (1.775), and a zeta potential of -15.9 mV. Formulation 5 had a z-average size of 85.64 nm (1.653), PDI 0.171 (0.019), number size average 46.28 (3.193), and zeta potential -19.6 mV (0.208). Formulation 6 had a z-average size 69.93 nm (0.9203), PDI 0.157 (0.015), number size average 33.88 nm (9.232), and a zeta potential of -17.4 mV

(0.987). Formulation 7 had a z-average size of 60.69 nm (0.291), PDI 0.164 (0.007), number size average 34.33 (0.3386), and a zeta potential -15.3 mV (1). The general trend shows a decrease in the size of the particles with increasing amounts of DSPE-PEG-2K from 12.5 mg to 20 mg in 2.5 mg increments. The cell viability of A549 cells exposed to these formulations is shown in Figure 5.6. At the highest concentrations evaluated, all the formulations exhibit the same reduction in cellular viability. Below 2 mg/mL, however, the formulation containing 12.5 mg of DSPE-PEG-2K shows a marginally better biocompatibility by virtue of having higher cell viability readings as compared to formulations containing higher amounts of DSPE-PEG-2K.

The role of the end functional group on the DSPE-PEG-2K was investigated by comparing methoxy terminated and COOH terminated DSPE-PEG-2K surfactants. Formulation 8, DSPE-PEG-2k-methoxy, had a z-average size of 95.84 nm (0.846), PDI 0.125 (0.019), number size average of 62.35 nm (4.73), and zeta potential of -18.7 mV (0.306). Formulation 9, DSPE-PEG-2K-COOH, had a z-average size 75.49 nm (0.7684), PDI 0.176 (0.004), number size average 44.88 nm (2.718), and zeta potential of – 32.8 mV (2.87).

The effects of using triglycerol monostearate as the co-surfactant showed the following results .Formulation 10 showed a z-average size of 68.04 nm (1.021), PDI 0.148 (0.015), number size average 38.15 (2.044), and zeta potential of -21 mV (0.557). Formulation 11 showed z-average particle size of 88.81 nm (1.057), PDI 0.131 (0.002), number size average 55.79 nm (1.76), and zeta potential of -23.1 mV (0.153). Formulation 12 showed a z-average size of 91.78 nm (0.5776), PDI 0.082 (0.011), number size average 67.95 nm (1.551), and zeta potential of -10.5 mV (1.13).

Formulation 13 showed z-average size of 71.83 nm (0.147), PDI 0.118 (0.005), number size 46.13 nm (0.7499), and zeta potential of -15.3 mV (0.451). The effects of the above formulations on the cell viability of A549 cells after 24 hours of exposure are shown in Figure 5.7.

5.3.6 Internalization of the lipid dispersions by A549 cells

The particles used for the internalization experiments had the following characteristics. Formulation one had a size z-average size of 77.08 nm (0.7965),PDI 0.153 (0.01), number size average 47.84 (3.932), and zeta potential of -16 mV (1.4). Formulation 2, DSPE-PEG-5K, had a z-average size of 99.02 nm (0.6158), PDI 0.086 (0.005), number size average of 70.6 nm (0.7554), and a zeta potential of -8.29 mV (0.353). After 24 hours of incubation, the lipid particles were internalized well by the A549 cells. There appears to be no difference in the ability of the particles to enter the intracellular compartment based on the size of the length of the PEG molecules used in the formulations that were investigated. Looking at the z-stack images, after 24 hours, both formulations were found across multiple layers inside the cells. Figure 5.8A shows the images of the same cells taken at different layers within the cells for formulation 1. Figure 5.8B shows the images of the same cells taken at different layers within the cells for formulation 2.

5.3.7 Gefitinib solubility in various lipid mixtures

The solubility of gefitinib in the lipid mixtures was as follows: 5.5 mg in 20 mg oleic acid and 30 mg trilaurin; 3.4 mg in 15 mg glycerol trioctanoate, 20 mg trilaurin, and 10 mg

stearic acid; 3.4 mg in 15 mg glycerol trioctanoate, 35 mg trilaurin, and 15 mg dipalmitoyl hydroxyproline; and 2.5 mg in 15 mg glycerol trioctanoate, 20 mg trilaurin, and 11 mg dipalmitoyl hydroxyproline. Gefitinib did not dissolve when 2 mg were mixed with 15 mg glycerol trioctanoate and 35 mg trilaurin.

5.3.8 Formulation of lipid dispersions using oleic acid with and without drug loading

The particles formulated with oleic acid without drug had the following characteristics: z-average size 123 nm (1.301), PDI 0.166 (0.022), number size average 68.1 nm (4.975), and zeta potential of -8.58 mV (0.43). The gefitinib loaded oleic acid containing formulation had the following characteristics: z-average size 131.3 nm (0.4041), PDI 0.154 (0.008), number size average 82.47 nm (6.438), and zeta potential -5.9 (0.486). When placed into media, both of the above formulations crashed out and a precipitate formed at the bottom of the vials. This led to the investigation of other carboxylic acid containing lipids for their potential to make lipid nanodispersions stable in media.

5.3.9 Ability of carboxylic acid containing lipids to form sub 200 nanometer lipid dispersions

Investigation into the ability of various carboxylic acid containing lipids revealed the following. Saturated fatty acids such as stearic acid, myristic acid, and palmitic acid added into the lipid core did not lead to the formation of lipid nanodispersions. After dilution into the ice cold buffer, the dispersions looked stable, however, after 24 hours all the formulations showed sign of phase separation by formation of a white precipitate at

the bottom of the glass vials. Eladic acid, the trans unsaturated fatty acid of stearic acid, also showed signs of phase separation by the appearance of a precipitate. The lipid dispersion created using 15 mg of erucic acid in the formulation had the following characteristics: z-average size 109.4 nm (0.7572), PDI 0.075 (0.012), number size average 81.41 nm (1.585), and zeta potential -8.48 mV (0.89). The erucic acid dispersion was stable in the formulation buffer, however, destabilized when placed in media as seen by the formation of a precipitate. The dispersion had the following characteristics when measured in media: z-average size 159.9 nm (16.52), PDI 0.402 (0.062), and number size 72.47 (4.713). The destabilization is confirmed by the increase in the z-average size and the increase in the PDI from 0.075 to 0.402. When measured in normal saline, the lipid dispersion had the following characteristics: z-average size 109.6 nm (0.9074), PDI 0.083 (0.002), and number size average 79.27 nm (0.7275).

5.3.10 Formulation of gefitinib loaded lipid dispersions with dipalmitoyl hydroxyproline with and without DC-cholesterol

The gefitinib formulation one containing no DC-cholesterol had the following characteristics: z-average size 93.87 nm (0.8814), PDI 0.159 (0.018), number size average 53.77 nm (1.031), and zeta potential of -13.4 mV (0.929). The particles loaded with gefitinib containing DC-cholesterol had the following characteristics: z-average size 138.9 nm (1.3), PDI 0.13 (0.007), number size average 90.61 nm (1.748), and zeta potential -10.3 mV (0.115). The gefitinib loaded formulation without DC-cholesterol destabilized in media, however, the presence of DC-cholesterol in the formulation helped prevent the destabilization of the nanodispersion. This was confirmed by particle size measurements that showed the formulation containing DC-cholesterol and dipalmitoyl

hydroxyproline had the following characteristics when placed in media: z-average size 138.2 nm (0.5033), PDI 0.118 (0.01), and number size average of 96.63 nm (1.504).

5.4 Discussion

The optimization of the buffer, sonication parameters, and the max temperature reached has an important effect on the characteristics of the formulation. Early formulations that were performed using deionized water as the buffer and bath temperatures of 65 degrees Celsius led to the formation of particles with a PDI above 0.3 and dispersions with a z-average size and number size difference of nearly 100 nanometers. The difference of these two measurements can partly be described by the presence of surfactant micelles in the formulation. The high temperatures reached during sonication of aqueous solutions can alter the solubility of the surfactants used for the stabilization of the lipid dispersions. As the temperature increases, some of the surfactants experience an increase in their aqueous solubility to such an extent that they do not localize at the interface of the lipid and aqueous phases. When the dispersion is then cooled after sonication, the free surfactants experience a decrease in solubility and organize into micellar structures that have a much different size than dispersed lipid droplets. The optimization of the temperature used during preparation and the use of buffers helps control the solubility of the surfactants in the aqueous phase and allow them to better exist at the interface of the two phases. It is important to use a buffer of the correct ionic strength as too strong of a buffer will lead to destabilization of the lipid dispersion as seen in our experiments.

The use of alcohols in the formulation of microemulsions shows they can be used in the formulation of submicron size lipid dispersions.[19, 73-75] Here, we evaluate the effects of ethanol on the size and biocompatibility of the fabricated lipid dispersions. Using the same components, the introduction of ethanol into the aqueous phase during formulation decreases the average size of the formulation as the alcohol content is increased from 0% to 5% to 10%. The decrease on the particle size can be attributed to the relaxation of the surfactants at the interface by their interaction with the alcohol. We have shown that the addition of alcohol can indeed reduce the particle size without having any deleterious effects on the biocompatibility of the formulations.

The effects of the solid lipid phase on cell viability shows there is a difference in the biocompatibility of the formulations as measured by MTT assay in A549 lung cancer cells. The first set of experiments comparing precirol, compritol, and cetyl palmitate offer an interesting insight into the factors that determine the compatibility of the lipids used for lipid nanoparticle fabrication. Of these three, precirol appears to be have the least effects on the cellular viability of the A549 cells. Precirol is a diglyceride of a mixture of palmitic and stearic acid with a melting point around 55 degrees Celsius as reported by the supplier. Compritol is a mixture of mono, di, and tri glycerides of behenic acid with a melting point near 67 degrees Celsius as reported by the supplier. Cetyl palmitate is a lipid ester of palmitic acid with cetyl alcohol with a melting point of 54 degrees Celsius as reported by the supplier. Looking at these lipids, the compritol appears to have a bigger decrease in the cell viability due to its higher melting point. The longer fatty acid tails of compritol may be too tightly bound to allow for effective cellular metabolism of the formulation leading to accumulation of the lipids in the endosomes and lysosomes of

the cells. Looking at the comparison of the precirol, geleol mono and diglycerides, gelucire 43/01, and trilaurin, we see a similar pattern emerge. Geleol mono and diglycerides is a lipid blend of mono, di, and triglycerides of stearic and palmitic acid has a melting point in the range of 55-65 degrees Celsius as reported by the supplier. Gelucire 43/01 is a lipid blend of predominantly triesters of C8-C18 fatty acids with a melting point between 42-46 degrees Celsius as reported by the supplier. Trilaurin is a triglyceride if the 12 carbon fatty acid lauric acid and has melting point around 46 degrees Celsius as reported by TCI America which manufactured the lipid. Looking at this set of experiments, similar results are observed. The higher melting point lipids appear to decrease the cell viability of A549 cells to a greater extent as compared to those that have a lower melting point. Taking these results into consideration, it is recommended to use lower melting point lipids during the fabrication of lipid nanodispersions that can be internalized by cells.

Comparing the long term stability of nanodispersions with various solid lipids, it is clear that triglyceride lipids should make up the majority of the dispersed phase. Of the four formulations that were evaluated, precirol and geleol both showed the propensity to aggregate and precipitate. These lipid blends both have a high percentage of either mono or diglycerides making up the lipid core. It is possible that the presence of the added hydroxyl groups in the lipid matrix leads to a destabilization of the lipid nanodispersions upon long term storage. The trilaurin and gelucie 43/01 core lipids are made of predominantly the triglyceride form. When they are forming the core of the lipid particles, they are able to form a network of hydrophobic interactions that is uninterrupted by hydroxyl groups found in such blends as precirol.

Our studies show that the optimal surfactant blends used for the fabrication of lipid nanodispersions can have a great effect on the toxicity of the nanocarrier. When comparing the use of tween 60 and pegylated phospholipids, the pegylated phospholipids appear to be more biocompatible. This can be potentially explained by the structure of the two surfactant molecules. The tween 60 molecule is a pegylated sorbitan ester containing one stearic acid acid chain as its hydrophobic portion. The pegylated phospholipids used contain two stearic acid chains as the hydrophobic portion of the molecule. After the formation of the lipid nanodispersions, the two fatty acid tails of the pegylated phospholipids may be more prone to localize at the interface and remain bound to the lipid nanoparticle while the tween 60 can desorb from the interface more easily and interact with the cell membrane. A similar pattern is seen in our experiments evaluating various co-surfactants. Span 60 was compared to triglycerol monostearate. These two have the same fatty acid chain but differ in the makeup of their hydrophilic portion. The Span 60 has a sorbitan sugar as its hydrophilic portion. The triglycerol monostearate has a hydrophilic group that is made up of three glycerol molecules that have been covalently bonded together. The Span 60 has three hydroxyl groups and one oxygen in its hydrophilic segment meaning it has three hydrogen bond donors and one hydrogen bond acceptor. Triglycerol monostearate has three oxygens that can act as hydrogen bond acceptors and four hydroxyl groups that can act as hydrogen bond donors. Taken together, the triglycerol monostearate can have more hydrophilic interactions water while also having the potential to hydrogen bond with any nearby triglycerol monostearate molecules. This can help strengthen the bond of the particles at the interface leading to less surfactant that can break free to interact with cell membranes. As we saw in our

experiments, the formulations created using triglycerol monostearate as a co-surfactant did not reach the IC:50 at concentrations at just above 4 mg/mL. Looking at the literature, this formulation has one of the highest IC:50 values that has been reported by various investigators.[70]

The ability of the optimized lipid dispersions containing trilaurin, glycerol trioctanoate, triglycerol monostearate, DSPC, and DSPE-PEG was evaluated. It was shown that the PEG 2K or 5K did not prevent the internalization of these lipid nanodispersions as after 24 hours of incubation, both lipid nanodispersions were detected at various z-sections of A549 cells.

The solubility of gefitinib in the various lipid phases shows that there is a need to have a free carboxylic acid in the lipid matric to dissolve gefitinib in a substantial amount reaching 10%. Looking at the structure of gefitinib, it can be seen that is has a number of aromatic rings in its structure, but it also has a tertiary amine that can interact with a weak acid. Based on the solubility results we have seen, it is likely that the carboxylic acid group of our lipids can interact with the amine group in the structure of gefitinib leading to the formation of an ionic interaction that leads to the increase in the solubility of gefitinib in lipids that contain free carboxylic acid groups.

The inability of unsaturated lipids containing carboxylic acid groups to form lipid dispersions shows the difficulty of forming media stable lipid nanodispersions. The use of unsaturated fatty acids such as oleic acid and erucic acid leads to the formation of nanodispersions stable in the formulation buffer. These were stable in the buffer, but destabilized when exposed to media. The issues of the lipid nanodispersions precipitating

in media was not seen with lipid dispersions that did not contain lipids with carboxylic acids as many were evaluated for cytotoxicity in media. It has been shown that various proteins are adsorbed onto the surface of lipid particles after incubation in human serum. [76] It is possible the adsorption of these proteins leads to the destabilization of lipid particles containing lipids with carboxylic acid groups. If it is not due to the proteins found in the media, it may be due to the many other components found in the media. The presence of elevated electrolyte concentration in the media was ruled out by showing the particle size of erucic acid containing lipid dispersions remained the same when placed in normal saline.

Strategies to help increase the stability of the formulated lipid dispersions in media were explored by the introduction of amine containing DC-cholesterol into the formulation. The addition of DC-cholesterol was able to stabilize the lipid nanodispersion when placed in media. The size of the dispersion with the DC-cholesterol was increased relative to formulations without DC-cholesterol. This can be attributed to the decrease in the charge stabilization provided by the anionic surfactants in the formulation as DC-cholesterol introduces positive charge into the formulation that is over all negatively charged as confirmed by measuring the zeta potential. Even though the size of the formulation increased, the formulation was stabilized by the addition of amine containing molecules at a 1:1 ratio to the carboxylic acid containing was made to the formulation.

5.5 Conclusions

The formulation of lipid nanoparticles needs to be optimized for a given application. Stable biocompatible lipid dispersions can be created by fine tuning the formulation parameters, lipid components, and surfactant blends. The size of the particles can be adjusted by changing the amount of ethanol in the aqueous phase as well as by controlling the amount of DSPE-PEG added to the lipid formulation. The long term stability of the particles is not only affected by the surfactants used in the formulation of lipid nanodispersions, but by the composition of the dispersed phase. Using triglyceride lipids in the fabrication of lipid nanodispersions increases long term stability of the lipid nanodispersions. The effective formulation of drug loaded nanodispersions requires identifying lipids that can solubilize the drug and be used for the formulation of stable dispersions.

Starting Temperature(˚C)	Amplitude	Pulse Settings (seconds)	Temperature at 5 minutes (˚C)	Temperature at 10 minutes (˚C)	Temperature at 15 minutes (˚C)
24˚C	35%	15 on: 5 off	43.4 ˚C	46.7 ˚C	
24.7 ˚C	35%	10 on: 5 off	39.9 ˚C	41.7 ˚C	
26.5 ˚C	35%	5 on : 5 off	41 ˚C	40.7 ˚C	
30 ˚C	35%	15 on : 5 off	49.8 ˚C	51.8 ˚C	52 ˚C
30 ˚C	40%	15 on : 5 off	52.1 ˚C	54.3 ˚C	55 ˚C
51 ˚C	35%	15 on : 5 off	68.1 ˚C	69.2 ˚C	
60.6 ˚C	25%	15 on : 5 off	72 ˚C	71.8 ˚C	
60.8 ˚C	35%	15 on : 5 off	74.3 ˚C	76.5 ˚C	
61.6 ˚C	50%	15 on : 5 off	81.1 ˚C	81.7 ˚C	

Table 5.1 Temperatures reached during sonication at various conditions.

Amplitude	Temperature at end of cycle ˚ C (std)
30% 5 minutes	51.03 (1.49)
35% 5 minutes	53.14 (1.69)
40% 5 minutes	55.71 (1.90)
45% 5 minutes	58.81 (1.84)

Table 5.2 A Temperatures reached during sonication using schedule 1.

Sonication Amplitude	Temperature after Sonication (s.dev)
35% 5 minutes	**53.8 ˚C (0.932)**
40 % 5 minutes	**57.7 ˚C (1.050)**
45 % 5 minutes	**60.7 ˚C (1.155)**
50% 5 minutes	**63.5 ˚C (0.955)**

Table 5.2B Temperatures reached during sonication using schedule 2.

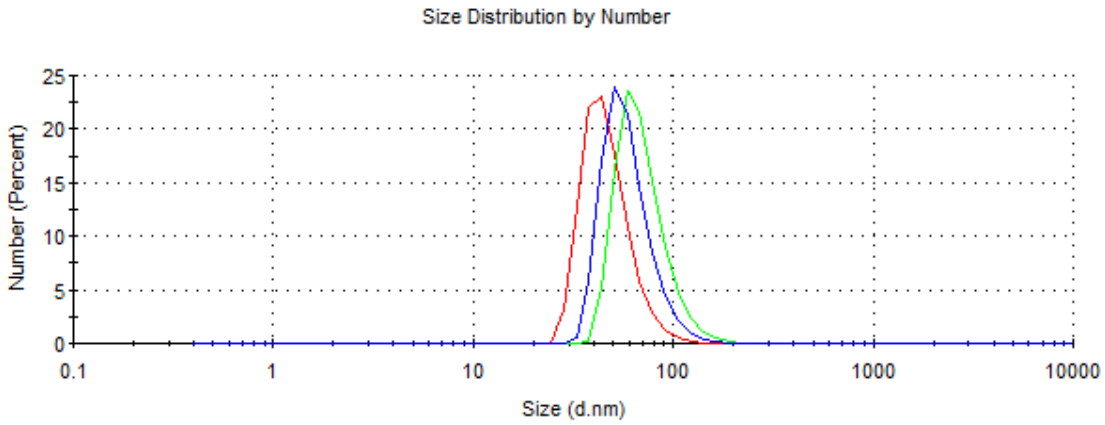

Figure 5.1. The number size distribution of lipid dispersions made with 0% ethanol 70.21nm average (green), 5% ethanol 59.68 nm average (blue), and 10% ethanol 46.93 nm average(red).

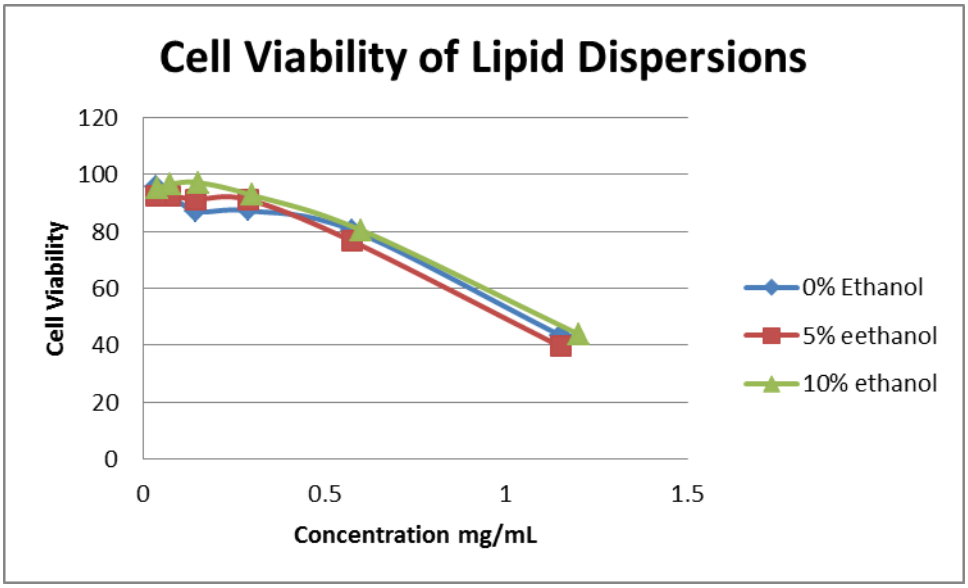

Figure 5.2. Cell viability of lipid dispersion made with the same components but varying amounts of ethanol in the aqueous phase. All the formulations have a similar IC:50 neat 1 mg/mL.

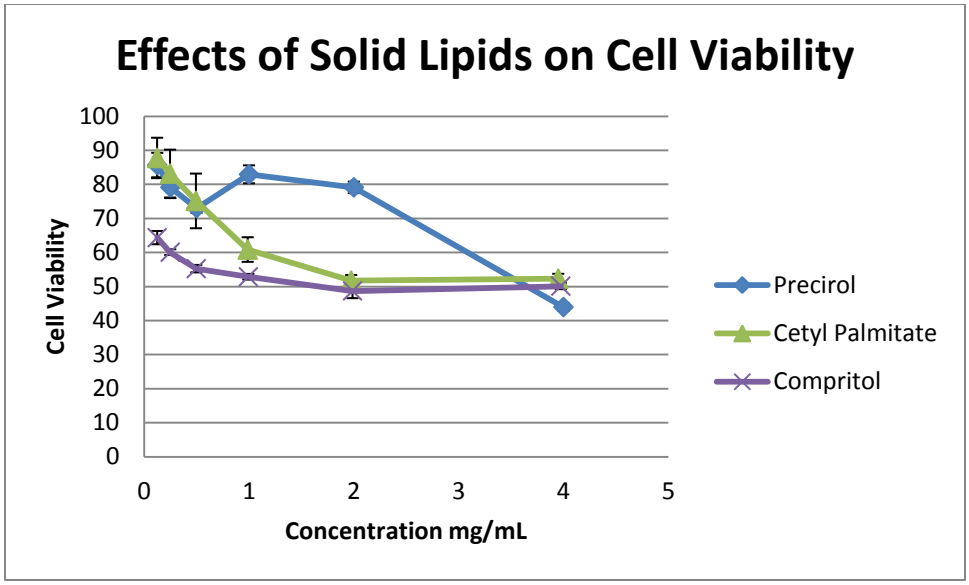

Figure 5.3A. Effects of cell viability of lipid nanodispersions made of the same components but differ in the solid lipids used, precirol(blue), cetyl palmitate (green), and compritol (purple).

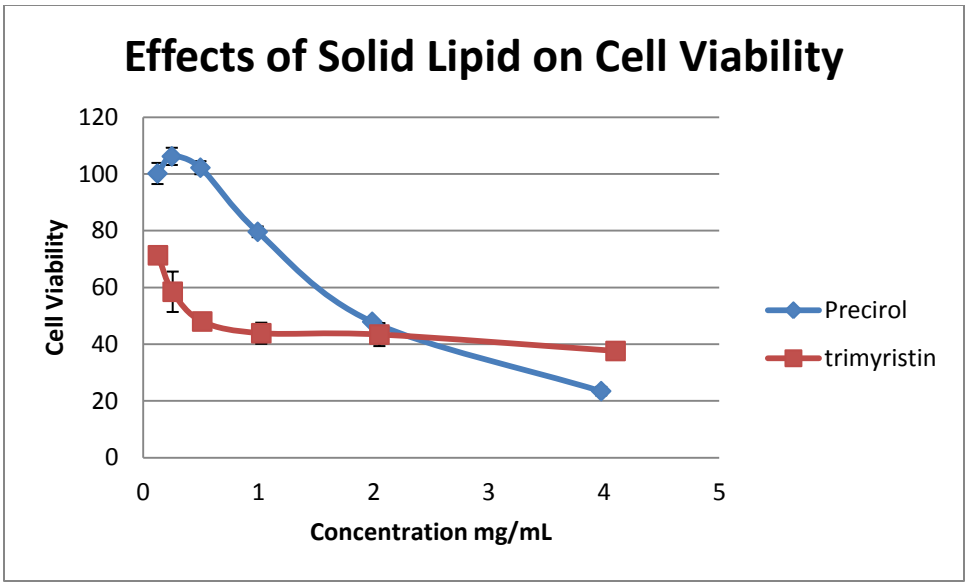

Figure 5.3B. Comparison of the cell viability of lipid dispersions that are the same except for the type of solid lipid used precirol (blue), trimyristin (red).

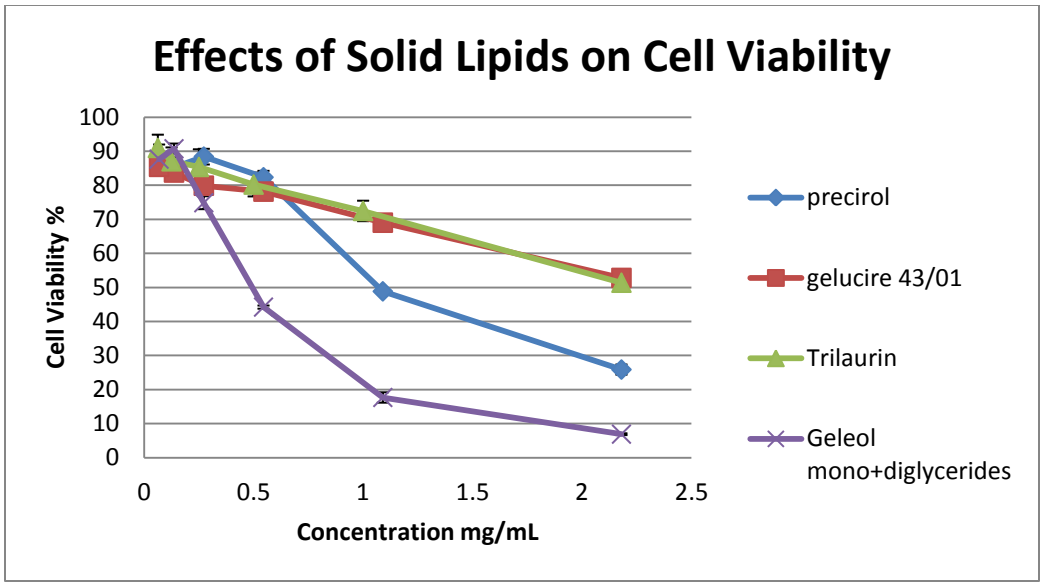

Figure 5.3C. Comparison of the cell viability of lipid dispersions that are the same except for the type of solid lipid used precirol (blue), gelucire 43/01 (red), Trilaurin (green), and geleol mono and diglycerides (purple).

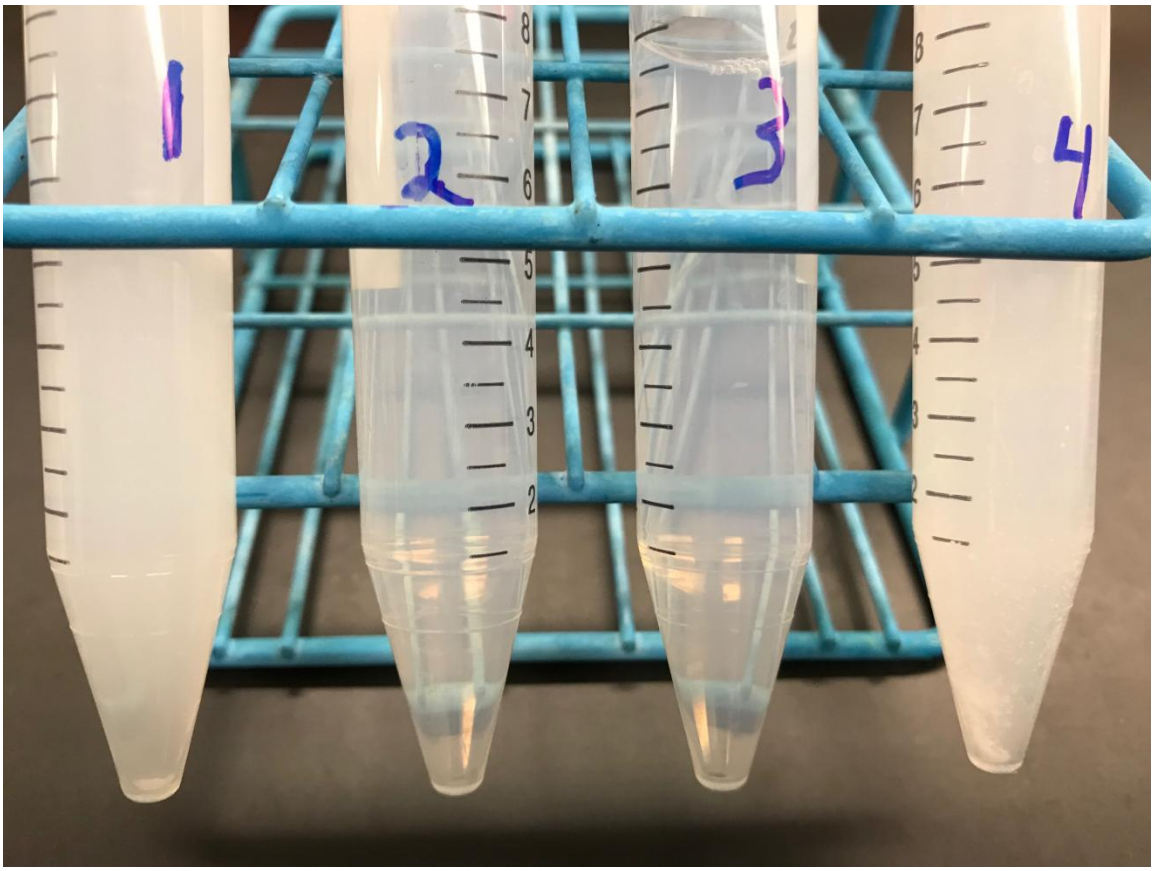

Figure 5.4. Depiction of phase separation behavior of batches after 6+ months of storage in 2-4 ˚C. 1. Precirol containing batch. 2. Gelucire 43/01 containing batch. 3. Trilaurin containing batch. 4. Geleol mono and diglycerides containing batch.

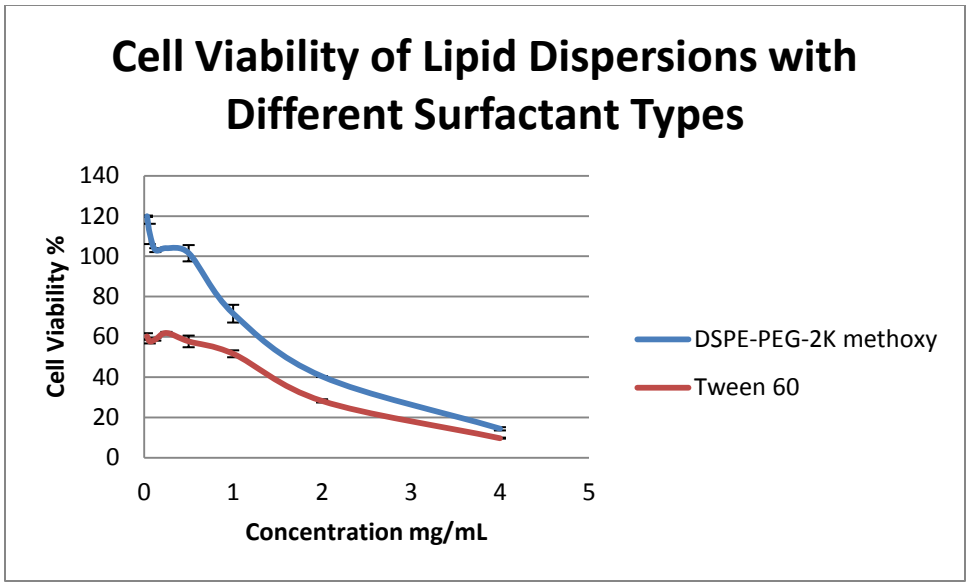

Figure 5.5 Cell viability of two lipid dispersions one stabilized with DSPE-PEG-2K-Methoxy (blue), and the other stabilized with tween 60.

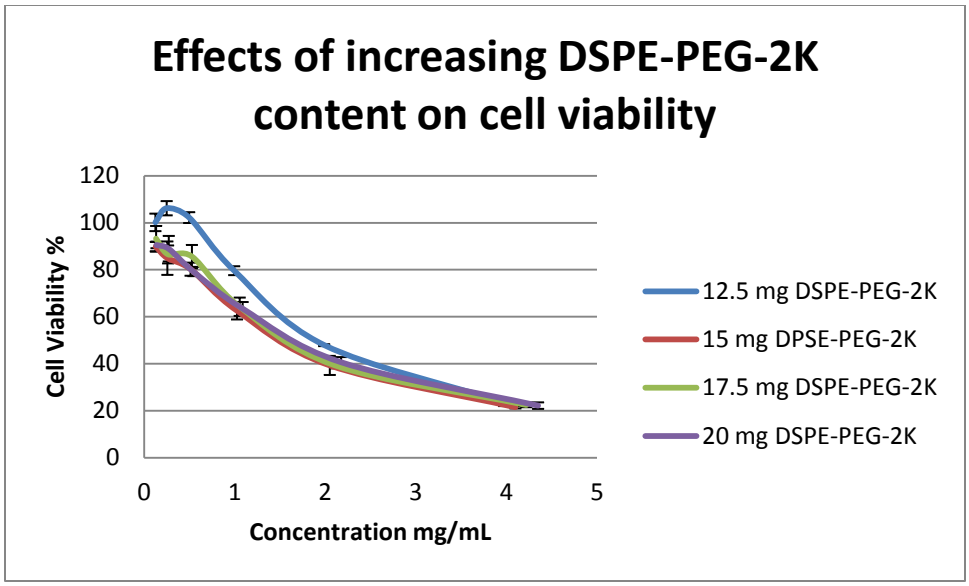

Figure 5.6 Effects of increasing DSPE-PEG-2K content in the formulation on cell viability.

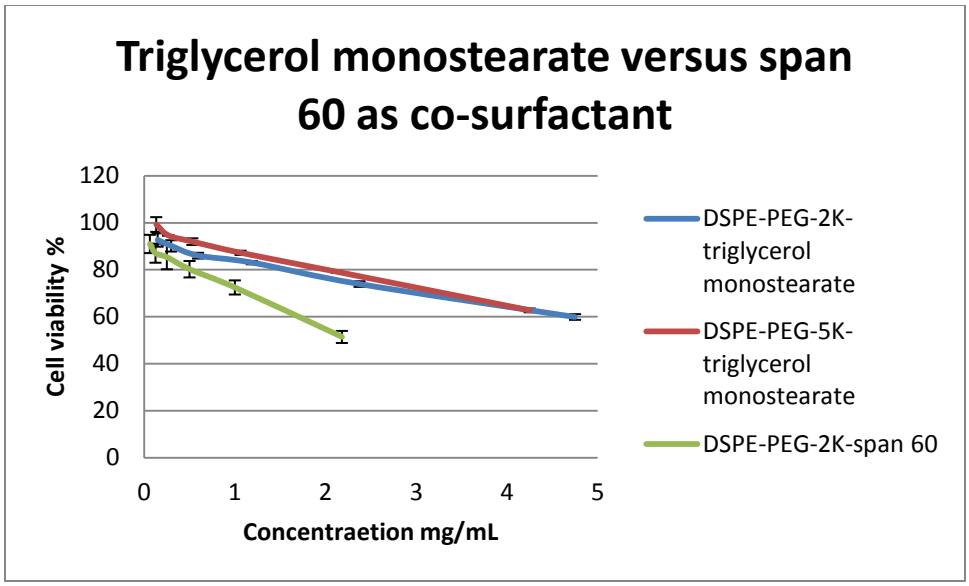

Figure 5.7. The effects of co-surfactants triglycerol monostearate and span-60 on the cell viability of A549 cells shows that triglycerol monostearate has greater biocompatibility as compared to the use of span 60 as a cosurfactant.

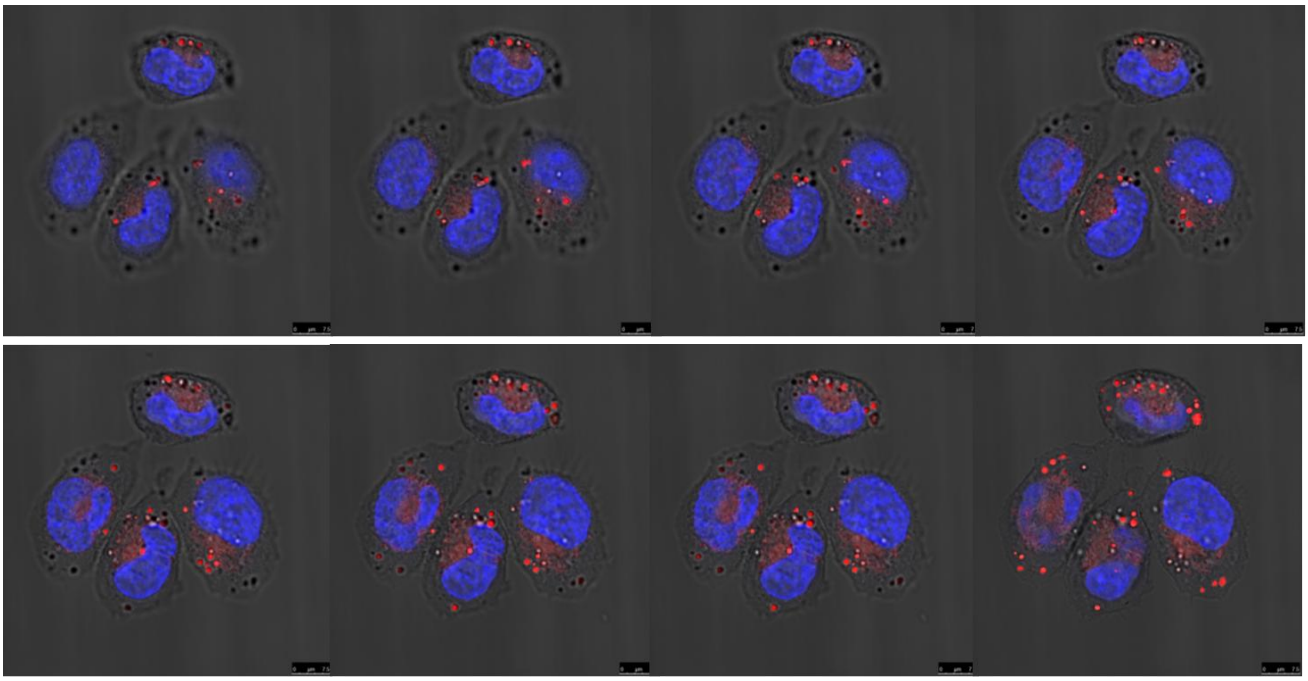

Figure 5.8A Light microscope image combined with the florescence images showing the localization of the lipid dispersion one at various depths with in the cells. Blue is the nuclei stained with DAPI. The red is the particles labeled with nile red.

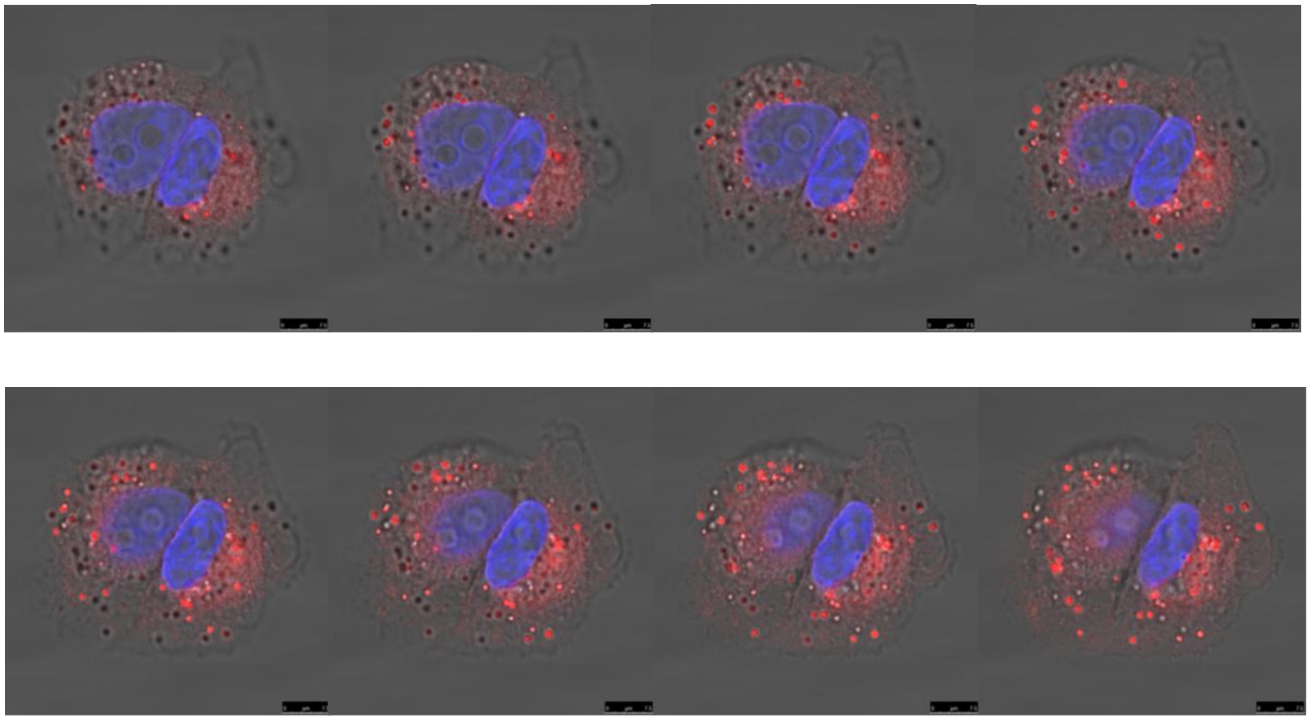

Figure 5.8B Light microscope image combined with the florescence images showing the localization of the lipid dispersion two at various depths with in the cells. Blue is the nuclei stained with DAPI. The red is the particles labeled with nile red.

6. Specific Aim 3: Investigation of the genes in the PI3K/AKT pathway that are differentially expressed in normal cell lines versus cancer cell lines.

6.1 Introduction

The PI3K/AKT pathway has been shown to harbor changes in a number of different types of cancers. Some genes in this pathway have even been shown to contribute to the development of drug resistance to ALK inhibitor therapy and gefitinib therapy. The PI3K/AKT pathway is activated after phosphorylation of the EGFR tyrosine kinase. [77] The pathway can also be activated by activation of HER2, VEGFR, and PDGFR membrane receptors. [78] The activation of these signaling pathways leads to the downstream activation of genes that can lead to cellular proliferation, cell cycle progression, and inhibition of apoptosis. [77] Studies of clinical samples have shown the over expression of PI3K and AKT correlate with a poor prognosis in non-small cell lung cancer and other cancer types as well. [62]Many inhibitors of the PI3K signaling cascade have been evaluated for their utility in the treatment of lung cancers. Currently, inhibitors of the pathway have only been shown effective when combined with other inhibitors, such as EGFR inhibitors. [78] To further investigate the role of the PI3K/AKT pathway in the progression of lung cancer, we compare the expression of 88 genes associated with the PI3K/AKT pathway in a small airway epithelial cell line as compared to A549 cell, PC-9 cells, and gefitinib resistant PC-9 cells. The analysis can help identify novel genes associated with cancer development in lung cancer cell lines with various sensitivities to gefitinib therapy.

6.2 Materials and Methods

6.2.1 Materials

RNA extraction kit was obtained from Qiagen(Germantown, MD). High capacity RNA to cDNA kit, and power up sybr green master mix were obtained from thermofisher scientific (Waltham, MA) . Gefitinib was obtained from Selleckchem(Houston, TX). 3-(4,5-Dimethylthiazol-2-yl)-2,5-Diphenyltetrazolium Bromide(MTT) and sodium dodecyl sulfate were purchased from Sigma Aldrich, St. Louis, Missouri.

6.2.2 Cell Culture

A549 lung cancer cells were grown using RPMI-1640 media (Morristown, NJ) mixed with 10% fetal bovine serum (Sigma, St. Louis, MO), 1% penicillin-streptomycin , and 2.5% sodium bicarbonate (Fisher Scientific, Waltham, MA). PC-9 and PC-9GR cells were grown using the same medium. Small airway epithelial cells were purchased from Lonza (Morristown, NJ) and grown in the recommended media provided by Lonza. The cells were grown in an incubator at 37° C and 5% (v/v) carbon dioxide. All experiments using cells were performed while the cells were in the exponential growth phase.

6.2.3 Development of Gefitinib Resistant PC-9 Cells

PC-9 cells were grown in 25 square centimeter growth flasks and treated with 50 micromolar gefitinib concentration for 24 hours. After 24 hours, the media was removed, the cells washed, and fresh media added to the flask. The cells were allowed to grow in fresh media for two weeks until they regained the ability to grow exponentially. The cells

were then again exposed to 50 micromolar gefitinib concentration. This was repeated until resistance developed in the newly established cell line.

6.2.4 Checking the sensitivity of PC-9, PC-9GR, and A549 cells to 72 hour gefitinib Treatment

To check the sensitivity of the various cell lines to gefitinib, a cell viability assay using MTT was performed. 3,000-3,500 cells of each cell line were plated into a 96 well plate and placed into the incubator for 24 hours. On the second day, the PC-9 and PC-9GR cells were treated with gefitinib concentrations ranging from 16 micromolar to 0.000977 micromolar. A549 cells were treated in triplicate with gefitinib concentrations ranging from 32 micro molar to 0.0625 micromolar. Non-treatment wells had their media replaced and acted as the controls. The cells were placed in the incubator for 72 hours. After 72 hours, the media from all the wells was removed, and 100 microliters of fresh media was added to all the wells. Next, 20 microliters of 5 mg/mL MTT yellow solution was added to all the wells and the plates were placed in the incubator for 3 hours. After three hours, 90 microliters of MTT clear solution was added to dissolve the formazan crystals that form from the MTT yellow reagent when it is cultured with living cells, and the cells were placed back into the incubator. The next day, the absorbance of the plates was read at a wavelength of 570 nm with a reference wavelength at 650 nm using a Tecan absorbance plate reader. The cell viability percent was calculated by comparing the average of the treated groups to the average of the controls.

6.2.5 RNA extraction and cDNA conversion

RNA was extracted from all cell lines, small airway epithelial cells, A549 cells, PC-9 cells, and PC-9GR cells when they were 70-80% confluent using a Qiagen Rneasy mini kit according to the manufacturer protocol. After RNA was obtained, the concentration was measured using a tecan absorbance reader and the RNA was either used immediately for cDNA conversion, or placed in storage at -80 degrees Celsius for cDNA conversion within one week. cDNA conversion was performed using Applied Biosystems high capacity RNA to cDNA kit according manufacturers protocol. In the final reaction mixture, 1,000 nanograms of RNA was added to each tube for conversion to cDNA. Upon completion of the reaction cycle, the cDNA samples were diluted to a final volume of 100 microliters to create a 10 nanogram per microliter solution of cDNA. The cDNA was stored in -20 degree Celsius until used for gene expression studies.

6.2.6 Expression studies of the genes associated with the PI3K/AKT pathway

A primer library of 88 genes involved in the PI3K/AKT signaling pathway was obtained from real time primers. Sybr green based PCR master mix was obtained from Fisher Scientific, and real time PCR was performed using a StepOnePlus instrument. The analysis was performed using the relative gene expression method or the delta,delta, Ct method. The small airway epithelial cells were used as the control cells and the expression of the 88 target genes was compared to the expression of the same gene in the

normal cell line. The reactions were run in triplicate with two different extractions of each cancer cell line evaluated to confirm the results. The total reaction volume for each PCR reaction was 20 microliters. 10 nanograms of cDNA was used in each reaction. The final primer concentration of the forward and reverse primer in each PCR reaction was 300 nanomolar as recommended by the manufacturer of the SYBR green master mix. When evaluating the A549 cells, TBP and RPL13A were used as the house keeping genes. When evaluating the PC-9 cells, TBP and PGK1 were used as the house keeping genes. When evaluating the PC-9GR cells, B-actin and PGK-1 were used as the house keeping genes.

6.3 Results

6.3.1 Gefitinib sensitivity of the cancer cell lines.

The sensitivity of the three cell lines to gefitinib was evaluated after treatment for 72 hours. Figure 6.1 shows the results of all three cell lines graphed at the same time. Of the three cell lines evaluated, A549 cells have the highest IC:50 value that is between 8 and 16 micromolar gefitinib. The IC:50 value for the PC-9GR cells appears to be between 0.25 and 0.125 micro molar gefitinib, although the cell viability of PC-9GR cells is near 50% in the range from 0.125 to 4 micromolar gefitinib treatment. PC-9 cells are the most sensitive to treatment with gefitinib with an IC:50 value between 0.0156 and 0.03125 micromolar gefitinib treatment. The sensitivity of PC-9 cells to gefitinib is at least 10 times higher than PC-9GR cells if we look at the lowest estimates of the IC:50.

6.3.2 Gene expression profile of A549, PC-9, and PC-9GR cells as compared to small airway epithelial cells

The relative expression of the 88 genes in A549 cells is shown in table 6.1. As the table shows, some of the genes could not be analyzed for relative expression as they were not expressed in one or both cell lines. These genes include AEBP1, BAD, BRAF, INS, IRS1, and others. Genes that were under expressed in A549 cells were noted with a decimal. If the gene expression of a target was said to be 50% lower in A549 cells, its relative expression was reported as 0.5X. If gene was said to be two times over expressed in A549 cells as compared to the small airway epithelial cells, the relative expression was reported as 2x. Of all the genes reported, the ones highlighted in yellow showed the greatest difference in expression as compared to the control cell line. These genes are ones that are targets for further studies evaluating the role they play in cancer disease maintenance and progression.

The relative expression of the 88 genes evaluated in PC-9 and PC-9GR cells is shown if table 6.3. The gene expression was noted in the same manner as used to show the relative expression for A549 cells. The ones highlighted in yellow represent the genes that are targeted for further evaluation for their role in cancer progression and resistance mechanisms.

6.4 Discussion

Looking at the gene expression profile of A549 cells, the genes that are candidates for future studies include E2F1, and PDE3B genes. SPP1 gene is also highly over expressed,

and it has been previously investigated by cancer researchers and found to correlate with cancer metastasis.[79-83] PDE3B is only found to be highly over expressed in A549 cells and provides an interesting target for future studies. Previous studies by Tanzawa et al. have found that levels of PDE3B are over expressed in head and neck cancer cell lines that have developed resistance to cisplatin.[84, 85] The role of PDE3B in the development of resistance in human lung cancer cell lines may warrant further investigation as this gene has not been explored for its role in promoting survival of lung cancer cell lines.

E2F1, in normal cells, plays a role in controlling cell cycle progression and is regulated by the retinoblastoma protein. E2F1 plays a role in induction of apoptosis and autophagy as well, however, E2F1 has also been found to be over expressed in a number of cancers. The role of E2F1 in cancer progression and aggressiveness has been documented in melanoma, bladder, renal, and lung cancers. [86-93] E2F1 has also been implicated in resistance to chemotherapy by activation of the ATP-binding cassette gene ABCG2. Rosenfeldt et al. reported that ABCG2 expression is directly controlled by E2F1 which can have implications for the development of treatments of chemotherapy resistant cancers. [93]

Looking at the expression profile of the PC-9 and PC-9GR cells, we see that the BCL-2 gene is over expressed in the resistant cell line. Being a regulator of non-pump resistance to apoptosis, it is not surprising that BCL-2 is over expressed in the gefitinib resistant cell line.[57] It is interesting to note that in both PC-9 and PC-9GR cells the level of E2F1 expression is elevated as compared to that of small airway epithelial cells. In PC-9GR cells, however, the level of over expression in PC-9GR cells was at least 39 times greater

than in small airway epithelial cells as compared to 13-17x greater in PC-9 cells. These results show that E2F1 is over expressed in cancer cells that have developed resistance to gefitinib. These results are in agreement with results published by Takezawa et al. that show elevated levels of expression of E2F1 in the PC-9 resistant cell line they developed in their laboratory.[94] It is possible that E2F1 may play a role in modulating resistance to gefitinib, or its over expression is due to other mechanisms that develop in resistant cells.

6.5 Conclusions

The analysis of the expression of 88 genes associated with the PI3K/AKT pathway identified a number of genes that are found to be over expressed in cancer cells as compared to normal cells. These genes are candidates for further evaluation in identifying the role they play in the development of cancer and drug resistant disease. These results can help guide development of future interventions in the treatment of lung cancer.

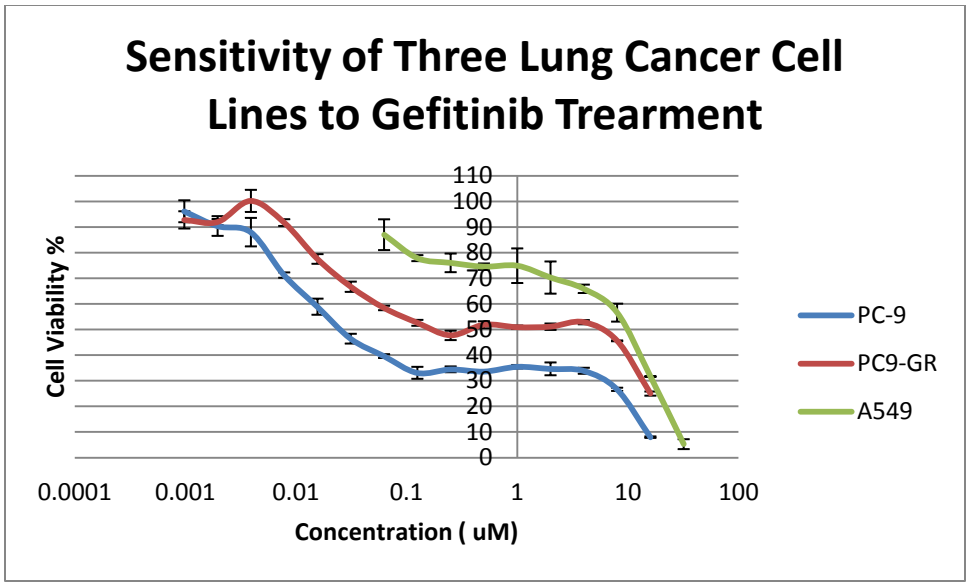

Figure 6.1. The sensitivity of three cancer cell lines to treatment with gefitinib.

GENES	Relative Expression in A549 cells
A1 ABL1	0.65X
A2 ACACA	0.6X
A3 ACOX1	0.75X
A4 AEBP1	NO EXPRESSION IN A549
A5 AKT1	1X
A6 AKT2	1.3X
A7 AKT3	9.5-10X
A8 ANG	5.5X
A9 ARAF	1X
A10 BAD	No amplification in either cells
A11 BCL2	2.5-3x
A12 BCL2L1	1.75-2.5x
B1 BRAF	No amplification in either cells
B2 BTK	1x, ct 35+
B3 CAP1	0.29x
B4 CASP9	0.25x
B5 CBL	0.55-0.6x
B6 CCND1	1.2-1.5x
B7 CCR2	1x
B8 CCR5	3.25-3.7x
B9 CD4	1.6-1.7x
B10 CD40	0.35-0.45x
B11 CDC42	0.41-0.43x
B12 CDH1	0.115-0.121x
C1 CDKN1A	Ct.35
C2 CDKN1B	Multiple Tm peaks
C3 CDKN2A	No amp in A549 Multi Tm in saec
C4 CREB1	0.6x
C5 CTNNB1	0.25-0.3x
C6 CXCR4	2x
C7 E2F1	10x
C8 EGFR	0.27-0.28x Ct. 23
C9 ERBB2	1x
C10 FRAP1	0.427-0.43x
C11 GRB2	No amp in cell lines
C12 GSK3A	1.7-1.9x
D1 GSK3B	No amp in cell lines
D2 GYS1	0.345-0.357x
D3 HK2	0.03x
D4 HRAS	0.65-0.7x
D5 IGF1	2x
D6 IGF1R	1x
D7 IGF2	Ct 35
D8 IGF2R	0.4x
D9 INS	No amp
D10 INSR	4.8-6.4x
D11 IRS1	No amp

Genes	Expression
D12 IRS2	0.75-0.8x
E1 IRS4	2.75-3.75x
E2 ITGB1	1x
E3 ITGB3	2.75-3.25x
E4 JAK2	0.65-0.7x
E5 KIT	Ct > 35
E6 KRAS	1x
E7 LCK	No amp
E8 LEP	1x
E9 MAP2K1	0.65-0.7x
E10 MAPK1	No amp
E11 MAPK14	Ct>35
E12 MAPK8	No amp
F1 MYC	0.1-0.15x
F2 NFKB1	0.15x
F3 NFKBIA	1x
F4 NOS	14-18x
F5 PAK1	No amp
F6 PDE3B	250-275x
F7 PDPK1	No amp
F8 PIK3C2B	3.5x
F9 PIK3C3	0.6-0.7x
F10 PIK3CA	0.4-0.5x
F11 PIK3R1	No amp
F12 PIK3R4	1x
G1 PRKCA	No amp
G2 PRKCE	4.5x
G3 PRKCG	No amp
G4 PTEN	1x
G5 RAC1	1x
G6 RAF1	1.3x
G7 RELA	1x
G8 RHOA	1x
G9 SGK1	0.7x
G10 SHC1	Ct >35
G11 SOS1	No amp
G12 SPP1	150,000x
H1 SRC	No amp
H2 SYK	0.025x
H3 TLR4	No amp
H4 TNF	0.2x

Table 6.1. Relative expression of the target genes in A549 cells as compared to small airway epithelial cells.

GENES	PC9 Expression	PC9GR Expression
A1 ABL1	0.5-0.6x	0.59x
A2 ACACA	1x	1.7-2x
A3 ACOX1	1x	0.7-1x
A4 AEBP1	0.006x	Ct>35
A5 AKT1	0.85x	1x
A6 AKT2	1x	2x
A7 AKT3	27.5-37.5x	31-35x
A8 ANG	1x	.9-1.4x
A9 ARAF	0.75x	1x
A10 BAD	No amp	No amp
A11 BCL2	1x	5.5-6.5x
A12 BCL2L1	2.25x	1.2-1.6x
B1 BRAF	No amp	No amp
B2 BTK	Ct>35	Ct >35
B3 CAP1	0.48x	0.35-0.39x
B4 CASP9	1.3x	3.1-3.6x
B5 CBL	0.46x	1x
B6 CCND1	1x	1x
B7 CCR2	1x	1-2x
B8 CCR5	1x	1.3-2x
B9 CD4	1x	1.8-2.6x
B10 CD40	2.25x	1.1-1.5x
B11 CDC42	0.5x	0.4x
B12 CDH1	1x	1x
C1 CDKN1A	0.04x	0.05x
C2 CDKN1B	4-5x	8.3-9.5x
C3 CDKN2A	4-6x	1.7-2.5x
C4 CREB1	0.9x	1x
C5 CTNNB1	0.41x	0.25x
C6 CXCR4	5-6x	2.6-3.3x
C7 E2F1	13-17x	39-41x
C8 EGFR	0.8x	1x
C9 ERBB2	1x	1x
C10 FRAP1	0.9x	0.7x
C11 GRB2	1x	1x
C12 GSK3A	1.25x	1x
D1 GSK3B	Ct >35	Ct 35
D2 GYS1	0.45-0.55x	0.3x
D3 HK2	0.344-0.377x	0.7x
D4 HRAS	0.42-0.52x	0.5x
D5 IGF1	2x	2-2.7x
D6 IGF1R	0.35x	0.35x
D7 IGF2	3.25-3.5x	1.5-2.2x
D8 IGF2R	0.65x	0.45x
D9 INS	No amp	No amp
D10 INSR	2.75-3.5x	1.7-3x
D11 IRS1	1x	0.5x

Genes	Expression	Expression
D12 IRS2	0.8x	1.5-1.8x
E1 IRS4	1x	1.7x
E2 ITGB1	0.39x	0.2-0.3x
E3 ITGB3	0.3x	0.018-0.027x
E4 JAK2	0.31x	0.177-0.23x
E5 KIT	No amp	Ct>35
E6 KRAS	1.6x	2x
E7 LCK	No amp.	No amp.
E8 LEP	0.375x	1x
E9 MAP2K1	0.6x	0.7-1x
E10 MAPK1	Ct >35	Ct>35
E11 MAPK14	1x	1x
E12 MAPK8	No amp	No amp
F1 MYC	0.95x	1x
F2 NFKB1	0.1x	0.12-0.14x
F3 NFKBIA	0.55x	0.44-0.47x
F4 NOS	5-10x	6-18x
F5 PAK1	1x	Ct>35
F6 PDE3B	Ct>35	Ct>35
F7 PDPK1	1.6x	0.3-0.6x
F8 PIK3C2B	10x	17.6-20.07x
F9 PIK3C3	0.65x	0.33-0.407x
F10 PIK3CA	0.83x	0.539-0.619x
F11 PIK3R1	No amp	No amp
F12 PIK3R4	1.5-1.6x	1.5x
G1 PRKCA	Ct>35	Ct >35
G2 PRKCE	2x	2.54-2.64x
G3 PRKCG	Ct 28 no amp in control	Ct 32, no amp in SAEC
G4 PTEN	0.23x	0.35-0.45x
G5 RAC1	1x	1.3x
G6 RAF1	1.25x	1.6x
G7 RELA	1.2-1.3x	1.2x
G8 RHOA	0.8x	0.8x
G9 SGK1	0.4x	0.09-0.15x
G10 SHC1	0.177x	0.16x
G11 SOS1	No amp	No amp
G12 SPP1	19-23,000x (ct 21 vs 35.8)	1,507-1,087x
H1 SRC	Ct >35	Ct>35
H2 SYK	1.3-1.5x	1.3-1.5x
H3 TLR4	No amp	No amp
H4 TNF	0.15-0.2x	0.04-0.06x

Table 6.2. The relative expression of genes in epithelial cells versus sensitive and resistant PC-9 lung cancer cells.

7. References

1. Garbuzenko, O.B., et al., *Inhibition of lung tumor growth by complex pulmonary delivery of drugs with oligonucleotides as suppressors of cellular resistance.* Proc Natl Acad Sci U S A, 2010. **107**(23): p. 10737-42.
2. Shim, M.S. and Y.J. Kwon, *Efficient and targeted delivery of siRNA in vivo.* FEBS J, 2010. **277**(23): p. 4814-27.
3. Puri, A., et al., *Lipid-based nanoparticles as pharmaceutical drug carriers: from concepts to clinic.* Crit Rev Ther Drug Carrier Syst, 2009. **26**(6): p. 523-80.
4. Muchow, M., P. Maincent, and R.H. Muller, *Lipid nanoparticles with a solid matrix (SLN, NLC, LDC) for oral drug delivery.* Drug Dev Ind Pharm, 2008. **34**(12): p. 1394-405.
5. Azarmi, S., W.H. Roa, and R. Lobenberg, *Targeted delivery of nanoparticles for the treatment of lung diseases.* Adv Drug Deliv Rev, 2008. **60**(8): p. 863-75.
6. Weber, S., A. Zimmer, and J. Pardeike, *Solid Lipid Nanoparticles (SLN) and Nanostructured Lipid Carriers (NLC) for pulmonary application: a review of the state of the art.* Eur J Pharm Biopharm, 2014. **86**(1): p. 7-22.
7. Dharap, S.S., et al., *Tumor-specific targeting of an anticancer drug delivery system by LHRH peptide.* Proc Natl Acad Sci U S A, 2005. **102**(36): p. 12962-7.
8. Gutiérrez, J.M., et al., *Nano-emulsions: New applications and optimization of their preparation.* Current Opinion in Colloid & Interface Science, 2008. **13**(4): p. 245-251.
9. Tadros, T., et al., *Formation and stability of nano-emulsions.* Adv Colloid Interface Sci, 2004. **108-109**: p. 303-18.

10. Rao, J. and D.J. McClements, *Food-grade microemulsions, nanoemulsions and emulsions: Fabrication from sucrose monopalmitate & lemon oil.* Food Hydrocolloids, 2011. **25**(6): p. 1413-1423.

11. Mehnert, W. and K. Mader, *Solid lipid nanoparticles: production, characterization and applications.* Adv Drug Deliv Rev, 2001. **47**(2-3): p. 165-96.

12. Lee, L.L., et al., *Emulsification: Mechanistic understanding.* Trends in Food Science & Technology, 2013. **31**(1): p. 72-78.

13. Cucheval, A. and R.C. Chow, *A study on the emulsification of oil by power ultrasound.* Ultrason Sonochem, 2008. **15**(5): p. 916-20.

14. Burguera, J.L. and M. Burguera, *Analytical applications of emulsions and microemulsions.* Talanta, 2012. **96**: p. 11-20.

15. Solans, C., et al., *Nano-emulsions.* Current Opinion in Colloid & Interface Science, 2005. **10**(3-4): p. 102-110.

16. Shang, L., K. Nienhaus, and G.U. Nienhaus, *Engineered nanoparticles interacting with cells: size matters.* J Nanobiotechnology, 2014. **12**: p. 5.

17. Oh, N. and J.H. Park, *Endocytosis and exocytosis of nanoparticles in mammalian cells.* Int J Nanomedicine, 2014. **9 Suppl 1**: p. 51-63.

18. Donsì, F., et al., *Infusion of essential oils for food stabilization: Unraveling the role of nanoemulsion-based delivery systems on mass transfer and antimicrobial activity.* Innovative Food Science & Emerging Technologies, 2014. **22**: p. 212-220.

19. Roohinejad, S., et al., *Formulation of oil-in-water beta-carotene microemulsions: effect of oil type and fatty acid chain length.* Food Chem, 2015. **174**: p. 270-8.

20. Teixeira, P.C., et al., *Antimicrobial effects of a microemulsion and a nanoemulsion on enteric and other pathogens and biofilms.* Int J Food Microbiol, 2007. **118**(1): p. 15-9.

21. Kuo, Y.C. and J.F. Chung, *Physicochemical properties of nevirapine-loaded solid lipid nanoparticles and nanostructured lipid carriers.* Colloids Surf B Biointerfaces, 2011. **83**(2): p. 299-306.

22. Lee, L. and I.T. Norton, *Comparing droplet breakup for a high-pressure valve homogeniser and a Microfluidizer for the potential production of food-grade nanoemulsions.* Journal of Food Engineering, 2013. **114**(2): p. 158-163.

23. O'Sullivan, J., et al., *Comparison of batch and continuous ultrasonic emulsification processes.* Journal of Food Engineering, 2015. **167**: p. 114-121.

24. Ramisetty, K.A., A.B. Pandit, and P.R. Gogate, *Ultrasound assisted preparation of emulsion of coconut oil in water: Understanding the effect of operating parameters and comparison of reactor designs.* Chemical Engineering and Processing: Process Intensification, 2015. **88**: p. 70-77.

25. Solans, C. and I. Solé, *Nano-emulsions: Formation by low-energy methods.* Current Opinion in Colloid & Interface Science, 2012. **17**(5): p. 246-254.

26. Kumar, S. and J.K. Randhawa, *High melting lipid based approach for drug delivery: solid lipid nanoparticles.* Mater Sci Eng C Mater Biol Appl, 2013. **33**(4): p. 1842-52.

27. Danhier, F., et al., *PLGA-based nanoparticles: an overview of biomedical applications.* J Control Release, 2012. **161**(2): p. 505-22.

28. Manisha mishra, P.M., K.Surya prabha, P.Sobhita rani, I . A.Satish babu , I. Sarath Chandiran , G.Arunachalam and S.Shalini and . *Basics and Potential Applications of Surfactants - A Review.* International Journal of PharmTech Research, 2009. **1** (4): p. 1354-1365.

29. Severino, P., et al., *Current State-of-Art and New Trends on Lipid Nanoparticles (SLN and NLC) for Oral Drug Delivery.* J Drug Deliv, 2012. **2012**: p. 750891.

30. *U.S. Cancer Statistics Working Group. United States Cancer Statistics: 1999-2009 Incidence and Mortality Web-based Report. Atlanta: U.S. Department of Health and Human Services, Centers for Disease Control and Prevention and National Cancer Institute; 2013. Available at: www.cdc.gov/uscs <http://www.cdc.gov/uscs>.*

.

31. *Tsao Anne S, Glisson Bonnie S, "Chapter 11. Small Cell Lung Cancer" (Chapter). Kantarjian HM, Wolff RA, Koller CA: MD Anderson Manual of Medical Oncology: <http://www.accessmedicine.com/content.aspx?aID=2788378>.*

.

32. *Frieze DA, Adams VR. Chapter 137. Lung Cancer. In: Talbert RL, DiPiro JT, Matzke GR, Posey LM, Wells BG, Yee GC, eds. Pharmacotherapy: A Pathophysiologic Approach. 8th ed. New York: McGraw-Hill; 2011. http://www.accesspharmacy.com/content.aspx?aID=8008333. Accessed May 24, 2018.*

33. *Johnson Faye M, Pisters Katherine M, "Chapter 12. Non-Small Cell Lung Cancer" (Chapter). Kantarjian HM, Wolff RA, Koller CA: MD Anderson Manual of Medical Oncology: <http://www.accessmedicine.com/content.aspx?aID=2788738>.*

.

34. *Ettinger S. David, Akerley Wallace, Borghaei Hossein, et al. (2013).National Comprehensive Cancer Network Clinical Practice Guidelines in Oncology: Non-Small Cell Lung Cancer. Version 2. Available at www. nccn.org*

35. Mitsudomi, T., et al., *Gefitinib versus cisplatin plus docetaxel in patients with non-small-cell lung cancer harbouring mutations of the epidermal growth factor receptor (WJTOG3405): an open label, randomised phase 3 trial.* Lancet Oncol, 2010. **11**(2): p. 121-8.

36. Kuzmov, A. and T. Minko, *Nanotechnology approaches for inhalation treatment of lung diseases.* J Control Release, 2015. **219**: p. 500-18.

37. Anderson, P.M., et al., *Aerosol granulocyte macrophage-colony stimulating factor: a low toxicity, lung-specific biological therapy in patients with lung metastases.* Clin Cancer Res, 1999. **5**(9): p. 2316-23.

38. Arndt, C.A., et al., *Inhaled granulocyte-macrophage colony stimulating factor for first pulmonary recurrence of osteosarcoma: effects on disease-free survival and immunomodulation. a report from the Children's Oncology Group.* Clin Cancer Res, 2010. **16**(15): p. 4024-30.

39. Markovic, S.N., et al., *A dose-escalation study of aerosolized sargramostim in the treatment of metastatic melanoma: an NCCTG Study.* Am J Clin Oncol, 2008. **31**(6): p. 573-9.

40. Rao, R.D., et al., *Aerosolized granulocyte macrophage colony-stimulating factor (GM-CSF) therapy in metastatic cancer.* Am J Clin Oncol, 2003. **26**(5): p. 493-8.

41. Otterson, G.A., et al., *Phase I study of inhaled Doxorubicin for patients with metastatic tumors to the lungs.* Clin Cancer Res, 2007. **13**(4): p. 1246-52.

42. Otterson, G.A., et al., *Phase I/II study of inhaled doxorubicin combined with platinum-based therapy for advanced non-small cell lung cancer.* Clin Cancer Res, 2010. **16**(8): p. 2466-73.

43. Lemarie, E., et al., *Aerosolized gemcitabine in patients with carcinoma of the lung: feasibility and safety study.* J Aerosol Med Pulm Drug Deliv, 2011. **24**(6): p. 261-70.

44. Zarogoulidis, P., et al., *Feasibility and effectiveness of inhaled carboplatin in NSCLC patients.* Invest New Drugs, 2012. **30**(4): p. 1628-40.

45. *Medina PJ, Shord SS. Chapter 135. Cancer Treatment and Chemotherapy. In: DiPiro JT, Talbert RL, Yee GC, Matzke GR, Wells BG, Posey LM, eds. Pharmacotherapy: A Pathophysiologic Approach. 8th ed. New York: McGraw-Hill; 2011. http://www.accesspharmacy.com/content.aspx?aID=8007280. Accessed June 10, 2013.*

46. Minko, T., et al., *New generation of liposomal drugs for cancer.* Anticancer Agents Med Chem, 2006. **6**(6): p. 537-52.

47. Kruh, G.D. and M.G. Belinsky, *The MRP family of drug efflux pumps.* Oncogene, 2003. **22**(47): p. 7537-52.

48. Keppler, D., *Multidrug resistance proteins (MRPs, ABCCs): importance for pathophysiology and drug therapy.* Handb Exp Pharmacol, 2011(201): p. 299-323.

49. Bellamy, W.T., *P-glycoproteins and multidrug resistance.* Annu Rev Pharmacol Toxicol, 1996. **36**: p. 161-83.

50. Ambudkar, S.V., et al., *Biochemical, cellular, and pharmacological aspects of the multidrug transporter.* Annu Rev Pharmacol Toxicol, 1999. **39**: p. 361-98.

51. Dumontet, C., et al., *Resistance mechanisms in human sarcoma mutants derived by single-step exposure to paclitaxel (Taxol).* Cancer Res, 1996. **56**(5): p. 1091-7.

52. Youle, R.J. and A. Strasser, *The BCL-2 protein family: opposing activities that mediate cell death.* Nat Rev Mol Cell Biol, 2008. **9**(1): p. 47-59.

53. Motoyama, N., et al., *Massive cell death of immature hematopoietic cells and neurons in Bcl-x-deficient mice.* Science, 1995. **267**(5203): p. 1506-10.

54. Rinkenberger, J.L., et al., *Mcl-1 deficiency results in peri-implantation embryonic lethality.* Genes Dev, 2000. **14**(1): p. 23-7.

55. Bouillet, P., et al., *Degenerative disorders caused by Bcl-2 deficiency prevented by loss of its BH3-only antagonist Bim.* Dev Cell, 2001. **1**(5): p. 645-53.

56. Print, C.G., et al., *Apoptosis regulator bcl-w is essential for spermatogenesis but appears otherwise redundant.* Proc Natl Acad Sci U S A, 1998. **95**(21): p. 12424-31.

57. Kelly, P.N. and A. Strasser, *The role of Bcl-2 and its pro-survival relatives in tumourigenesis and cancer therapy.* Cell Death Differ, 2011. **18**(9): p. 1414-24.

58. Shortt, J. and R.W. Johnstone, *Oncogenes in cell survival and cell death.* Cold Spring Harb Perspect Biol, 2012. **4**(12).

59. Jeannot, V., et al., *The PI3K/AKT pathway promotes gefitinib resistance in mutant KRAS lung adenocarcinoma by a deacetylase-dependent mechanism.* Int J Cancer, 2014. **134**(11): p. 2560-71.

60. Yang, L., et al., *Blocking the PI3K pathway enhances the efficacy of ALK-targeted therapy in EML4-ALK-positive nonsmall-cell lung cancer.* Tumour Biol, 2014. **35**(10): p. 9759-67.

61. Ibuki, Y., et al., *Cigarette sidestream smoke induces histone H3 phosphorylation via JNK and PI3K/Akt pathways, leading to the expression of proto-oncogenes.* Carcinogenesis, 2014. **35**(6): p. 1228-37.

62. Jiang, A.G., H. Yu, and J.A. Huang, *Expression and clinical significance of the phosphatidylinositol 3-kinase/protein kinase B signal transduction pathway in non-small cell lung carcinoma.* Oncol Lett, 2014. **8**(2): p. 601-607.

63. Taratula, O., et al., *Surface-engineered targeted PPI dendrimer for efficient intracellular and intratumoral siRNA delivery.* J Control Release, 2009. **140**(3): p. 284-93.

64. Shi, B., et al., *Biodistribution of small interfering RNA at the organ and cellular levels after lipid nanoparticle-mediated delivery.* J Histochem Cytochem, 2011. **59**(8): p. 727-40.

65. Xue, H.Y. and H.L. Wong, *Tailoring nanostructured solid-lipid carriers for time-controlled intracellular siRNA kinetics to sustain RNAi-mediated chemosensitization.* Biomaterials, 2011. **32**(10): p. 2662-72.

66. *Chabner Bruce A, Bertino Joseph, Cleary James, Ortiz Taylor, Lane Andrew, Supko Jeffrey G, Ryan David, "Chapter 61. Cytotoxic Agents" (Chapter). Brunton LL, Chabner BA, Knollmann BC: Goodman & Gilman's The Pharmacological Basis of Therapeutics, 2011, 12e: <http://www.accessmedicine.com/content.aspx?aID=16680251>.*

.

67. Subedi, R.K., K.W. Kang, and H.K. Choi, *Preparation and characterization of solid lipid nanoparticles loaded with doxorubicin.* Eur J Pharm Sci, 2009. **37**(3-4): p. 508-13.

68. Liu, D., et al., *Nanostructured lipid carriers as novel carrier for parenteral delivery of docetaxel.* Colloids Surf B Biointerfaces, 2011. **85**(2): p. 262-9.

69. Gao, W., et al., *Chemotherapeutic drug delivery to cancer cells using a combination of folate targeting and tumor microenvironment-sensitive polypeptides.* Biomaterials, 2013. **34**(16): p. 4137-49.

70. Doktorovova, S., E.B. Souto, and A.M. Silva, *Nanotoxicology applied to solid lipid nanoparticles and nanostructured lipid carriers - a systematic review of in vitro data.* Eur J Pharm Biopharm, 2014. **87**(1): p. 1-18.

71. Leong, T.S., et al., *Minimising oil droplet size using ultrasonic emulsification.* Ultrason Sonochem, 2009. **16**(6): p. 721-7.

72. Garces, A., et al., *Formulations based on solid lipid nanoparticles (SLN) and nanostructured lipid carriers (NLC) for cutaneous use: A review.* Eur J Pharm Sci, 2018. **112**: p. 159-167.

73. Ghosh, V., et al., *Antibacterial microemulsion prevents sepsis and triggers healing of wound in wistar rats.* Colloids Surf B Biointerfaces, 2013. **105**: p. 152-7.

74. Aggarwal, N., S. Goindi, and R. Khurana, *Formulation, characterization and evaluation of an optimized microemulsion formulation of griseofulvin for topical application.* Colloids Surf B Biointerfaces, 2013. **105**: p. 158-66.

75. Rao, J. and D.J. McClements, *Lemon oil solubilization in mixed surfactant solutions: Rationalizing microemulsion & nanoemulsion formation.* Food Hydrocolloids, 2012. **26**(1): p. 268-276.

76. Goppert, T.M. and R.H. Muller, *Protein adsorption patterns on poloxamer- and poloxamine-stabilized solid lipid nanoparticles (SLN).* Eur J Pharm Biopharm, 2005. **60**(3): p. 361-72.

77. Ganti, A.K., *Epidermal growth factor receptor signaling in nonsmall cell lung cancer.* Cancer Invest, 2010. **28**(5): p. 515-25.

78. Fumarola, C., et al., *Targeting PI3K/AKT/mTOR pathway in non small cell lung cancer.* Biochem Pharmacol, 2014. **90**(3): p. 197-207.

79. Guo, H., et al., *Nitric Oxide-Dependent Osteopontin Expression Induces Metastatic Behavior in HepG2 Cells.* Digestive Diseases and Sciences, 2005. **50**(7): p. 1288-1298.

80. Weber, G.F., *Molecular mechanisms of metastasis.* Cancer Lett, 2008. **270**(2): p. 181-90.

81. Wu, X.L., et al., *Osteopontin knockdown suppresses the growth and angiogenesis of colon cancer cells.* World J Gastroenterol, 2014. **20**(30): p. 10440-8.

82. Rangaswami, H., A. Bulbule, and G.C. Kundu, *Osteopontin: role in cell signaling and cancer progression.* Trends Cell Biol, 2006. **16**(2): p. 79-87.

83. Wai, P.Y. and P.C. Kuo, *The role of Osteopontin in tumor metastasis.* J Surg Res, 2004. **121**(2): p. 228-41.

84. Yamano, Y., et al., *Identification of cisplatin-resistance related genes in head and neck squamous cell carcinoma.* Int J Cancer, 2010. **126**(2): p. 437-49.

85. Uzawa, K., et al., *Targeting phosphodiesterase 3B enhances cisplatin sensitivity in human cancer cells.* Cancer Med, 2013. **2**(1): p. 40-9.

86. Alla, V., et al., *E2F1 in melanoma progression and metastasis.* J Natl Cancer Inst, 2010. **102**(2): p. 127-33.

87. Lee, S.R., et al., *Activation of EZH2 and SUZ12 Regulated by E2F1 Predicts the Disease Progression and Aggressive Characteristics of Bladder Cancer.* Clin Cancer Res, 2015. **21**(23): p. 5391-403.

88. Imai, M.A., et al., *Overexpression of E2F1 associated with LOH at RB locus and hyperphosphorylation of RB in non-small cell lung carcinoma.* J Cancer Res Clin Oncol, 2004. **130**(6): p. 320-6.

89. Hung, J.J., et al., *Clinical significance of E2F1 protein expression in non-small cell lung cancer.* Exp Hematol Oncol, 2012. **1**(1): p. 18.

90. Eymin, B., et al., *Distinct pattern of E2F1 expression in human lung tumours: E2F1 is upregulated in small cell lung carcinoma.* Oncogene, 2001. **20**(14): p. 1678-87.

91. Stoleriu, M.G., et al., *A new strategy in the treatment of chemoresistant lung adenocarcinoma via specific siRNA transfection of SRF, E2F1, Survivin, HIF and STAT3.* Eur J Cardiothorac Surg, 2014. **46**(5): p. 877-86.

92. Ma, X., et al., *Overexpression of E2F1 promotes tumor malignancy and correlates with TNM stages in clear cell renal cell carcinoma.* PLoS One, 2013. **8**(9): p. e73436.

93. Rosenfeldt, M.T., et al., *E2F1 drives chemotherapeutic drug resistance via ABCG2.* Oncogene, 2014. **33**(32): p. 4164-72.

94. Takezawa, K., et al., *Enhanced anticancer effect of the combination of BIBW2992 and thymidylate synthase-targeted agents in non-small cell lung cancer with the T790M mutation of epidermal growth factor receptor.* Mol Cancer Ther, 2010. **9**(6): p. 1647-56.